

Author:
Ankit Verma

Graduation Supervisors:
ir. M.B. Zaaijer
dr. J.A. Poulis
Prof. dr. G.J.W. van Bussel

Date:
November 2011

ADHESIVE BONDED TOWERS FOR WIND TURBINES

Design, Optimization and Cost Analysis

Ankit Verma

Master Thesis

ADHESIVE BONDED TOWERS FOR WIND TURBINES

Design, Optimization and Cost Analysis

*Submitted in Partial Fulfillment of the Requirements
for the Degree of Master of Science
in
Sustainable Energy Technology
Track: Wind Energy*

*Author:
Ankit Verma*

November 2011

Department of Aerospace Engineering
Delft University of Technology

Department of Mechanical Engineering
Eindhoven University of Technology

Adhesive Bonded Towers for Wind Turbines

Copyright © 2011 by Ankit Verma

All rights reserved

Supervised by:

ir. M.B. Zaaijer (Michiel)

dr. J.A. Poulis (Hans)

Prof. dr. G.J.W. van Bussel (Gerard)

Wind Energy Research Group

Delft University of Technology

Kluyverweg 1

2629 HS Delft

The Netherlands

Abstract

In an increasingly competitive energy market, the cost of a wind power plant has become more important. A tubular steel tower supporting a wind turbine can amount to up to 20% of the overall turbine costs and its optimization may lead to substantial savings with regard to the costs and the use of materials.

One important aspect of the design is connections between the tower's sections and between the cans. The towers usually consist of steel segments, made of several welded cans (conical subsections), which are further connected by welded flanges. The welded connections have high risk of fatigue failure leading to the thick tower wall. Also, the flanges are very expensive. This research is focused on improving wind turbine towers by using adhesive bonded joints instead of welded joints and flanges. This idea is investigated and the principles of bonded connection are presented. Fatigue resistance is treated as the main discerning factor between the existing design and the proposed solution in this study.

The first part of the project focuses on providing a design solution for replacing the bottom-most flange with the bonded joints. A comparative cost study of the proposed solution is also provided in this project. In the second part, optimization of the thickness has been investigated for the entire tower when the cans are bonded circumferentially using adhesives instead of welds.

For the cost analysis of the proposed solution, an 80m reference tower was designed based on the stability and the fatigue assessment of the welds. The approach is use a reference 3MW wind turbine model in GH Bladed. The proposed bonded joint is a tubular-single lap joint based on implementation of simple analytical Volkersen Model. A design guideline for the adhesive bonded joint is presented. Furthermore, particular focus was given to the factors affecting a joint strength and their behavior in a bonded joint. Finally, the benefits in terms of fatigue strength, design simplicity, and cost savings are addressed in detail.

According to this study, the replacement of the bottom-most flanges with an adhesive bonded joint provides a maximum cost reduction of 17%. This seems to be an economically feasible assembly solution. For the bonding of entire cans in the tower, only the top two cans can be bonded economically, keeping the remaining cans to be welded to each other. The replacement of welds in the entire tower by bonded joints is possible, however, in comparison to the existing solution it is not a feasible solution in terms of material and cost saving.

Acknowledgement

The work reported is the final research project towards obtaining my masters degree (MSc.) in the Wind Energy Section of Delft University of Technology. This project work was done under the supervision of Michiel Zaaijer. First, I would like to express my gratitude to him for his constant guidance and valuable advices during the last 12 months at TU Delft. He helped me to visualize this project from scratch and has provided valuable assistance during the entire project. The numerous discussions we had have contributed greatly in shaping my thesis and thoughts.

Part of the work was done under the guidance of dr. J.A. Poulis, Director of the Adhesion Institute, TUDelft. I thank him for initiating this project as well as for giving valuable inputs and guidance during this project. Besides, invaluable suggestions from members of the adhesive department are much appreciated.

I also thank the master students at Section Wind Energy whose contributions, via informative discussions, were invaluable and also to the entire team at Section Wind Energy for making my experience here most memorable.

I would like to take this opportunity to thank all my friends from TUDelft and TU/e. Their company made this a truly eventful two years. Finally, I would like to thank my dear parents for their continuous support and motivation. Without them, none of this would have been possible.

Table of Contents

Abstract.....	i
Acknowledgement	iii
List of figures.....	ix
List of tables	xi
List of symbols.....	xiii
Acronyms	xvii
1. Introduction	1
1.1. Preliminary research	1
1.2. Objective	2
1.3. Approach.....	2
1.4. Report layout	2
2. Tubular steel tower.....	3
2.1. Introduction	3
2.2. Welded tubular steel tower	3
2.3. Bolted ring flange connections	4
3. Design of a reference tower with flanges and welds.....	7
3.1. Introduction	7
3.2. Tower design procedure	7
3.3. Turbine configuration	8
3.3.1. Turbine model in GH Bladed	8
3.3.2. Tower properties.....	9
3.3.3. Foundation geometry	11
3.3.4. Flange geometry at the tower base	11
3.3.5. Tower input in GH Bladed	12
3.4. IEC class and Wind conditions.....	13
3.5. Design loads	18
3.5.1. Static loads	18
3.5.2. Fatigue loads	21
3.6. Redesign of tubular tower	22
3.6.1. Stability check	22

3.6.2.	Fatigue check	23
3.6.2.1.	Welding details in a tubular tower.....	23
3.6.2.2.	Detail categories of welded joints.....	23
3.6.2.3.	S-N curve	24
3.6.2.4.	Palmgren-miner's rule.....	26
3.6.2.5.	Fatigue damage calculation	26
3.6.2.6.	Approach for dimensioning the wall thickness.....	27
3.6.3.	Natural frequency check	29
3.7.	Conclusion.....	31
4.	Adhesive bonding.....	33
4.1.	Introduction	33
4.1.1.	Introduction to adhesive.....	33
4.1.2.	Definitions	33
4.1.3.	Adhesive bonded joint	34
4.1.4.	Advantages and disadvantages of adhesive bonding	35
4.2.	Factors affecting the joint strength	36
4.2.1.	Adhesive properties	37
4.2.2.	Adherend properties.....	37
4.2.3.	Overlap lengths	37
4.2.4.	Adhesive thicknesses	38
4.2.5.	Environmental effects.....	39
4.3.	Method to improve the joint strength.....	40
4.4.	Conclusion.....	41
5.	Design of adhesive bonded joints.....	43
5.1.	Adhesive bonding design procedure	43
5.2.	Selection of a joint type	44
5.2.1.	Various types of joints.....	44
5.2.2.	Considerations for selecting a suitable type of joint	45
5.3.	Joint geometry and loading	46
5.4.	Material properties	46
5.5.	Closed-form models.....	47
5.5.1.	Types of models	47

5.5.2.	Volkersen model	48
5.5.3.	Selection of failure criterion	50
5.5.4.	Linear elastic analysis.....	50
5.6.	Design checks.....	52
5.6.1.	Resistance at ULS	52
5.6.2.	Fatigue check of the bonded joint	54
5.6.2.1.	S-N curve of adhesive.....	54
5.6.2.2.	Safety factor for bonded joints	55
5.6.2.3.	S-N curve for structural steel	56
5.7.	Modification in the can geometry	56
6.	Bonding of tower base to the foundation instead of flange and cost comparison	59
6.1.	Results of bonding tower base to the foundation.....	59
6.2.	Final geometry	61
6.3.	Cost analysis.....	62
6.3.1.	Flange fabrication cost.....	62
6.3.2.	Flange welding cost.....	62
6.3.3.	Adhesive bonding cost	63
6.4.	Cost comparison	64
7.	Bonding of the cans instead of welds and cost comparison.....	67
7.1.	Results of bonding the cans	67
7.2.	Cost comparison	68
8.	Conclusion and recommendations	69
8.1.	Conclusion.....	69
8.2.	Recommendations for future work	70
9.	Bibliography	71
Appendix A.	Load case descriptions.....	75
Appendix B.	Definition of adhesive related terms.....	78
Appendix C.	Adhesive and material properties	79
Appendix D.	Matlab code for Volkersen Model.....	80
Appendix E.	Table showing the failure loads for fillet	82

List of figures

Figure 2-1: Construction of a tubular steel tower from welded cans.....	4
Figure 2-2: Bolted ring flange connection [14]	5
Figure 3-1: Overview of the design procedure for a wind turbine tower.....	8
Figure 3-2: Blade configuration in GH Bladed.....	8
Figure 3-3: Turbine configurations and components mass details.....	9
Figure 3-4: Tower design, Vestas 3MW, Onshore [19]	10
Figure 3-5: (a) Cylindrical structural element [20] and (b) its geometry details.....	11
Figure 3-6: Design of a flange which is welded to the foundation and tower base	11
Figure 3-7: The Bladed input of initial tower properties along with the flanges as point masses	12
Figure 3-8: Wind speed distribution from GH Bladed	15
Figure 3-9: Extreme operating gust at $V_{hub} = 25\text{m/s}$	17
Figure 3-10: Coordinate system for the design loads on a tower [7]	19
Figure 3-11: Typical weld details in a tubular tower a) weld at flange b) weld between two cans	23
Figure 3-12: The stress cycle [21].....	24
Figure 3-13: S-N curve for welds category 80 and 71.....	25
Figure 3-14: Approach for dimensioning the wall thickness	27
Figure 3-15: Dimensioning of cans adjacent to bottom flange	29
Figure 3-16: Campbell diagram for the final designed tower.....	30
Figure 3-17: Dimensioning of the tower wall thickness according to stability and fatigue check	31
Figure 4-1: Different types of loads in an adhesive bonded joint [27]	33
Figure 4-2: Components of a typical adhesive joint [30]	35
Figure 4-3: Comparison of load transfer in various types of joints [4].	35
Figure 4-4: S–N curves of lap joints [4]	36
Figure 4-5: Overlap effect on Linear analysis: brittle adhesive (Redux326) and high-strength steel [34] .	38
Figure 4-6: Adhesive thickness effect on linear analysis: adhesive(Hysol9321) and high-strength steel .	38
Figure 4-7: Fatigue of 1.5 mm AISI 304L stainless steel adhesive joints.....	40
Figure 4-8: Load transfer and shear stress distribution in SLJs (1) with fillet and (2) without fillet [29]....	41
Figure 5-1: Steps for the design of a adhesive bonded joint	43

Figure 5-2: Joint configurations for (a) Lap joints [30] (b) strap joints (c) tubular joint with a taper [29] .	44
Figure 5-3: Tubular single lap joint [29]	45
Figure 5-4: Rotation of joints in (a) Single lap plate joint (b) Single lap tubular joint [42]	45
Figure 5-5: Deformations in loaded single-lap joints with elastic adherends [8].	48
Figure 5-6: Single-lap joint analyzed by Volkersen [8]: (a) Geometry and (b) Elemental diagram.....	49
Figure 5-7: Principle of the proposed adhesive bonded connection.....	51
Figure 5-8: Shear stress variation along the overlap length $l=400\text{mm}$, $t_a=10\text{mm}$, $t_t=36.5\text{mm}$, $t_b=55\text{mm}$.	52
Figure 5-9: Shear stress variation against overlap length at thickness 10mm , $t_t=36.5\text{mm}$ and $t_b=55\text{mm}$	53
Figure 5-10: Effect of varying thicknesses of adherend in a joint on the peak stress	53
Figure 5-11: S-N curve for simple lap joint bonded with toughened epoxy system, DP 490.	54
Figure 5-12: Dynamic fatigue of steel double-box hat structures [47]......	54
Figure 5-13: S-N curve for simple lap joint bonded with a toughened epoxy system (DP 490)	55
Figure 5-14: S-N curve for the structural steel.....	56
Figure 5-15: Transition in butt welds of unequal thicknesses	57
Figure 6-1: Shear stress variation along the overlap length for (a) both wall thickness 55mm , $l = 770\text{mm}$ and (b) both wall thickness 60mm and $l = 660\text{mm}$	60
Figure 6-2: Campbell diagram for the turbine with bonded tower base to foundation.	61

List of tables

Table 3-1: Basic parameters for wind turbine classes [7]	13
Table 3-2: Design load case parameters	13
Table 3-3: Extreme load cases descriptions.....	18
Table 3-4: Partial safety factors for the load cases.....	18
Table 3-5: Design loads at tower base for different load cases.....	19
Table 3-6: Extreme design loads at each welded sections	20
Table 3-7: Fatigue load case description	21
Table 3-8: Partial safety factors for fatigue analysis.....	21
Table 3-9: Wall thicknesses dimensioned according to stability check.....	22
Table 3-10: Detail categories for common welds in a tubular tower [22].....	23
Table 3-11: Redesign of tower thicknesses according to fatigue damage	28
Table 3-12: Tower natural frequencies from modal analysis in the Bladed	30
Table 5-1: Material properties of adherend and adhesive	47
Table 5-2: Comparison between different analytical models [32]	48
Table 5-3: Partial safety factors for fatigue analysis of adhesively bonded connections.....	55
Table 5-4: Detail Categories and tapering slope for welded parts of a component [48]	57
Table 6-1: Effect on overlap length and material volume with increase in adherend wall thicknesses	59
Table 6-2: Cost of foundation flange connection	63
Table 6-3: Dimension of bottommost can before and after bonding.....	63
Table 6-4: Cost of adhesive connection	64
Table 7-1: Detailed analysis of bonding cans with adhesive	68
Table 7-2: Cost saving from the circumferential bonding	68

List of symbols

Latin symbols

I_{15}	characteristic turbulence intensity at 15 m/s	[%]
I_{Ref}	expected value of the turbulence intensity at 15 m/s	[%]
t	tower shell thickness	[m]
e	equivalent geometrical imperfection	[m]
m	inverse slope of S-N curve	[-]
m_0	inverse slope in the range $N \leq 5 \cdot 10^6$; 3 for welded joints	[-]
n_i	number of stress cycles of the i^{th} stress range	[-]
t_w	wall thickness of the tower	[m]
b	joint width	[m]
l	overlap length	[m]
t_t	top adherend thickness	[m]
t_b	bottom adherend thickness	[m]
t_a	adhesive thickness	[m]
$f_{v,ad}$	limiting shear strength value of adhesive	[Pa]
k_F	labour cost factor = 1\$/min	[\$/min]
t_{sH}	wall thickness at height H set according to stability check	[m]
t_{fH}	wall thickness at height H set according to fatigue check	[m]
z	height above ground	[m]
I_{turb}	turbulence intensity	[%]
k	shape parameter of the Weibull function	[-]
V_{ref}	reference wind speed average over 10 min	[m/s]
A	category for higher turbulence characteristics	[-]
B	category for medium turbulence characteristic	[-]
C	category for lower turbulence characteristics	[-]
V_{ave}	annual average wind speed at hub height	[m/s]
V_r	Rated hub-height wind speed	[m/s]
P_{rated}	Rated power	[MW]
$P_w(V_{hub})$	weibull probability function	[-]
$P_R(V_{hub})$	rayleigh probability function	[-]

V_{hub}	10-min mean of the wind speed at hub height	[m/s]
V_{ave}	annual mean wind speed	[m/s]
C	scale parameter of the Weibull function	[m/s]
$V(z)$	wind speed at the height z	[m/s]
$V_N(z)$	the expected extreme wind speed with a recurrence period of N years	[m/s]
V_{gust}	hub height gust magnitude	[m/s]
D	rotor diameter	[m]
V_{in}	cut in wind speed	[m/s]
V_{out}	cut out wind speed	[m/s]
V_r	rated wind speed	[m/s]
F_x	rotor thrust	[N]
M_y	tilting moment	[Nm]
M_z	torsional moment	[Nm]
N_d	design axial force	[N]
M_d	design bending moment	[Nm]
N_{el}	euler force for a cantilever beam	[Nm]
R	tower radius	[m]
S	stability check value	[-]
N_i	number of cycles to failure	[-]
D_o	outer diameter of the tower section	[m]
D_i	inner diameter of the tower section	[m]
$I_{\text{tower section}}$	moment of inertia of the tower section	[kg·m ²]
P	applied load	[N]
E	adherend modulus	[Pa]
G_a	adhesive shear modulus	[Pa]
L_{wi}	circumference of the can	[m]
V_{total}	total volume of two sections getting welded	[m ³]
K_{cir}	longitudinal weld cost	[\$]

Greek symbols

Γ	gamma function	[-]
σ_1	fixed turbulence standard deviation	[-]
Λ_1	turbulence scale parameter, according to the equation 3-1	[-]
γ_f	partial safety factor for load	[-]
γ_m	partial safety factor for material	[-]
γ_n	partial safety factor for consequences of failure	[-]
σ_{\max}	maximum upper stress of a stress cycle	[N/mm ²]
σ_{\min}	maximum lower stress of a stress cycle	[N/mm ²]
$\Delta\sigma_R$	fatigue strength reference value of S-N curve at $2 \cdot 10^6$ cycles of stress range	[N/mm ²]
$\Delta\sigma$	stress range	[N/mm ²]
$\gamma_{M,adh}$	material factor for adhesive bonded joints	[-]
σ_{sheet}	stress in the sheet due to axial loads and bending moments	[N/mm ²]
κ	number of element to be assembled	[-]
Θ_w	difficulty factor expressing the complexity of the assembly	[-]
ρ	density of the material	[kg/m ³]
τ_{avg}	average shear stress	[Pa]

Acronyms

DLC	Design Load Case
DOWEC	Dutch Offshore Wind Energy Converter
ETM	Extreme Turbulence Model
EOG	Extreme Operating Gust
EWM	Extreme Wind Speed Model
FEA	Finite Element Analysis
FEM	Finite Element Model
FOS	Factor of Safety
GH	Garrad Hassan
GL	Germanischer Lloyd
IEC	International Electrotechnical Commission
MCA	Multi Criteria Analysis
NREL	National Renewable Energy Laboratory
NWP	Normal Wind Profile
NTM	Normal Turbulence Model
PPI	Producer Price Index
SLJ	Simple Lap Joint
ULS	Ultimate Limit State

1. Introduction

The increasing prices of fossil fuels during the last decades have sparked increasing interest and investments in wind power plants to expand their share of electricity production and improve wind turbines technology with new and more economical inventions and sustainable solutions. In 2009 a total of 37,500MW of new wind energy capacity was installed worldwide - an increase in 31 percent compared to the previous year. By 2030, the International Energy Agency (IEA) considers just under 1,100,000 MW of global wind energy capacity to be a real possibility [1].

A tubular steel tower represent up to 20% of the total turbine costs [2]. The wind industry installed over 5,000 commercial-scale wind turbines in 2008 in USA, which translates into 15,000 tower sections and 2.4 million bolts in tower flange. By 2011 the number of tower flange splice bolts required annually will likely reach 5 million [3]. The optimized design of a tower in terms of tower diameter and wall thickness may therefore lead to substantial savings with regard to the costs and the use of materials.

One important aspect of the design of a tubular steel tower in a wind turbine is the joints between the tower's sections and among the cans. While the loads acting on a tower are highly dynamic, the currently used solutions (flanges, bolts and welding) are intrinsically prone to fatigue and thus impose limitations on the design and impair the overall efficiency. Also, the flanges are expensive, need lots of machining and long delivery time. This gives an opportunity to look for a new alternative way of assembling the tower. The proposed solution in this study is adhesive bonded joints (or also termed as adhesive bonded connections).

The major application of adhesive in a wind turbine industry is bonding the internal wind turbine blade structure. In this study, the focus is on the tower, which is designed according to fatigue failure of the welded connections. These connections have high risk of fatigue failure leading to the thick tower wall. However, there is possibility that if the tower cans are bonded with adhesive, the fatigue damage can be reduced. This is because adhesive bonded joints are less sensitive to fatigue [4]. Thus, there is opportunity for the wall thickness to be reduced and save material in the cans along the tower.

1.1. Preliminary research

This thesis is the next step, after what was done in the system integration project-II "Adhesive Bonded Wind Turbine Assemblies" [5]. In this project, an alternative method of assembly was proposed to bond the parts together with adhesives instead of welded and bolted connections. All the existing connections in a wind turbine were also reviewed. These connecting locations were considered as the potential areas for adhesive bonding. Different drivers were set to eliminate some connections. The disassembly property of the adhesives was set as a major driver. Next, a multi criteria analysis (MCA) was applied to find the optimal potential area to be bonded with adhesive. The MCA concluded that 'the foundation to tower base connection' was the best optimal potential location for adhesive bonding. The second best possible connection was the 'circumferential welding of the top can'.

1.2. Objective

The current work aims to study the possibility of using adhesive bonded joints for improving the tower design. The focuses are on the following two tasks:

- 1) To assess the potential cost benefits of using adhesive, instead of flanges, for bonding a tower base with a foundation section.
- 2) To investigate the thickness optimization of entire tower when the cans are bonded circumferentially using adhesives instead of welds.

1.3. Approach

The first step in the research will be extensive literature study about adhesive bonding and the design procedure of a wind tower. A reference model of 3MW wind turbine is taken in GH Bladed [6]. Extreme and dynamic loads will be calculated according to IEC standard [7]. The tower will be redesigned after the design checks for stability and fatigue strength of the tower. The natural frequencies of the tower will be checked to avoid resonance

The next step will be designing an adhesive bonded joint between the tower base and the foundation. A simple Volkersen model [8] will be implemented to optimize the overlap length, adhesive thickness and wall thickness. A detailed analysis of bonding each tower can with adhesive, instead of welding will be carried out. This is to check for the feasibility of reducing the tower thickness. Finally the adhesive bonded connection will be compared economically with the flanged and welded connections.

1.4. Report layout

The layout of the report will follow the steps involved in the approach described above. In chapter 2, detailed configurations of a tubular steel tower with their definitions will be discussed. Chapter 3 details the design of a reference tower in a Bladed model of 3MW wind turbine with the design checks for stability and fatigue. It also includes the flange and the foundation geometry and wind conditions for the load calculations. Chapter 4 introduces the relevant knowledge about adhesive bonding and the factors influencing the joint strength with the guidelines to increase it. Chapter 5 presents a design procedure for an adhesive bonded joint with the selection of joint type, analytical models chosen, determination of loadings and adhesive properties. The implementations of the design procedure and the results for both of the objectives are given in Chapter 6 and Chapter 7. These two chapters also include the detailed cost analysis for the bonded joints and cost comparison with the existing design. Finally, the conclusions and recommendations are discussed in Chapter 8.

2. Tubular steel tower

2.1. Introduction

A wind turbine tower supports the nacelle and the rotor at the top of a wind turbine. It provides rotor a necessary elevation up to a level where higher and more uniform speeds are found. Most modern turbines installed onshore are multi-megawatt machines with nominal outputs between 1.5MW and 3MW. Their rotor diameters range between 70m and 100m. Nowadays, tubular towers dominate the wind turbine market as they are a prominent compromise between economical, aesthetical and safety considerations.

This section will deal primarily with the detailed configurations of a tubular steel tower. Different parts of the tower will be defined. These definitions will be used throughout the report.

2.2. Welded tubular steel tower

A wind turbine tower typically comprises of a number of tubular steel tower segments (or rings) mounted on top of each other, where each tower segment is made of different conical subsections (or cans) as shown in Figure 2-1. Each conical subsection is a steel plate rolled into a slightly tapered circular shape and welded with a seam lengthwise to constitute a closed ring, plus a circumferential welding seam to connect to the next can of the tower's ring [9]. The cans are manufactured and welded in the workshop and finally assembled on site.

Tubular steel towers are currently available for the multi-megawatt turbines with hub height up to about 100m. The towers are designed as truncated cones with their diameter increasing towards the base in order to increase their strength and at the same time to save material. The wall thickness of the tower varies among the segments usually decreasing from the base to the top. The wall thickness can vary from less than 10mm for the upper sections to 40mm for the lower sections [10]. In order to meet the strict requirements of the fatigue design, all welds are designed as full penetration butt welds of high quality [11]. Transportation constraints impose limits on the diameter and length of the elements. Typically the diameter should be lower than about 4.3m to pass under bridges [12] and the elements length ranges between 20m and 30m.

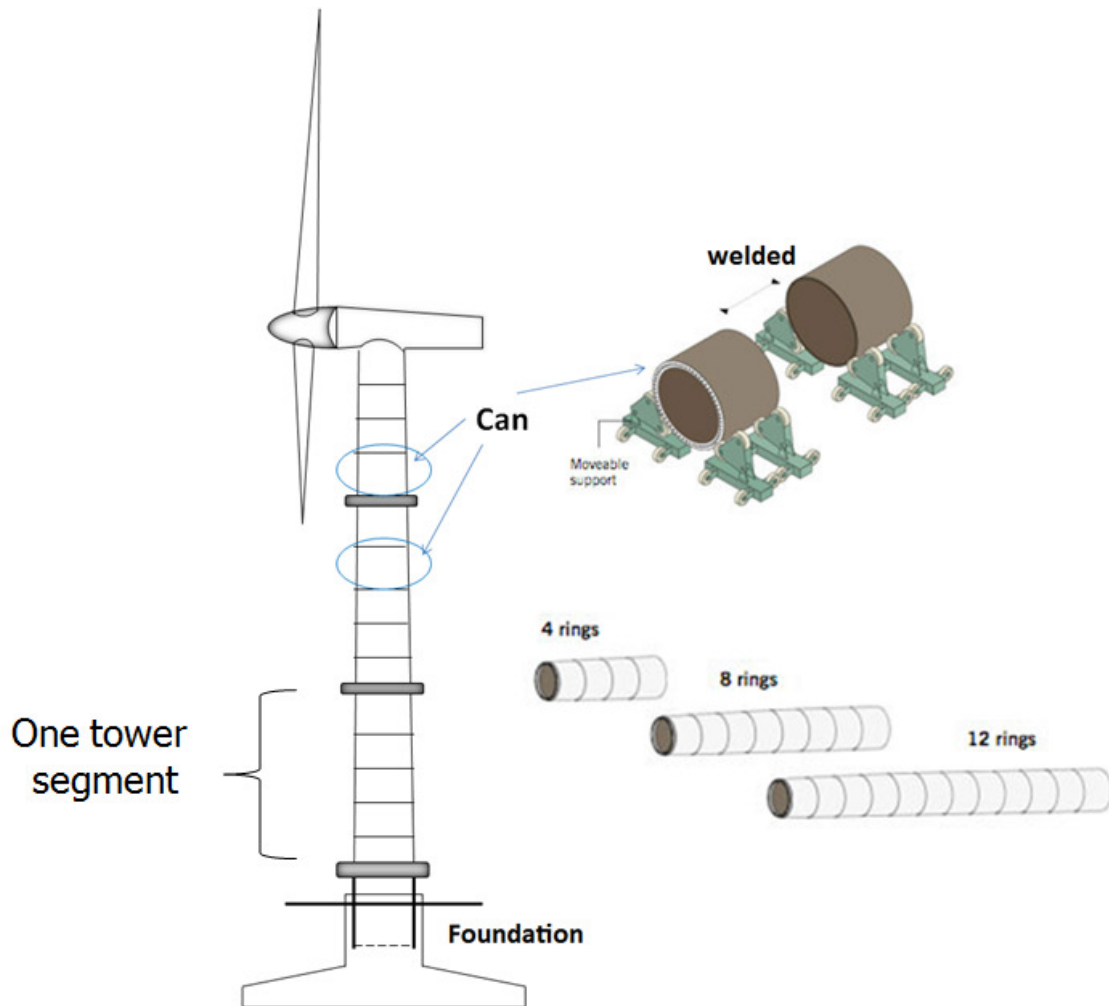


Figure 2-1: Construction of a tubular steel tower from welded cans [13] → flanged tower segment → complete tower

2.3. Bolted ring flange connections

The tower segments from the factory assembly are transported to the erection site, where the segments are connected by ring flanged joints as shown in Figure 2-2. A combination of welding and preloaded bolting is employed to join the flanges and the tower segments. The flanges are welded to the either end of the tower segment in the factory itself. The flange width is determined by the bolt size and varies between 100mm and 300mm. The thickness depends on the required stiffness and is typically more than 100mm for a bottom flange. The bolts diameters are typically M36 to M42 but can go up to M48 [12].

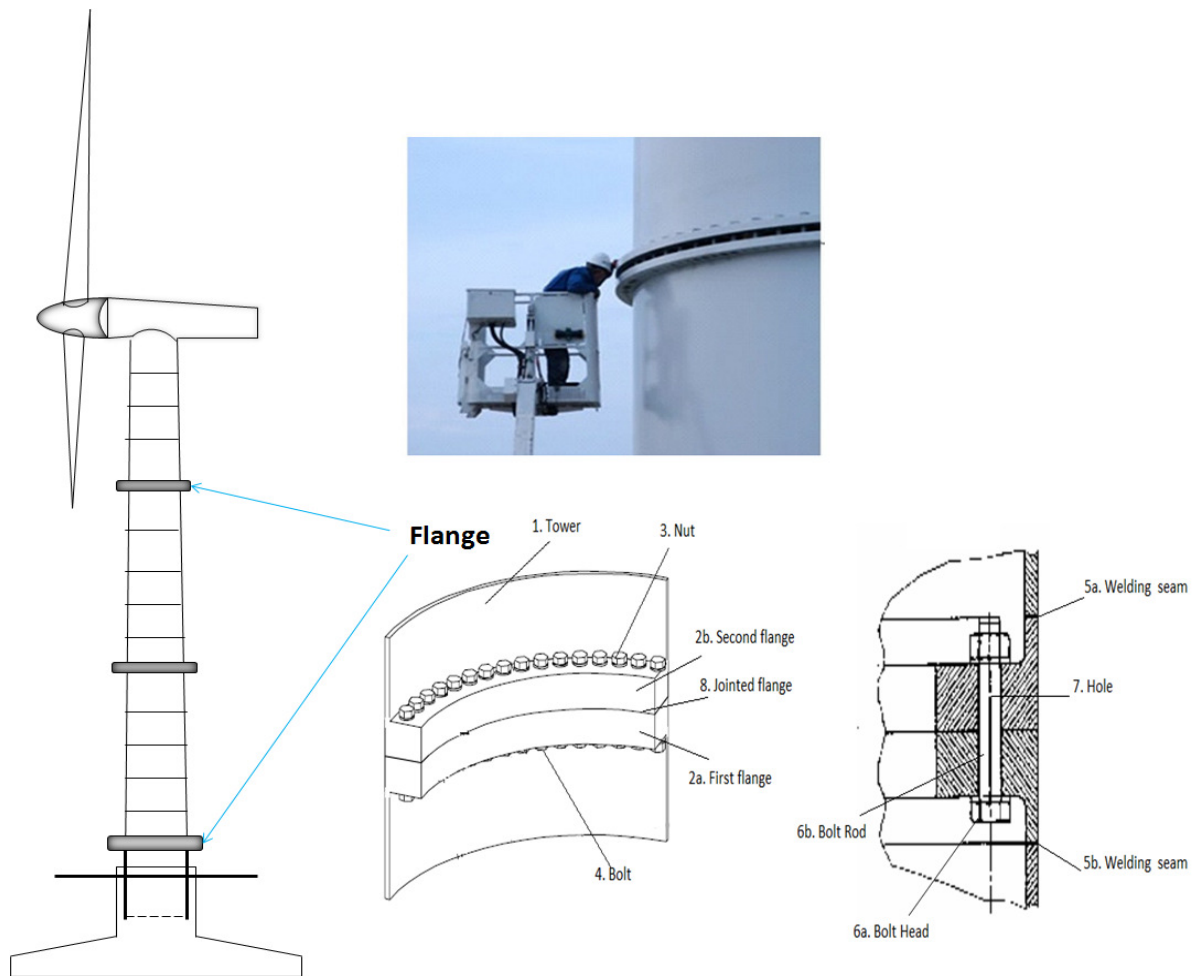


Figure 2-2: Bolted ring flange connection [14]

The fabrication of a flange is very costly and takes a long delivery time. The flanges can be forged or more economically rolled from flat profiles and welded. They are then machined to the required dimensions and welded to the tubes. Welding may introduce additional geometrical imperfections and if the tolerances are not met for the welded flange, a second machining operation is necessary. To ensure perfect alignment of paired flanges with the bolts, the holes are drilled using CNC machines [15]. Flange flatness deviation should be within the tolerance limit to avoid the influence on the resistance.

The design of the flange is often governed by the fatigue resistance. Fatigue resistance of bolts is intrinsically low due to stress concentrations introduced at the thread foot. Depending on the fabrication process and method used to derive the fatigue loads they are ranked in detail categories¹ 36, 50 or 71 [15].

¹ Fatigue strength reference value of S-N curve at 2 million cycles of stress range

3. Design of a reference tower with flanges and welds

This chapter starts with the explanation for the purpose of designing a reference tower. The factors governing its design are also discussed. It also includes the tower preliminary design procedures, reference wind turbine model in GH bladed, the flange and foundation geometry, wind conditions and the design loads. The design checks to be performed are discussed briefly along with the S-N curve for the typical welds in a tower. The chapter concludes with the designed wall thicknesses along the tower height.

3.1. Introduction

The current assembly solutions for a wind turbine tower are the flanged and the welded connections. The new assembly solution proposed in this research work is the adhesive bonded joint. A reference tower is needed for the cost analysis of the existing and the proposed solution. In this chapter, a preliminary design of the reference tower is presented with a focus on the flanged and welded connections. The design of tower connections is often governed by the fatigue resistance. The design of the flange and the tower wall thickness is both independent. The flange design is dependent on the bolt, whose low fatigue resistance leads to oversized flange. Whereas, dimensioning of the wall thickness is based on the fatigue resistance of the 'welds between the cans' and 'flange welding to the cans'. This leads to conclusion that the tower wall is to be designed with the focus only on the welded connections. Therefore, the flange has not been designed in this report but for comparison, a reference flange has been taken from the Vestas V90 turbine [16].

3.2. Tower design procedure

An overview of the design procedure with the main design checks is given on Figure 3-1. The first step is to input the turbine and wind data for determining the extreme and fatigue loads on the turbine. The tower geometry is then defined from an existing tower². To make the design procedure simple, the tower will be assigned a linearly varying diameter throughout the entire design, with the base and top diameter from an existing tower. Only the thickness will be optimized according to all design checks. The natural frequencies of turbine and tower must be adjusted to avoid resonance. Accordingly the wall thicknesses are increased or decreased.

Using the extreme loads, it is checked whether the tower will resist failure due to buckling or yielding. Subsequently, a fatigue check is performed for 20 years of turbine operation. If the extreme load checks and the fatigue check indicate that the wall thickness is insufficient, the wall thickness must be increased. If both of the checks show that the wall thickness is significantly larger than required, the wall thickness should be reduced and the buckling and fatigue damage should be re-assessed. After optimizing the wall thickness, the natural frequency of the support structure should be re-assessed.

² The existing tower gives the details for tower sections, base and top diameter, bolts specifications and flanges to be directly taken for the final design of tower (also shown in Figure 3-4).

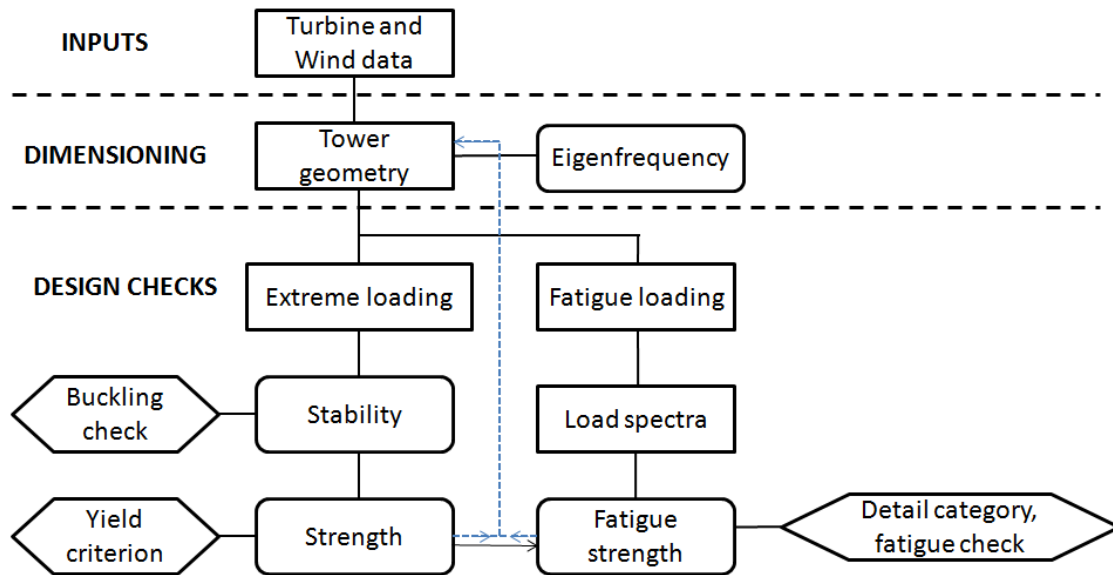


Figure 3-1: Overview of the design procedure for a wind turbine tower

3.3. Turbine configuration

3.3.1. Turbine model in GH Bladed

A reference Bladed model of Vestas V90, 3MW wind turbine is taken for the design of the wind turbine tower. The blade is designed with the DU97W300 airfoil model as shown in the Figure 3-2. The Vestas V90 Bladed model is not validated, however, it gives the loads in the correct order of magnitude [17].

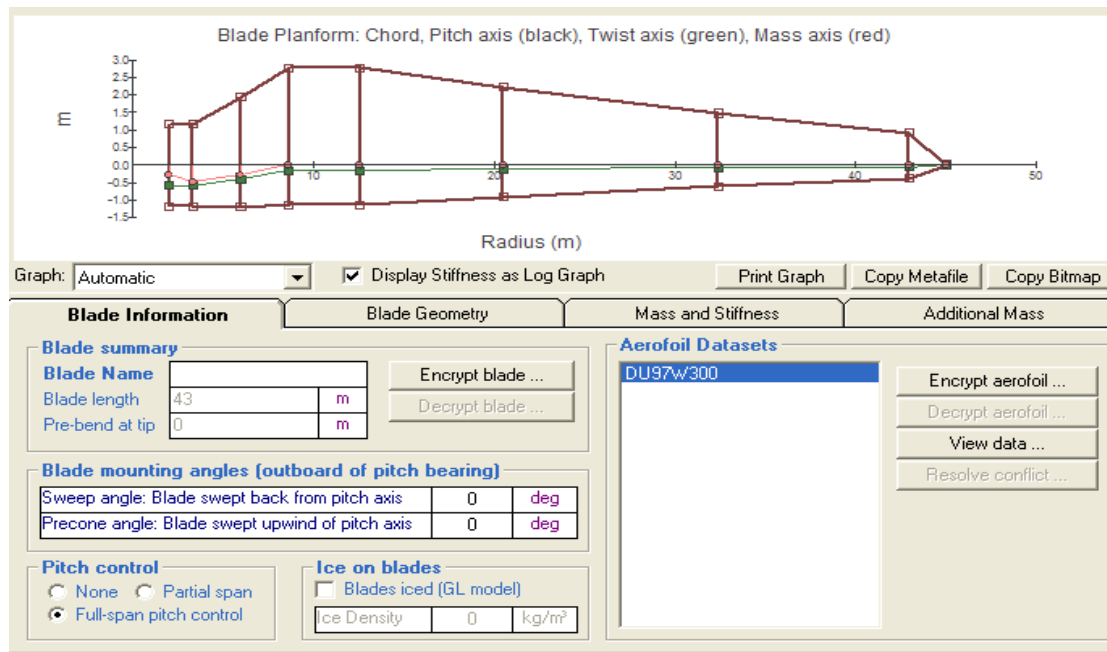


Figure 3-2: Blade configuration in GH Bladed

The turbine and rotor details with component's mass data have been shown in the Figure 3-3. The Bladed version 3.85 has been used for the tower design, loads calculation and the fatigue analysis.

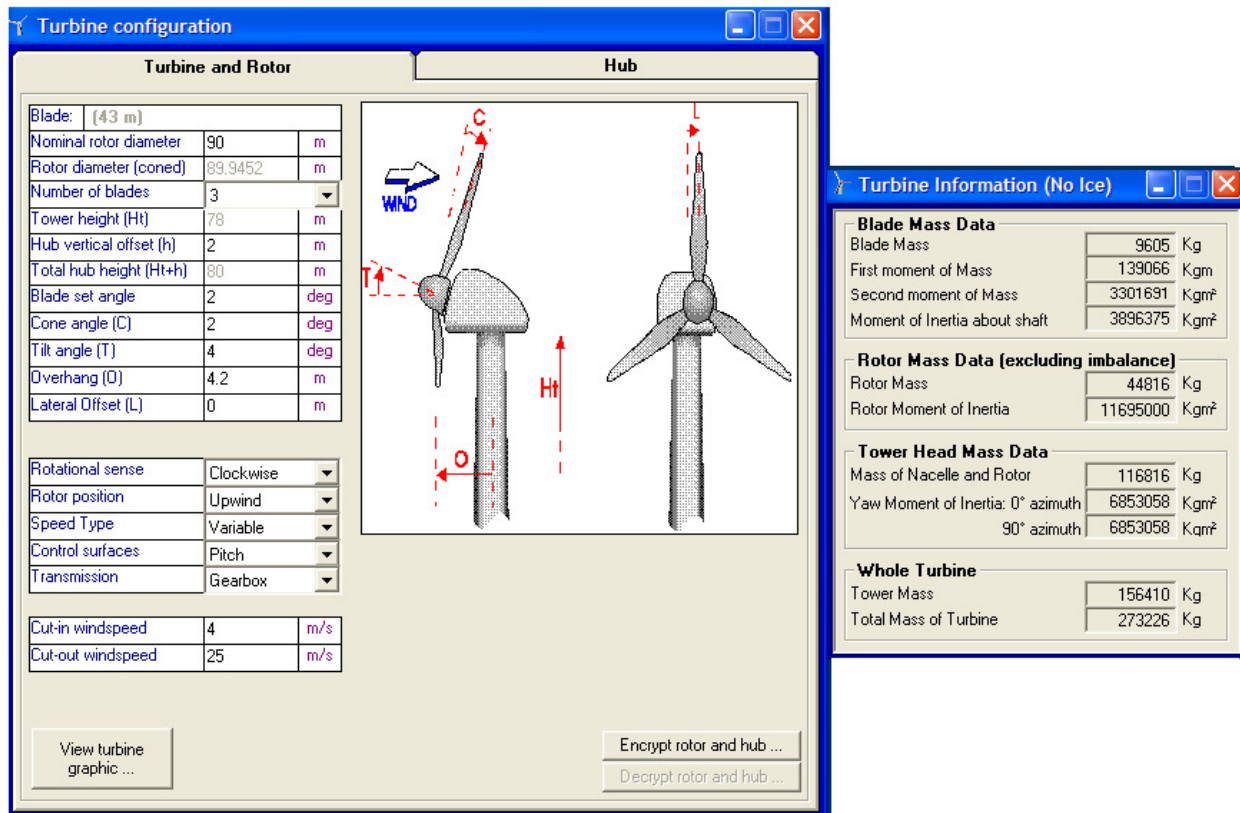


Figure 3-3: Turbine configurations and components mass details

3.3.2. Tower properties

The tubular shaped tower is assumed to have a linear diameter and thickness distribution. This is a necessary simplification in the beginning because more detailed (non-linear) specifications of the eventual structure are not available. The tower base diameter (4.19m) and top diameter (2.316m) are taken from the Vestas V90 turbine [16]. The details of the existing tower sections along with the flanges and bolts specification are presented in Figure 3-4. The thickness distribution along the tower will be dimensioned later in this project according to design checks. The effective mechanical steel properties of the tower are based on the DOWEC study [18]. The Young's modulus, the shear modulus and the density of the steel are taken as 210 GPa, 80.8 GPa, 8,000 kg/m³ respectively. The density of 8,000 kg/m³ is meant to be an increase above steel's typical value of 7,850 kg/m³ to account for paint, bolts and welds that are not accounted for in the tower thickness data.

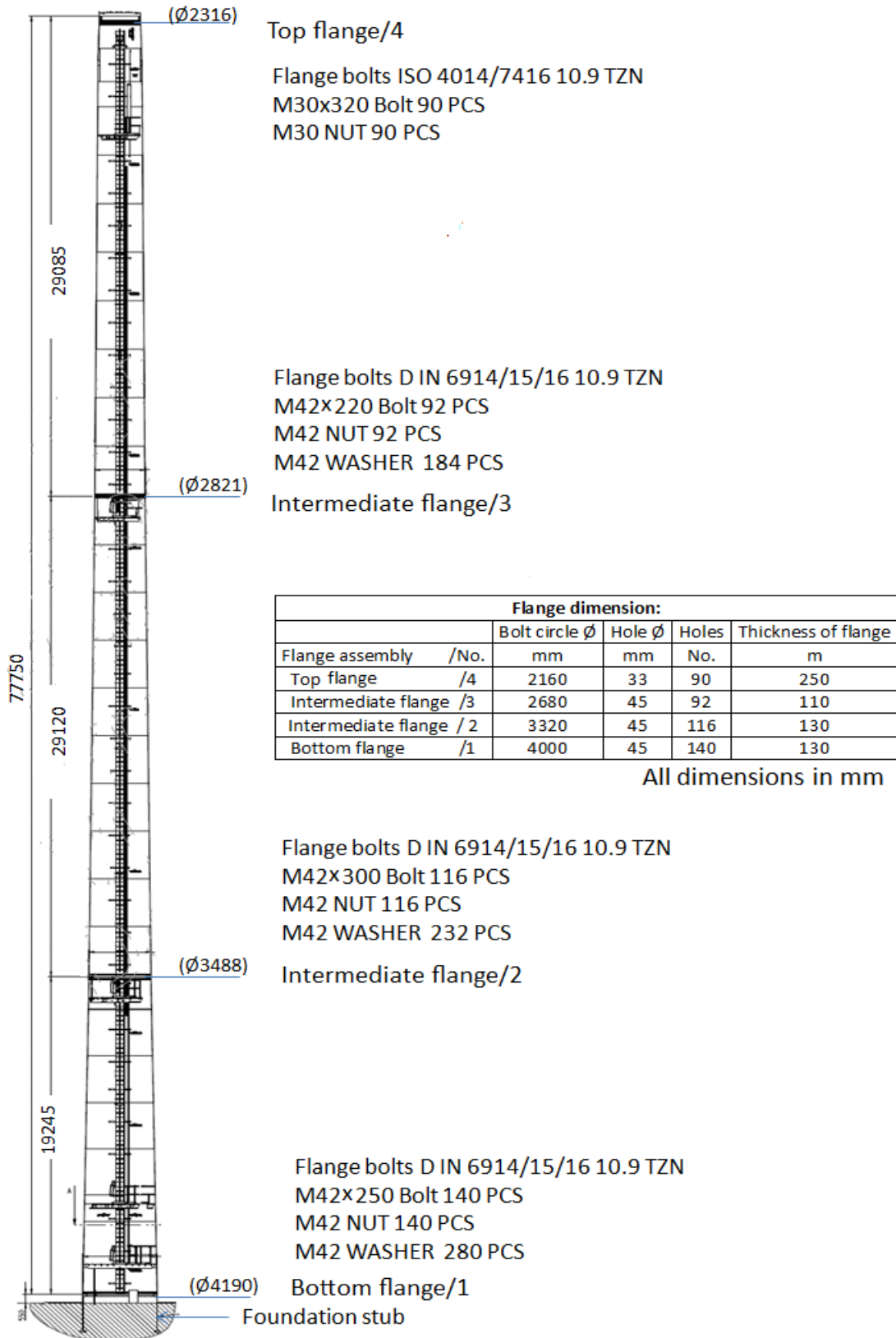


Figure 3-4: Tower design, Vestas 3MW, Onshore [19]

3.3.3. Foundation geometry

The foundation system considered in this project is the cylindrical structural element (embedded tower stub) as shown in Figure 3-5 with its specifications. The cylindrical structural element is set on the blinding layer and precisely aligned with the adjusting bolts. Once the foundation is completed, the tower is flanged together with the foundation section.

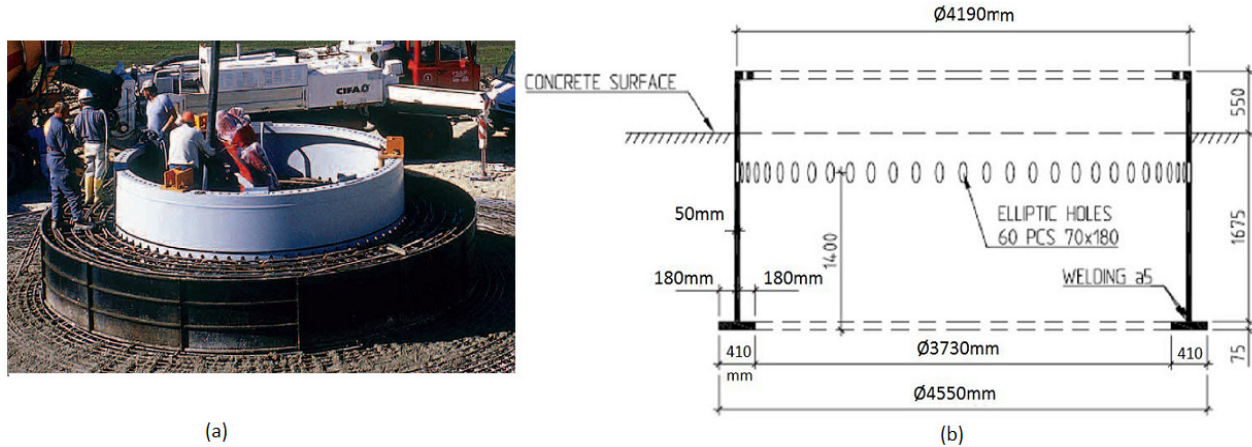


Figure 3-5: (a) Cylindrical structural element [20] and (b) its geometry details

3.3.4. Flange geometry at the tower base

The reference flange at the tower base and the foundation has been dimensioned similar to Vestas V90 flange. The flange's geometry has been shown in Figure 3-6. In the Bladed, the flanges are modelled as point masses as shown in Figure 3-7 (marked with circle), but not by an increase in wall thickness.

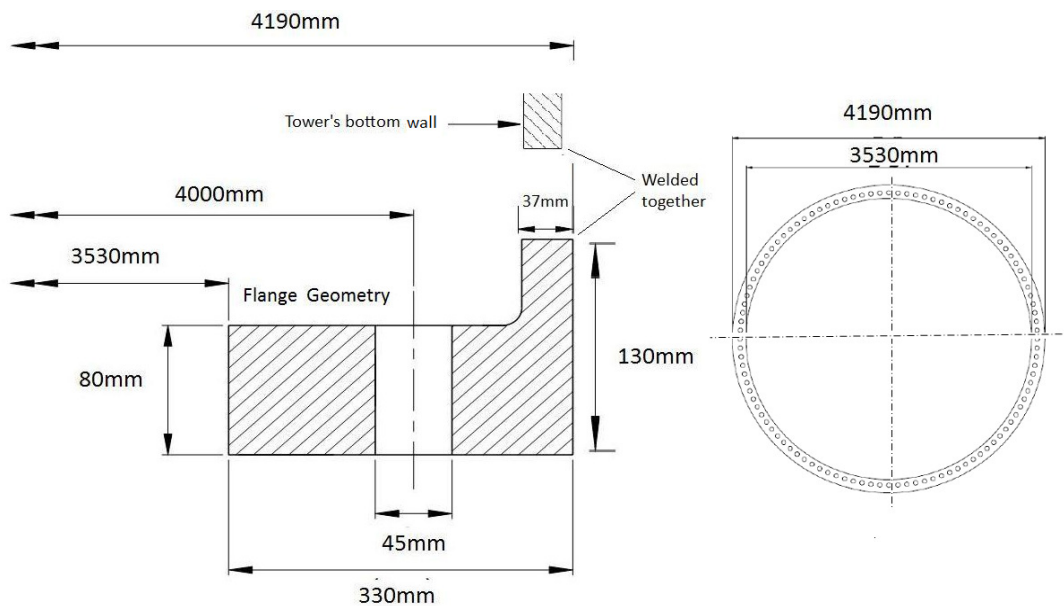


Figure 3-6: Design of a flange which is welded to the foundation and tower base

3.3.5. Tower input in GH Bladed

The tower diameter is assumed to be linearly tapered from tower base (4.19m) to tower top (2.316m) as shown in the table of Figure 3-7. The diameter will not be optimized throughout the design procedure. To begin with the wall thickness optimization, the thickness has been varied linearly from 30mm at the base to 14mm at the top. At the top, a flange with 250mm thickness has been welded to raise the tower height up to 78m. The addition of hub vertical offset (2m) brings the hub height to 80m. The input specification for the structural properties of tower is shown in the Figure 3-7.

The structural damping³ of the tower is assumed to have a damping of 1% of critical damping⁴ in all modes of the tower (without the top mass present), which corresponds to the values used in the DOWEC study [18].

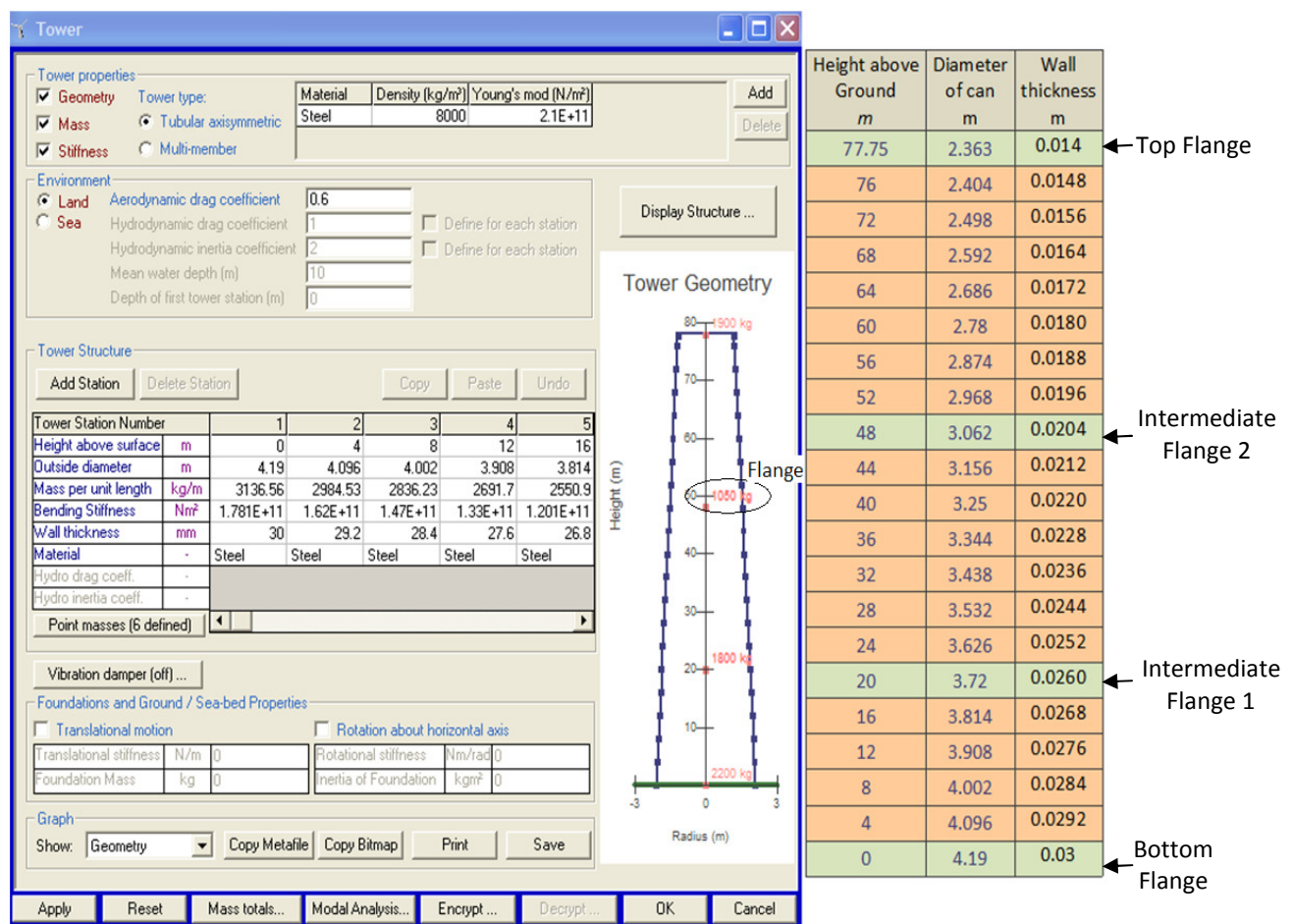


Figure 3-7: The Bladed input of initial tower properties along with the flanges as point masses

³ The structural damping of a system is usually defined as the percentage decrease of two peaks of an oscillation and this value is called as the logarithmic damping decrement δ .

⁴ Critical damping (ζ) is the amount of damping at which system returns to equilibrium as quickly as possible without oscillating. ($\zeta = \delta/(2\pi)$)

3.4. IEC class and Wind conditions

IEC Class

Wind turbine classes are defined in terms of wind speed and turbulence parameters as shown in Table 3-1, according to IEC61400-1 edition 3 [7]. The load calculations are performed according to wind class IA in this project. The design lifetime for wind turbine is 20 years.

Table 3-1: Basic parameters⁵ for wind turbine classes [7]

Wind turbine class	I	II	III	S
V_{ref} (m/s)	50	42,5	37,5	Values specified by the designer
A I_{ref} (-)	0,16			
B I_{ref} (-)	0,14			
C I_{ref} (-)	0,12			

Where,

V_{ref} is the reference wind speed average over 10 min

A designates the category for higher turbulence characteristics

B designates the category for medium turbulence characteristic

C designates the category for lower turbulence characteristics

I_{ref} is the expected value of the turbulence intensity at 15 m/s

General information

The chosen location for the wind turbine is onshore. The reference turbine considered in this project is of the type Vestas V90 with three blades of diameter each 90m. The wind conditions for the load calculations are presented in Table 3-2.

Table 3-2: Design load case parameters

Rated hub-height wind speed, V_r	12.3m/s
Wind class	IEC I _A
Air density	1.225 kg/m ³
Characteristic turbulence intensity at 15 m/s, I_{15}	16%
Hub height	80m
Annual average wind speed at hub height, V_{ave}	10m/s
Reference wind speed average over 10 min, V_{ref}	50m/s

⁵ The parameter values apply at hub height

Wind conditions are the primary external conditions affecting the structural integrity. The wind regime for load and safety considerations is divided into the normal wind conditions, which will occur frequently during normal operation of a wind turbine, and the extreme wind conditions that are defined as having a 1-year or 50-year recurrence period.

The wind conditions include a constant mean flow combined, in many cases, with either a varying deterministic gust profile or with turbulence. In all cases, the influence of an inclination of the mean flow with respect to a horizontal plane of up to 8° is considered. The expression turbulence denotes variability in the wind speed from 10 min. averages.

The longitudinal turbulence scale parameter, Λ_1 , at hub height z is given by

$$\Lambda_1 = \begin{cases} 0.7z & z \leq 60m \\ 42m & z \geq 60m \end{cases} \quad 3-1$$

Based on the normal and extreme wind conditions, the following models are defined:

- Normal wind models
 - Wind speed distribution
 - Normal Wind Profile (NWP)
 - Normal Turbulence Model (NTM)
- Extreme wind models
 - Extreme Wind speed Model (EWM)
 - Extreme Operating Gust (EOG)
 - Extreme Turbulence Model (ETM)

The turbulent variation in wind speed has been modeled using a one component Von Karman model with a characteristic turbulence intensity set according to the Normal Turbulence Model (as defined in IEC 61400-1 edition 3).

In the following paragraphs, the wind models are described for the chosen wind class IA according to IEC standard.

Wind speed distribution

The wind speed distribution at the site is significant for the wind turbine design, because it determines the frequency of occurrence of the individual load components. The wind speed distribution is given by the probability density function, which is used to describe the distribution of wind speeds over an extended period of time. The distribution function for most sites is expressed by Weibull distribution as:

$$P_w(V_{hub}) = 1 - \exp [-(V_{hub}/C)^k] \quad 3-2$$

$$\text{where: } V_{ave} = \begin{cases} C\Gamma(1 + \frac{1}{k}) \\ C\sqrt{\pi}/2, \text{ if } k = 2 \end{cases}$$

For design in the standard wind turbine classes, the Rayleigh distribution shall be taken for the load calculations. The Rayleigh function is identical to the Weibull function if $k = 2$ is selected and is given by

$$P_R(V_{hub}) = 1 - \exp [-\pi(V_{hub}/2V_{ave})^2] \quad 3-3$$

Where

$P_w(V_{hub})$	is Weibull probability function
$P_R(V_{hub})$	is Rayleigh probability function
V_{hub}	is 10-min mean of the wind speed at hub height [m/s]
V_{ave}	is the annual mean wind speed [m/s] = $0.2V_{ref}$
C	is the scale parameter of the Weibull function [m/s]
k	is the shape parameter of the Weibull function
Γ	is the gamma function

The Weibull wind speed distribution at hub height for annual mean wind speed of 10m/s and Weibull shape factor 2 is shown in Figure 3-8.

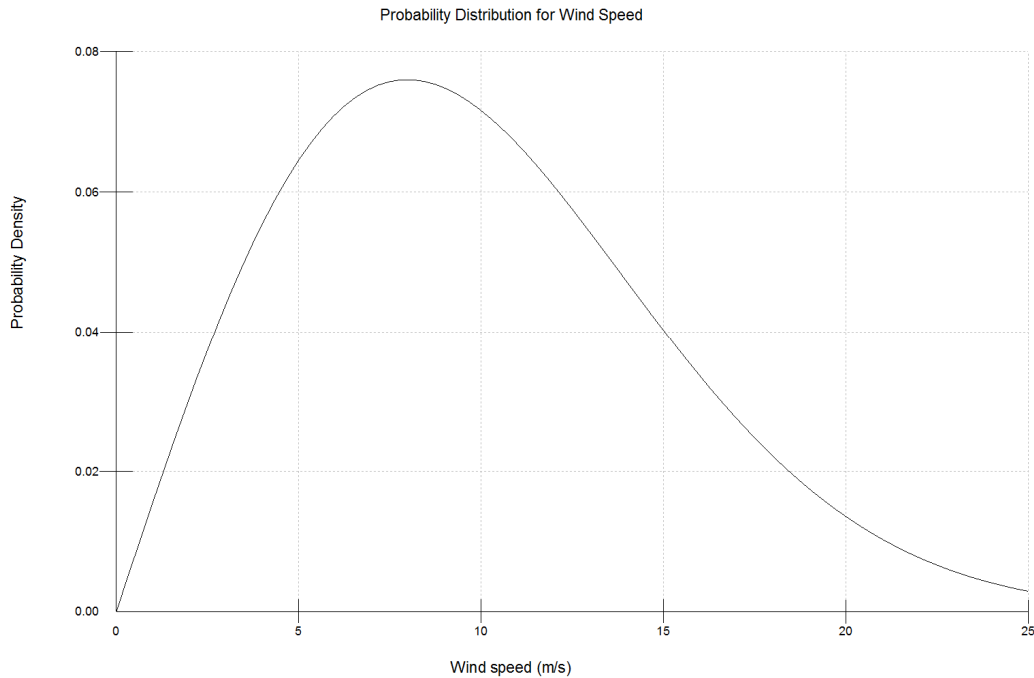


Figure 3-8: Wind speed distribution from GH Bladed

Normal Wind Profile Model (NWM)

The wind profile, $V(z)$ denotes the average wind speed as a function of height z , above the ground. The assumed wind profile is used to define the average vertical wind shear across the rotor swept area.

$$V(z) = V_{hub} \left(\frac{z}{z_{hub}} \right)^{0.2} \quad 3-4$$

Where

$V(z)$ is wind speed at the height z [m/s]

z is height above ground [m]

Normal Turbulence Model (NTM)

For the normal turbulence model, the representative value of the turbulence standard deviation, σ_1 , shall be given by the 90 % quantile for the given hub height wind speed. This value for the standard wind turbine classes shall be given by

$$\sigma_1 = 0.16 \cdot (0.75 \cdot V_{hub} + 5.6) \quad 3-5$$

The turbulence intensity is given by

$$I_{turb} = \frac{\sigma_1}{V_{hub}} \quad 3-6$$

Extreme Wind Speed Model (EWM)

The EWM can be either a steady or a turbulent wind model. The wind models are based on the reference wind speed, V_{ref} , and a fixed turbulence standard deviation, σ_1 . For the turbulent extreme wind speed model, the 10 min average wind speeds as functions of z with recurrence periods of 50 years and 1 year, respectively, are given by

$$V_{50}(z) = V_{ref} \cdot \left(\frac{z}{z_{hub}} \right)^{0.11} \quad 3-7$$

$$V_1(z) = 0.8 \cdot V_{50}(z) \quad 3-8$$

Where

$V_N(z)$ The expected extreme wind speed (averaged over 10 minutes), with a recurrence period of N years. V_1 and V_{50} represent 1 and 50 years.

The longitudinal turbulence standard deviation⁶ is defined as

$$\sigma_1 = 0.11 \cdot V_{hub} \quad 3-9$$

Extreme Operating Gust (EOG)

The extreme operating gust EOG50 is also known as the ‘Mexican hat’. It is the ‘worst gust’ to be expected during operation with a recurrence period of 50 years. The hub height gust magnitude V_{gust} for the wind turbine class A is given by the following relationship:

⁶ The turbulence standard deviation for the turbulent extreme wind model is not related to the NTM or ETM

$$V_{gust} = \min \left\{ 1.35(V_{e1} - V_{hub}); 3.3 \left(\frac{\sigma_1}{1 + 0.1 \cdot \left(\frac{D}{\Lambda_1} \right)} \right) \right\} \quad 3-10$$

Where

σ_1 is given in equation 3-5

Λ_1 is the turbulence scale parameter, according to the equation 3-1

D is the rotor diameter

The wind speed as a function of height and time is defined as following:

$$V(z, t) = \begin{cases} V(z) - 0.37 \cdot V_{gust} \cdot \sin\left(\frac{3\pi t}{T}\right) \left(1 - \cos\left[\frac{2\pi t}{T}\right]\right) & \text{for } 0 \leq t \leq T \\ V(z) & \text{otherwise} \end{cases} \quad 3-11$$

Where

$V(z)$ is defined in equation 3-4

T is 10.5s

As an example, for our case at $V_{hub} = 25\text{m/s}$, the extreme operating gust is shown in Figure 3-9

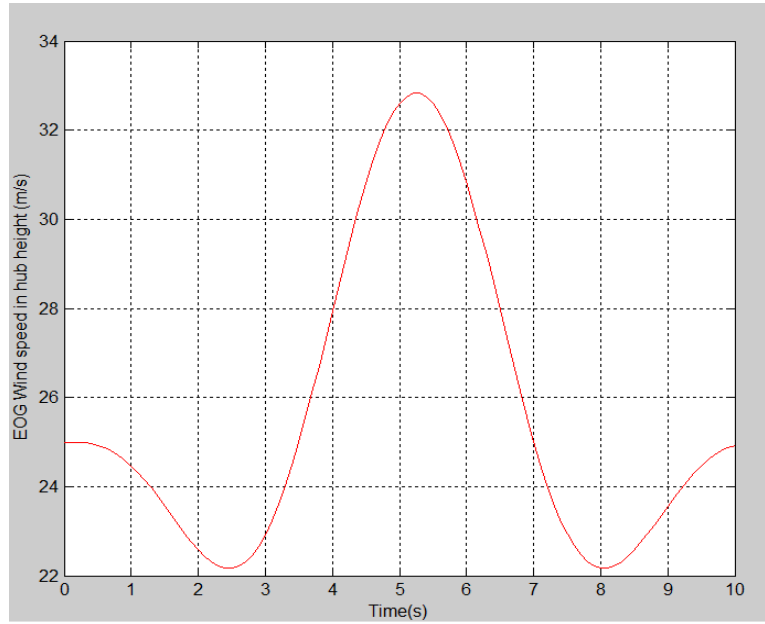


Figure 3-9: Extreme operating gust at $V_{hub} = 25\text{m/s}$

Extreme Turbulence Model (ETM)

The extreme turbulence model uses the normal wind profile model given by equation 3-4 and turbulence with longitudinal component standard deviation given by

$$\sigma_1 = c \cdot I_{ref} \left(0.072 \cdot \left(\frac{V_{ave}}{c} + 3 \right) \cdot \left(\frac{V_{hub}}{c} - 4 \right) + 10 \right); c = 2\text{m/s} \quad 3-12$$

3.5. Design loads

3.5.1. Static loads

The main loads acting on a wind turbine tower are:

- the self weight of the different elements, including the rotor, the nacelle and all the machinery,
- the actions of the wind (thrust and drag) on the blades, and,
- the wind pressure on the tower.

The static design loads usually are derived from information of the wind speed and its direction; with help of simplified models including the geometrical properties of the tower. The static loads are calculated for the Design Load Cases (DLCs) specified in the IEC standard. The Table 3-3 shows the loads cases that are analyzed in this project for extreme loads calculation on the tower.

Table 3-3: Extreme load cases descriptions

Design situation	DLC	Wind condition	Other conditions	Partial safety factor
Power production	1.3	ETM $V_{in} < V_{hub} < V_{out}$		N
Power production plus occurrence of fault	2.3	EOG50 $V_{hub} = V_r \pm 2m/s$ and V_{out}	Loss of electrical grid connection	A
Normal shutdown	4.2	EOG50 $V_{hub} = V_r \pm 2m/s$ and V_{out}		N
Emergency shutdown	5.1	NTM $V_{hub} = V_r \pm 2m/s$ and V_{out}		N
Idling	6.1	EWM 50-year recurrence period		N
Abbreviations: V_{in} - Cut in wind speed V_{out} - Cut out wind speed V_r - Rated wind speed EOG50 - Extreme operating gust with 50 years of recurrence period N - Normal A - Abnormal				

Partial safety factors for loads have been applied externally to the results of the dynamic simulations. Table 3-4 summarises the safety factors that have been used in each load case.

Table 3-4: Partial safety factors for the load cases

Load case type	Safety factor for loads, γ_f
Abnormal (DLCs 2.3)	1.10
Normal (all other DLCs)	1.35

The associated coordinate system for calculating the extreme loads on a tower, based on GL standard [7], is shown in Figure 3-10.

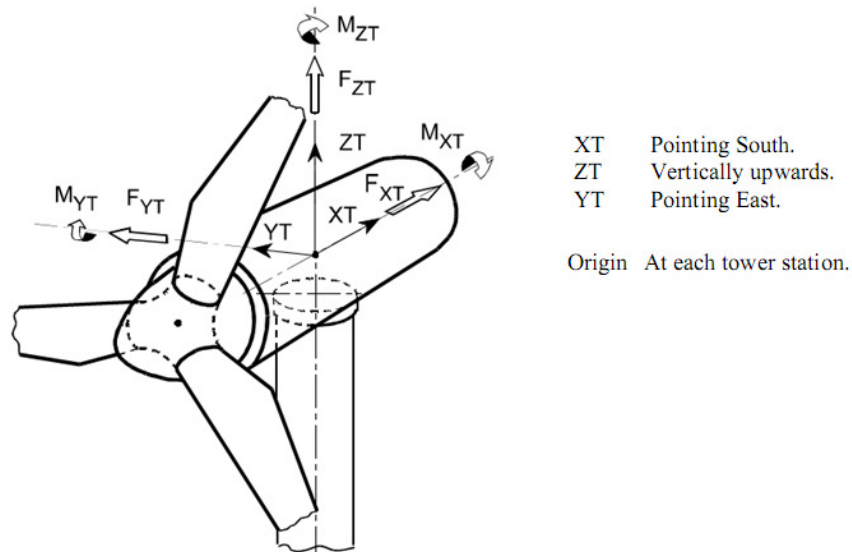


Figure 3-10: Coordinate system for the design loads on a tower [7]

Table 3-5 shows the maximum design loads that result from the each load case at the tower base. The detailed descriptions for each load case calculation are presented in Appendix A. The given loads are the design loads, i.e. they already include a safety factor which is given in the Table 3-4. Due to the long lever arm for the sections of interest in the design of the connections, the extreme shear forces in the x-direction usually correspond to the extreme bending moment. This load case is thus design driving. In the given load Table 3-5, the extreme load corresponds to load case DLC 2.3 which is the simulation of the 50-year-gust in combination with the loss of electrical grid connection.

Table 3-5: Design loads at tower base for different load cases

Load case		Tilting moment M_y (kNm)	Axial load F_z (kN)	Safety factor γ_f
DLC 1.3	Max	59880	-3510	1.35
	Min	3175	-3730	1.35
DLC 2.3	Max	85400	-3010	1.10
	Min	20590	-3065	1.10
DLC 4.2	Max	41600	-2660	1.35
	Min	-27800	-2700	1.35
DLC 5.1	Max	41100	-3560	1.35
	Min	-65400	-3640	1.35
DLC 6.1	Max	32400	-3350	1.35
	Min	-191	-3572	1.35

The thickness of each can has to be optimized in the entire tower during the second phase of this study i.e. bonding with the adhesive. The extreme loads at each tower section are also calculated for the load case DLC 2.3 and are put in Table 3-6.

Table 3-6: Extreme design loads at each welded sections

Welding location	Height H, m	Moment M_y, Nm	Axial load F_z, N
Top Flange	77.75	1.86E+06	-1.34E+06
Plate to plate	76	3.73E+06	-1.36E+06
	72	7.99E+06	-1.40E+06
	68	1.23E+07	-1.43E+06
	64	1.65E+07	-1.48E+06
	60	2.08E+07	-1.52E+06
	56	2.50E+07	-1.58E+06
	52	2.93E+07	-1.64E+06
Flange 2	48	3.37E+07	-1.72E+06
Plate to plate	44	3.81E+07	-1.81E+06
	40	4.24E+07	-1.88E+06
	36	4.68E+07	-1.97E+06
	32	5.12E+07	-2.06E+06
	28	5.55E+07	-2.15E+06
	24	5.98E+07	-2.25E+06
Flange 1	20	6.41E+07	-2.38E+06
Plate to plate	16	6.84E+07	-2.50E+06
	12	7.27E+07	-2.62E+06
	8	7.69E+07	-2.74E+06
	4	8.12E+07	-2.86E+06
Bottom Flange	0	8.54E+07	-3.01E+06

3.5.2. Fatigue loads

Fatigue loads are cyclic loads or repetitive loads, which cause cumulative damage in the materials of the structural components, and which eventually lead to structural failure. Fatigue loads are usually loads well below the load level that will cause static failure, and many load cycles are required before a fatigue failure will take place. This is commonly referred to as high-cycle fatigue. However, if the applied loads are high enough to cause plastic deformation, the fatigue life is considerably shorter and this is termed low cycle fatigue. Fatigue failure takes place by the initiation and propagation of a crack until the crack becomes unstable and propagates fast, if not suddenly, to failure. In some materials a limit is seen, below which fatigue failure does not occur, or fatigue damage progresses at a low enough rate to be considered negligible. This is known as the endurance limit or fatigue threshold.

Design load case

The fatigue loads has been calculated only for the power production case. This is because of the high occurrences of the power production case. The design load case simulated in the Bladed is shown in Table 3-7. The wind is divided in to 6 bins: 0-6, 6-10, 10-14, 14-18, 18-22 and 22-25m/s.

Table 3-7: Fatigue load case description

Design situation	DLC	Wind condition	Other conditions	Partial safety factor
Power production	1.2	NTM $V_{in} < V_{hub} < V_{out}$		1.265

Partial safety factor

The partial safety factors are given in Table 3-8 according to IEC61400-1 edition 3 [7]. The overall safety factor is applied to the cyclic stress range for assessing the increment of damage associated with each fatigue cycle.

Table 3-8: Partial safety factors for fatigue analysis

Type	Partial safety factor
Loads, γ_f	1.0
Material (for welded and structural steel), γ_m	1.1
Consequences of failure (non fail safe structure components), γ_n	1.15
Total ($\gamma_f \cdot \gamma_m \cdot \gamma_n$)	1.265

In general, consideration of the rotor thrust (F_x), tilting moment (M_y) and torsional moment (M_z) is sufficient. The tilting and tower torsional moments can be considered as orthogonal, so that the damages from tensile stresses (from M_y and F_x) can be derived separately from those from shear stresses (from M_z) [21]. As they are usually much smaller, the damages from the shear stresses will be neglected.

3.6. Redesign of tubular tower

3.6.1. Stability check

The tower has been checked for the breaking strength and buckling strength in this section. Breaking strength check is required for surviving extreme winds. However, as a result of the increasing weight optimisation in modern steel tubular towers, the buckling strength of the tower usually governs the tower design as far as shell thickness is concerned. The stability analysis has been performed according to the method suggested in the Danish standard [22]. This method checks for both the breaking strength and the buckling strength. According to this method, the following inequality must be fulfilled

$$\frac{N_d}{2\pi R t} + \frac{N_{el}}{N_{el} - N_d} * \frac{M_d + N_d e}{\pi R^2 t} < \sigma_{cr} \quad 3-13$$

(Source: DNV/Risø, 2002 [22])

For a unity check

$$\underbrace{\frac{\frac{N_d}{2\pi R t} + \frac{N_{el}}{N_{el} - N_d} * \frac{M_d + N_d e}{\pi R^2 t}}{\sigma_{cr}}}_{S} < 1 \quad 3-14$$

Where

N_d	design axial force [N]
M_d	design bending moment [kNm]
N_{el}	euler force for a cantilever beam [kNm]
R	tower radius [m]
t	tower shell thickness [m]
e	the equivalent geometrical imperfection [m]
S	stability check value

Using the *equation 3-14*, the entire tower wall thicknesses are subsequently optimized in order to attain the value S as close as possible to one. If S exceeds 1.0 the wall thickness must be increased and the check must be repeated. If S is below 1.0 the wall thickness is reduced until a value as close as possible to 1.0 is reached. The new designed tower thicknesses for each welded section according to stability check are put in Table 3-9. The details of stability check are presented in Table 3-11.

Table 3-9: Wall thicknesses dimensioned according to stability check

Height	0	4	8	12	16	20	24	28	32	36	40	44	48	52	56	60	64	68	72	76	77.75
Wall thickness	30	28	27.5	27.5	27	26.5	26	25.5	25	24.4	23.5	22.5	21.5	20.3	19	17.4	15.6	13.5	11	7.8	6.3

3.6.2. Fatigue check

To ensure that a structure will fulfill its intended function, fatigue assessment should be carried out for each type of structural detail, which is subjected to extensive dynamic loading. The extent of the analysis is influenced by the local stress range and/or the number of cycles due to fluctuating loads on the structure. Wind loading on the turbine is the main source of potential fatigue cracking. Fatigue design can be carried out by methods based on S-N curves from fatigue tests in the laboratory and/or methods based on fracture mechanics. In this project, the former method has been used for fatigue assessment according to Palmgren-Miner's rule. The fatigue check has been performed for each welded section of the entire tower in the Bladed.

3.6.2.1. Welding details in a tubular tower

Welds are, in general, treated in the same manner as the rest of the structure when a proper reduction factor for the weld quality and base material is included. Figure 3-11 shows typical welds at flange and between two cans of different thickness used for the design of tower in this project.

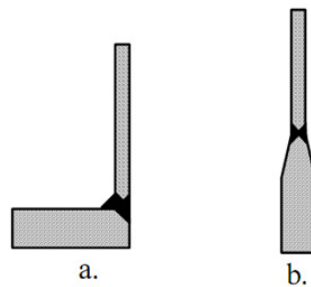


Figure 3-11: Typical weld details in a tubular tower a) weld at flange b) weld between two cans of different thickness [22]

3.6.2.2. Detail categories of welded joints

Corresponding to their notch effect, welded joints are normally classified into detail categories considering particulars in geometry and fabrication, including subsequent quality control. The Figure 3-10 contains detail categories for the fatigue assessment of these two welds according to the standards Eurocode 3 [23] and DS412 [24]. The detail category number (or $\Delta\sigma_R$) represent the fatigue strength reference value (at $2 \cdot 10^6$ cycles) for structures made of steel. The given detail categories assume 100% controlled full penetration butt welds of quality level B [22]. These categories have been used for fatigue analysis of welds in the tower. Also all welded joints on primary members shall be designed to provide a stress flow as smooth as possible without major internal or external notches, discontinuities in rigidity and obstructions to strains. To avoid stress concentration, the wall thickness is tapered with a slope not to be greater than 1:4.

Table 3-10: Detail categories for common welds in a tubular tower [22]

Weld	Categories ($\Delta\sigma_R$)
Can to can	80
Can to flange	71

3.6.2.3. S-N curve

Most components in wind turbines are subjected to stress ranges of great variation. This time series is extracted from the Bladed and converted to stress time history as explained in section 3.6.2.5. For illustrative purposes, the cycle is usually depicted as a sine function diagram as shown in Figure 3-12. σ_{max} is the maximum upper stress of a stress cycle and σ_{min} is the maximum lower stress of a stress cycle. $\Delta\sigma$ is the applied stress range $|\sigma_{max} - \sigma_{min}|$.

The mean stress is the algebraic average of σ_{max} and σ_{min} and given as:

$$\sigma_m = \frac{(\sigma_{max} + \sigma_{min})}{2} \quad 3-15$$

The amplitude of the stress cycle σ_{amp} , equals half of the stress range as:

$$\sigma_{amp} = \frac{|\sigma_{max} - \sigma_{min}|}{2} \quad 3-16$$

The R-ratio is calculated as the ratio of σ_{min} to σ_{max} :

$$R = \frac{\sigma_{min}}{\sigma_{max}} \quad 3-17$$

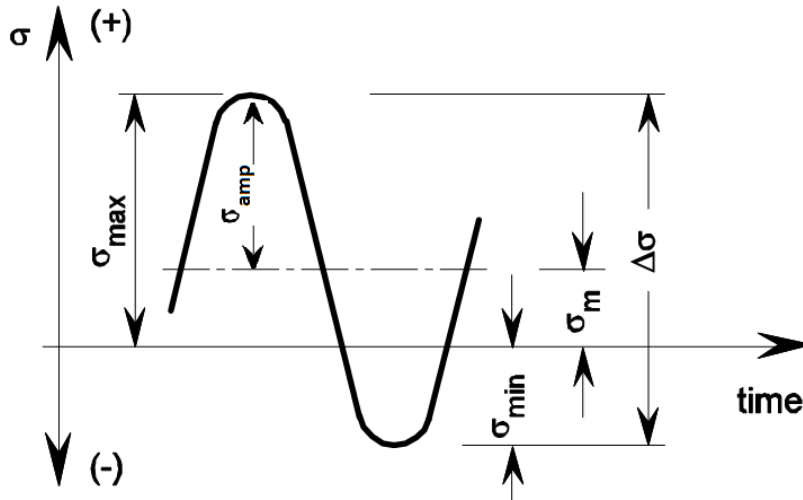


Figure 3-12: The stress cycle [21]

The loads acting on the structure are highly dynamic and the welds are intrinsically prone to fatigue. To perform the fatigue analysis the S-N curve for the welds was required and it was obtained from the GL standards [21]. The equations to determine the S-N curve are shown below in Equation 3-18 and Equation 3-19.

$$\log(N) = 6.69897 + m \cdot Q \quad 3-18$$

(Source: GL standard, 2005)

$$Q = \log(\Delta\sigma_R / \Delta\sigma) - 0.39794 / m_0 \quad 3-19$$

Where

m inverse slope of S-N curve

$m = m_0$ for $Q \leq 0$

$m = 2m_0 - 1$ for $Q > 0$

m_0 inverse slope in the range $N \leq 5 \cdot 10^6$; 3 for welded joints

$\Delta\sigma_R$ fatigue strength reference value of S-N curve at $2 \cdot 10^6$ cycles of stress range (or detail category number according to Table 3-10) [N/mm²]

$\Delta\sigma$ stress range [N/mm²]

N number of endured stress cycles according to S-N curve (= endured stress cycles under constant amplitude loading)

The S-N curves for both categories are constructed according to the information presented above and are shown below in Figure 3-13.

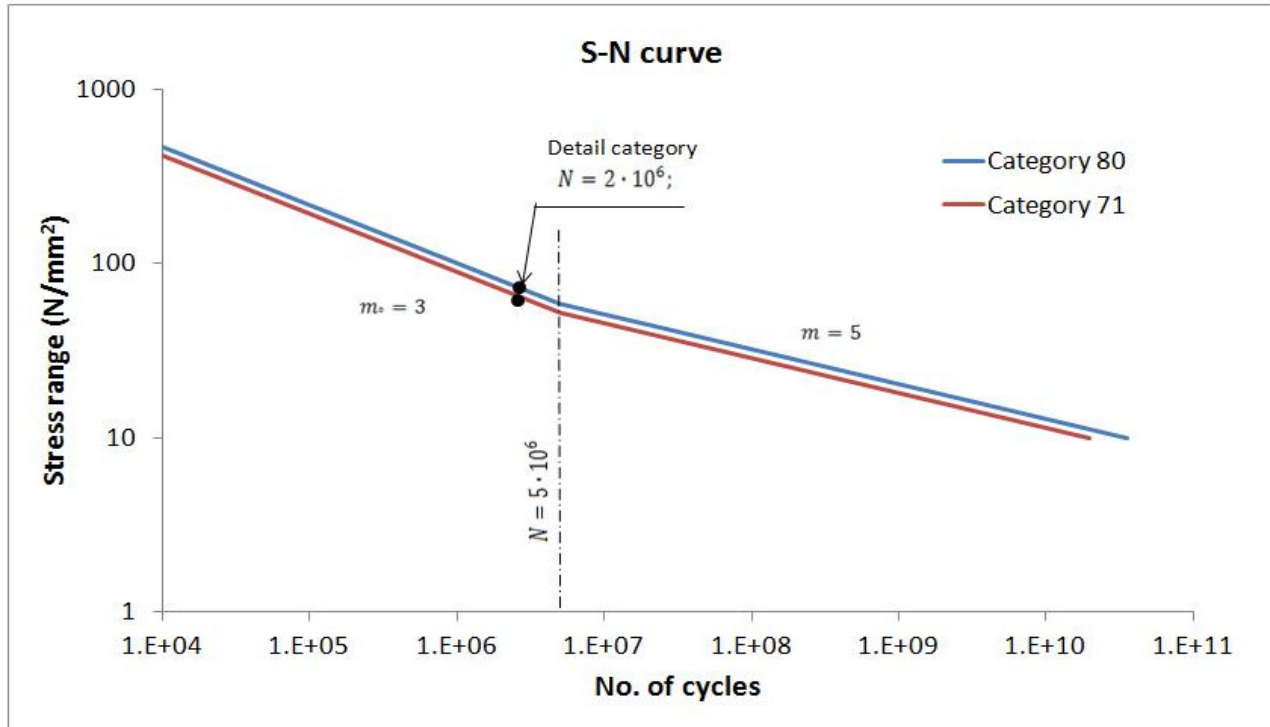


Figure 3-13: S-N curve for welds category 80 and 71

3.6.2.4. Palmgren-miner's rule

The fatigue life, or in other terms the cumulative damage, under varying loads can be predicted based on the S-N curve approach under the assumption of linear cumulative damage by Palmgren-Miner's rule. The total damage that a structure will experience during its design life may be expressed as the cumulative damage from each load cycle at different stress levels, independent of the sequence in which the stress cycles occur [22]. According to Palmgren-Miner's rule, the accumulated fatigue damage D can be predicted as follows:

$$D = \sum_i \frac{n_i}{N_i} \quad 3-20$$

Where

n_i is the number of stress cycles of the i^{th} stress range
 N_i is the corresponding number of cycles to failure

Failure might occur when the accumulated fatigue damage number exceeds 1.0. Thus, for the joint and member to survive for at least the planned service life of the turbine, the accumulated damage shall be less than or equal to 1.

3.6.2.5. Fatigue damage calculation

This calculation generates fatigue damage estimates from a stress history or a previously generated rainflow cycle count⁷, by taking account of the fatigue properties of the material. The Bladed did not show the stress history directly. Therefore, a suitable stress time history can be generated from load time histories by use of the channel combination and the equation 3-21.

$$\text{Stress range} = \frac{M_y * (D_o/2)}{I_{\text{tower section}}} \quad 3-21$$

Where

M_y is the bending moment at tower section
 D_o is the outer diameter of the tower section
 D_i is the inner diameter of the tower section
 $I_{\text{tower section}}$ is the moment of inertia = $\frac{\pi}{64} (D_o^4 - D_i^4)$

Selecting the multiple channels⁸ in fatigue analysis in the Bladed, the load cases and the variables to be processed in a single calculation are specified. The load cases are here the DLC 1.2 for different wind bins. The variables are the stress history at each welded section of the tower. The damage is calculated for the turbine lifetime of 20 years. The wind speed distribution is defined according to section 3.4. The material properties are entered in the look-up table in the Bladed with different stress range values and the corresponding number of cycles to failure as calculated from S-N curve in Figure 3-13.

⁷ Rain-flow counting method is used to establish distributions of stress ranges from a stress history.

⁸ Allow a whole list of variables to be processed across a whole list of load cases. If appropriate, the results are accumulated over the turbine lifetime (or any other desired period).

3.6.2.6. Approach for dimensioning the wall thickness

A systematic approach for dimensioning the wall thickness is shown in Figure 3-14. The fatigue check is performed for each welded section of the tower, applying the correct category values for the welded sections according to the Table 3-10. The entire tower wall thicknesses are optimized keeping the accumulated fatigue damage (D) as close as possible to one. If D exceeds 1.0, the wall thickness must be increased and the check must be repeated. If D is below 1.0, the wall thickness is reduced until a value as close as possible to 1.0 is reached. If the fatigue assessment leads to the wall thickness at one section to be less than the wall thickness that obtained from stability check, then final thickness is kept according to stability analysis. Else, the wall the thicknesses are finally set according to fatigue assessment. The dimensioned tower thicknesses for each welded section according to fatigue check are presented in Table 3-11, under the column 'fatigue check'.

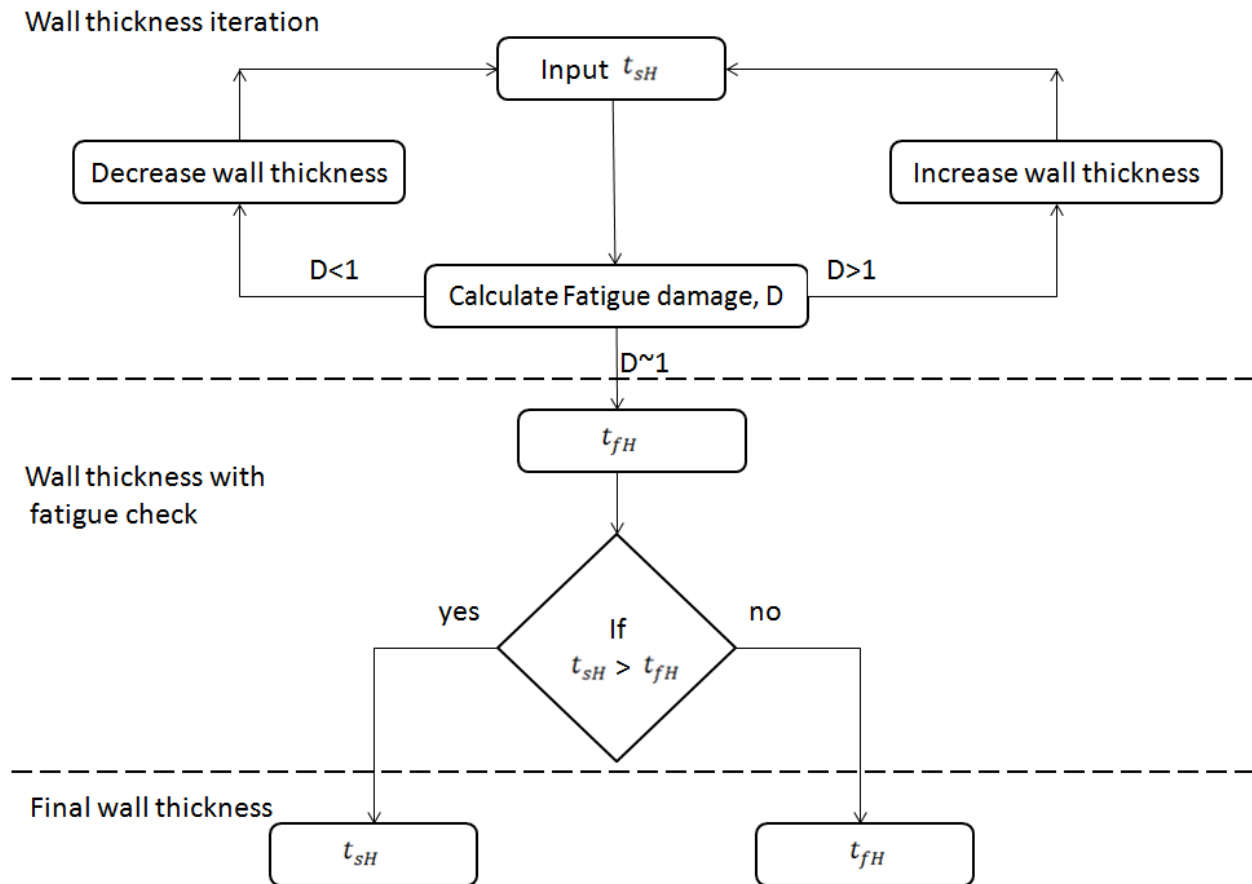


Figure 3-14: Approach for dimensioning the wall thickness

Where,

D accumulated fatigue damage

t_{sH} wall thickness at height H set according to stability check [mm]

t_{fH} wall thickness at height H set according to fatigue check [mm]

Table 3-11: Redesign of tower thicknesses according to fatigue damage

Detail Category $\Delta\sigma_R$ N/mm^2	Welding location	Height H, m	Stability Check			Fatigue check	
			Wall thickness according to stability check t_{sH}, mm	Stability check value (S)	Fatigue damage according to t_{sH}	Final thickness according to fatigue check t_{fH}, mm	Fatigue damage according to t_{fH}
Category 71	Top Flange	77.75	6.3	0.980	52.920	17.5	0.900
Category 80	Can to Can	76	7.8	1.001	15.750	17.5	0.900
		72	11.0	0.984	4.470	17.0	0.934
		68	13.5	1.031	2.536	18.0	0.900
		64	15.6	1.000	1.922	19.0	0.935
		60	17.4	1.000	1.670	20.5	0.940
		56	19.0	0.998	1.541	22.0	0.930
		52	20.3	0.996	1.500	23.0	0.950
Category 71	Flange 2	48	21.5	0.995	2.215	27.0	0.990
Category 80	Can to Can	44	22.5	0.997	1.488	27.0	0.930
		40	23.5	0.991	1.476	26.5	0.920
		36	24.4	0.985	1.465	27.5	0.930
		32	25.0	0.989	1.492	28.0	0.963
		28	25.5	0.993	1.522	28.5	0.960
		24	26.0	0.993	1.545	29.5	0.960
Category 71	Flange 1	20	26.5	0.991	2.329	34.0	0.962
Category 80	Can to Can	16	27.0	0.987	1.556	34.0	0.920
		12	27.5	0.979	1.543	31.0	0.970
		8	27.5	0.991	1.618	32.0	0.920
		4	28.0	0.980	1.581	32.0	0.950
Category 71	Bottom Flange	0	30.0	0.989	2.460	36.5	0.970

The Table 3-11 also summarizes the overview of entire tower design. First the tower wall thicknesses (t_{sH}) are designed according to stability check. But, the fatigue damage calculated at t_{sH} exceeds 1 as shown in the Table 3-11. Iterative steps are then applied by increasing the wall thicknesses until the fatigue damage is just less than 1. This action finally gives the wall thicknesses t_{fH} that keep the tower in safe fatigue limit and provides high stability.

The tower sections are connected by two welded flanges as shown in Figure 3-15. The tower thickness decreases from base to top. However, throughout one can, the thickness has been considered to be constant. The thicknesses of cans C1 and C2, adjacent to flanges are set according to fatigue assessment for category 71. Similarly, the wall thicknesses of the cans adjacent to other flanges in the tower are increased as shown in Table 3-11.

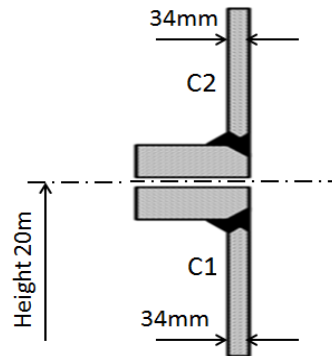


Figure 3-15: Dimensioning of cans adjacent to bottom flange

3.6.3. Natural frequency check

During operation, thrust loads are applied on the tower of the wind turbine. Due to these loads the tower will deflect or it will start vibrating at its natural frequency. The first natural frequency of the tower is a very important parameter as it determines the dynamic behaviour of the wind turbine. For wind turbines, it is important that the natural frequency of the tower does not interfere with the rotor frequency or blade passing frequency (or frequencies of excitation), as this can cause heavy resonance due to excitation. This leads to higher stresses in tower and, more importantly to higher stress ranges, an unfavourable situation with respect to the fatigue life of the wind turbine. Therefore it is important to ensure that the excitation frequencies with high energy levels do not coincide with the natural frequency of the tower.

The wind excitation frequencies that should be avoided are those that coincide with the range of rotational frequencies of the rotor. These frequencies are indicated as rotor frequency (1P) or blade passing frequency (3P) for a triple bladed turbine. Blade-passing frequency interval (3P) is equal to the rotational frequency interval times the number of blades. With a minimum rotational speed at the cut-in wind speed of 8.6 rpm and a maximum rotational speed of 18.4 rpm, the rotational frequency interval (1P) to stay clear of ranges from 0.143 Hz to 0.306 Hz.

Table 3-12 contains the calculated natural frequencies of the entire tower. The margin between the calculated first tower bending frequency and the rotor frequency (1P) at nominal speed seems sufficient: $0.32 \text{ Hz} / (16.1 \text{ rpm} / 60 \text{ s}) = 1.19\text{P}$. The tower bending frequency also lies above the maximum rotor speed in full load of 18.4rpm (0.306 Hz).

Table 3-12: Tower natural frequencies from modal analysis in the Bladed

Description	1 st mode, f [Hz]	2 nd mode, f [Hz]	3 rd mode, f [Hz]
Fore-aft, T_{fa}	0.32	1.83	4.10
Side-to-side, T_{sts}	0.32	1.54	3.80

One way to identify points of correspondence between natural frequencies and excitation of the rotor is to use a Campbell diagram, which shows the most important natural frequencies of the wind turbine as a function of rotor speed. Figure 3-16 shows the campbell diagram of the turbine with the final designed tower. From this diagram, it can be clearly seen that the first fore-aft and side-to-side tower frequencies are placed between the excitation frequencies (1P and 3P) throughout the operational range of the wind turbine. The Campbell diagram also shows that the rotor natural frequencies do not intersect the important excitation frequencies and avoid the resonance.

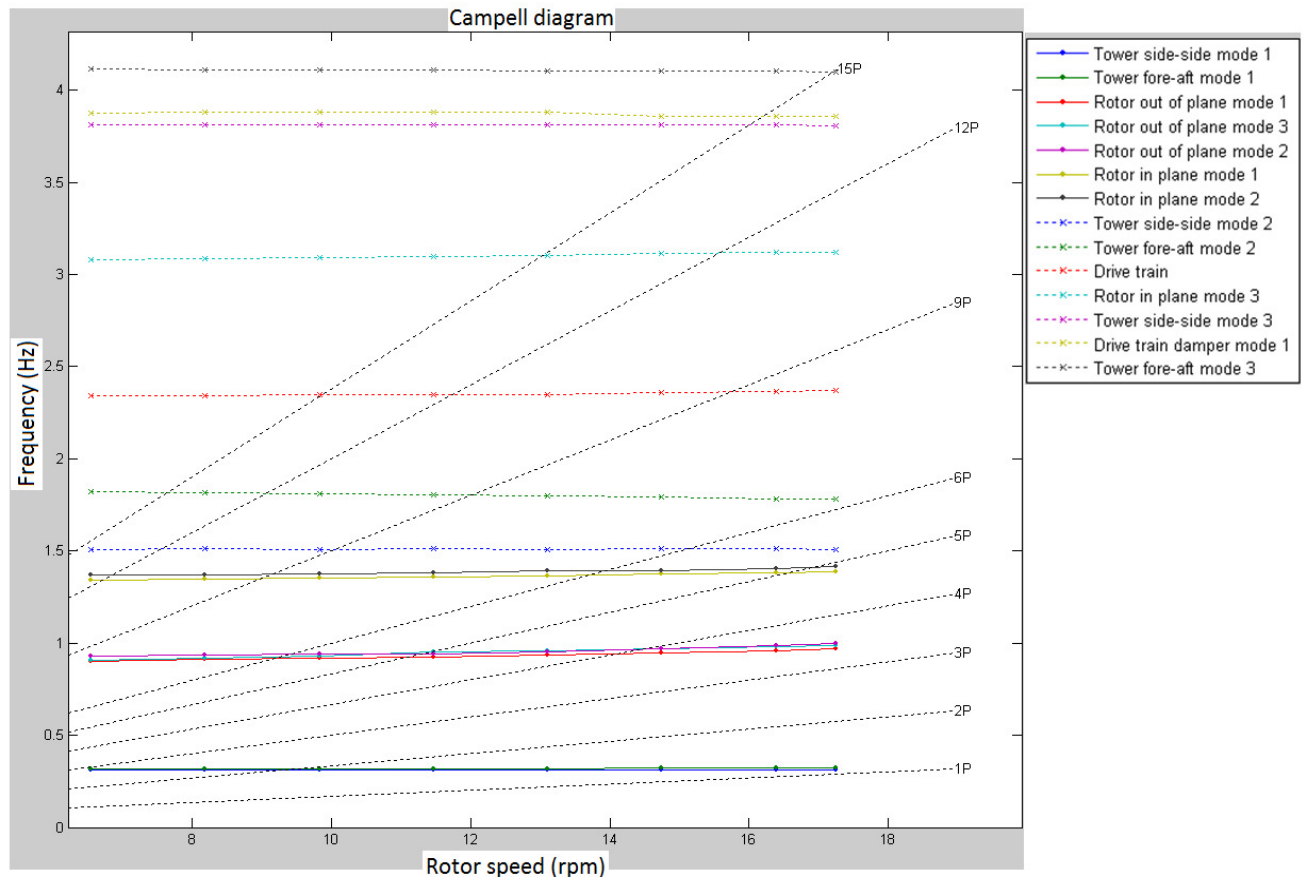


Figure 3-16: Campbell diagram for the final designed tower

3.7. Conclusion

The presented approach for the design of tower structure (reference tower) for wind turbines follows a well defined sequence of steps to come to a preliminary design of such a structure. The results obtained with this method give a good indication of the tower dimensions which are required for the given site conditions and for the selected turbine. The quick tower design approach lends itself well to this research purpose. This is because the adhesive bonded tower will be designed based on this reference tower and will give a fair cost comparison between the reference and adhesive bonded tower.

After performing the design checks for each section of the tower, the conclusion is drawn that the fatigue is the predominant phenomenon with regard to the determination of the wall thickness. This can be clearly seen in the Figure 3-17. This leads to wide scope for objective 2 of this research work by reducing the wall thickness from red colour to till blue colour, when tower is designed with the adhesive. This objective will be checked in the chapter 7.

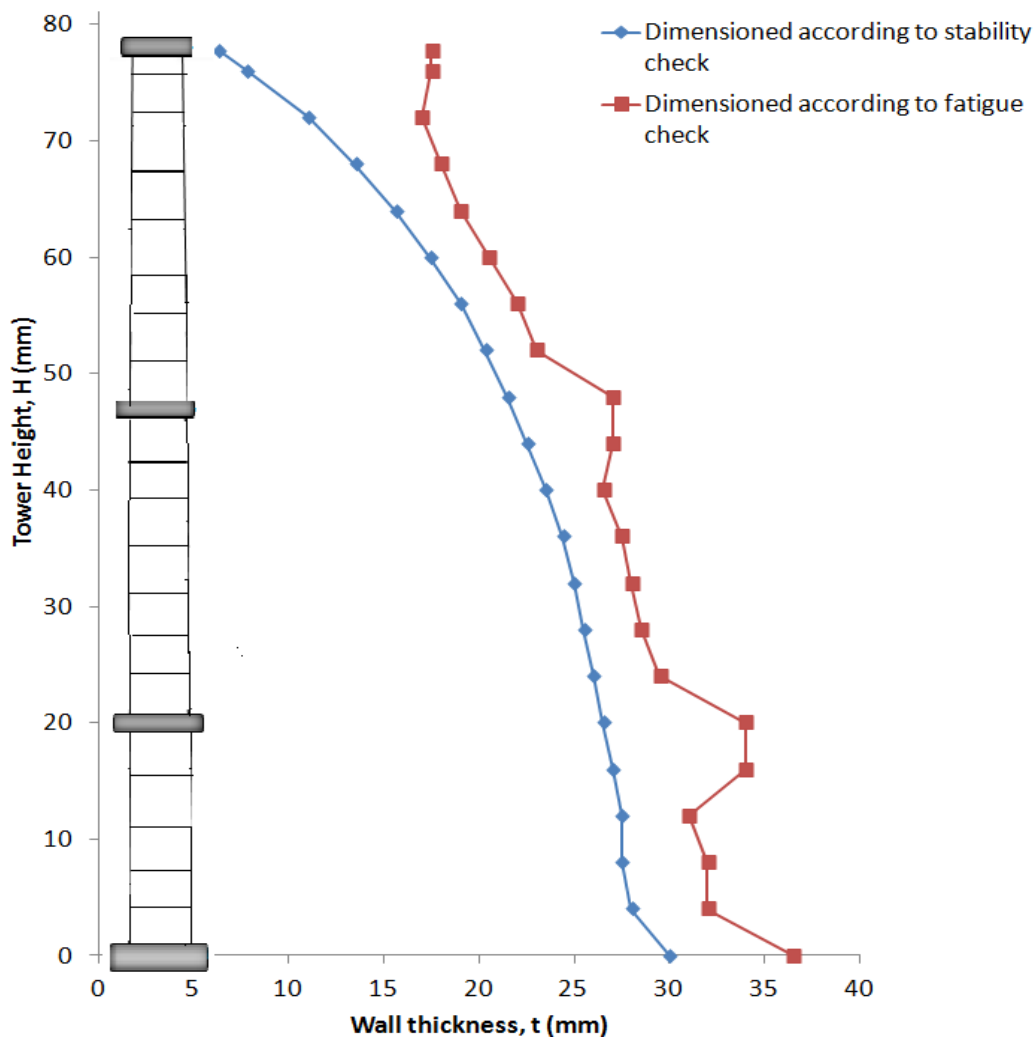


Figure 3-17: Dimensioning of the tower wall thickness according to stability and fatigue check

4. Adhesive bonding

This chapter presents the relevant knowledge of adhesive bonding with a brief introduction about adhesives, some definitions, formation of bonded joint and advantages and disadvantages of adhesives. Factors influencing the joint strength and the guidelines to increase it are discussed briefly from the literature studies. A method to improve the joint strength has also been presented. Finally, a conclusion will be made with a viewpoint for the bonded joint to be designed in this project.

4.1. Introduction

4.1.1. Introduction to adhesive

Adhesives have been used for thousands of years. Since about 1900, with the development of synthetic polymeric materials higher loaded joints in more demanding applications became possible. Today there many industrial uses of adhesives and it is difficult to imagine a product (in the home, in industry or in transportation) that does not use adhesives in some manner. According to Kinloch [25], an *adhesive* may be defined as a material which when applied to the surfaces of materials can join them together and resist separation. Adams et al. defined a *structural adhesive* as an adhesive that can resist substantial loads and that is responsible for the strength and stiffness of the structure [26]. Examples of structural adhesives are epoxy, thermosetting acrylic, and urethane systems.

4.1.2. Definitions

Before the adhesive bonding is discussed in details, certain key terms need to be defined. For basic definitions of common terms associated to adhesive technology please refer to Appendix B. Other terms and definitions that will specifically be used in this report are mentioned in this section.

Different types of loads arise in adhesive joints depending on the joint geometry and the direction of loading. These are often classified as tensile, shear, cleavage or peel as illustrated in Figure 4-1.

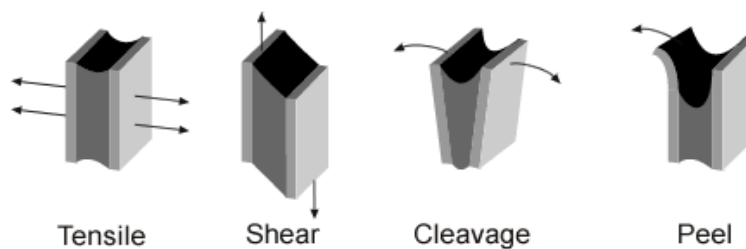


Figure 4-1: Different types of loads in an adhesive bonded joint [27]

- *Tensile*: Forces acting perpendicular to the plane of adhesive.
- *Shear*: Forces acting in the plane of adhesive.
- *Peel*: Forces applied to strip of a flexible member fastened with adhesive to another flexible or rigid member.
- *Cleavage*: Forces applied at one end of a rigid bonded assembly which tend to split the bonded members apart. It can be considered as peel of two rigid members.

Adherend: Body that is or intended to be held to another body by an adhesive.

Adhesion: Adhesion is the attraction between two substances resulting from intermolecular forces that establish between them.

Post-cure: Further treatment by time and/or temperature of an adhesive to obtain the required properties by curing.

Cure time: Time required to induce curing at a given temperature.

Fillet: Portion of an adhesive that bridges the adherends outside the bond-line.

Moisture: High humidity or wet conditions affecting the adhesive or adherend.

4.1.3. Adhesive bonded joint

Adhesive bonding is a joining technique similar to other joining techniques like welding, soldering, riveting, bolting etc. What is considered as adhesive bonded joint is explained by the following definition.

An adhesive bonded joint can be defined as a joint between two substrates of equal or different materials by means of a non-metallic third material that has good adhesion and has also sufficient cohesive strength to maintain the substrates fixed against each other during the operational life of the product, despite the forces acting on the joint [28].

The formation of bonded joint can be distinguished in three stages as [29]:

- Initially, the adhesive must behave as a liquid to be spread easily on the surface. It should also wet properly the adherends to be bonded for an intimate molecular contact between adhesive and the surface.
- Secondly, the liquid adhesive must harden in order to support sometimes continuous and sometimes variable load throughout their lives.
- Finally, they must transfer and distribute the load among the components in an assembly.

By preference, the load is transferred by shear stresses in the adhesive layer, whereas tensile, peel or cleavage loads should be avoided or minimized as much as possible. The strength of the joint not only depends on the shear strength of the adhesive itself, but also on the shear and peel stress distribution along the length of the overlap.

Sometimes a primer is used with adhesives. A primer is a substance which is applied to a surface prior to the application of an adhesive. This usually helps in improving the performance of the bond or protecting the surface until the adhesive or sealant can be applied. The bonded joint is the whole part formed by the adherends, the adhesive, the primer (if present), and the interphases and interfaces associated to it, as shown in Figure 4-2.

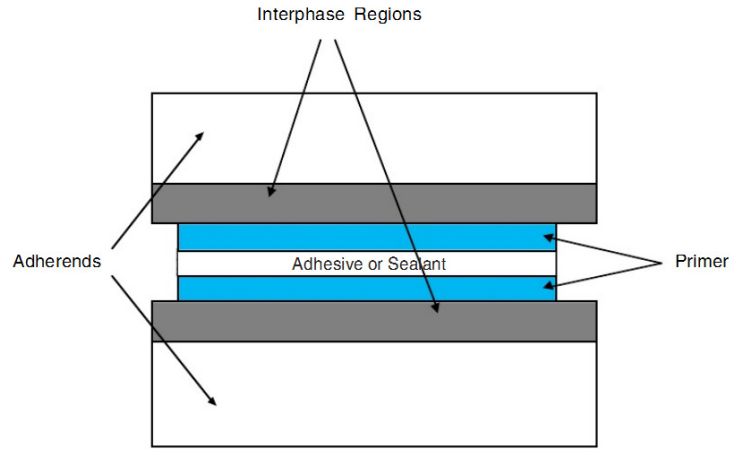


Figure 4-2: Components of a typical adhesive joint [30]

4.1.4. Advantages and disadvantages of adhesive bonding

Adhesive bonded joints are increasingly being used in engineering applications due to their improved mechanical performance over conventional mechanical fasteners. In contrast to other joining methods, such as riveting and bolting, adhesive bonding distributes the load transfer uniformly along the bonded joint as seen in Figure 4-3 and thus avoids stress concentration.

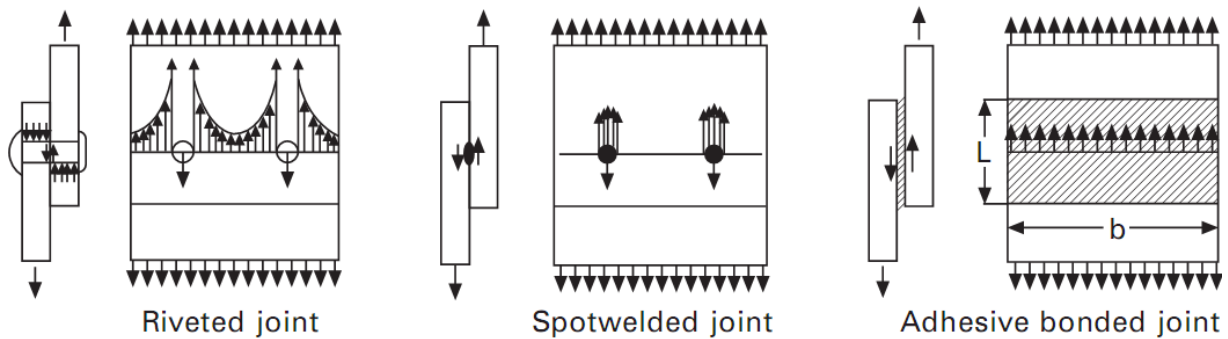


Figure 4-3: Comparison of load transfer in various types of joints [4].

Due to the polymeric nature of the adhesive, adhesive bonding of critical joints provides good damping properties which also enable an improvement in fatigue life [4]. This is because the polymer-based adhesives absorb mechanical energy applied to the joint and dissipate that energy as heat. Figure 4-4 shows typical fatigue curves for riveted and adhesively bonded joints, indicating the superiority of the latter. Where vibration is transmitted through joints, mechanically fastened components can sometimes show fretting due to very small amplitude relative movement normal to their mating surfaces. Adhesive bonding not only eliminates fretting but it can also serve to damp or attenuate the vibration [26].

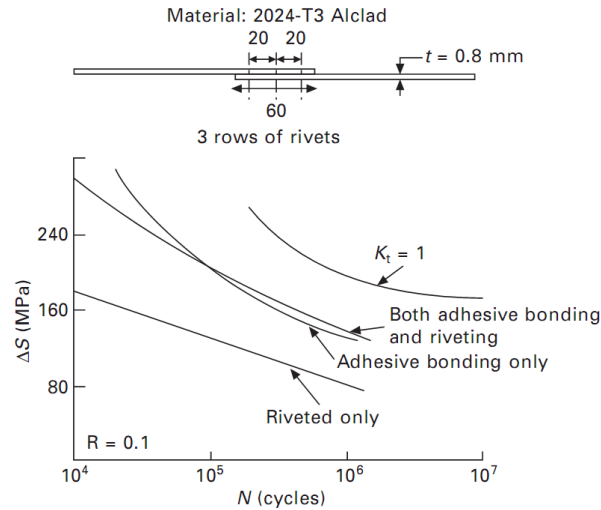


Figure 4-4: S–N curves of lap joints [4]

Adhesives can bond dissimilar materials with different coefficients of thermal expansion because the adhesive flexibility can compensate the difference. The adhesive creates an intimate contact between the bonded surfaces, which is good in structural terms and also for corrosion resistance.

Adhesive bonding is also associated to some disadvantages that leave room for more technological research and development. They have limited resistance to extreme temperature and humidity conditions. An adhesive bonded structure will most probably not be capable of being dismantled and re-assembled, at least without considerable cleaning and repetition of surface preparation [26]. However, a series of non-destructive techniques are now available. The curing needs high temperature for many adhesives and requires jigs and fixtures to maintain the substrate in position during this process. This is a big economical disadvantage. To have a good interfacial strength and a durable joint, a careful surface preparation is necessary such as solvent cleaning, mechanical abrasion, or chemical treatments.

4.2. Factors affecting the joint strength

The major factors that affect the joint strength of lap joints are the material properties (adherends and adhesive), the geometry (adherend and adhesive thickness, and the overlap) and the environment. Failure always occurs at the stress concentrations and it is fundamental to decrease these stress peaks if a joint strength improvement is required. There are general guidelines to increase the joint strength by minimizing the stress concentrations [30]:

- Use an adhesive with a low modulus and ductile behavior
- Use similar adherends or if not possible balance the stiffness
- Use a thin adhesive layer
- Use a large bonded area

Each of these factors is discussed in the following sections and the detailed design guidelines are provided.

4.2.1. Adhesive properties

The joint strength is a function of the adhesive strength and ability to distribute the load over a large area and reduce the stress concentration. However, the joint strength may not increase if a stronger adhesive is used. The joint strength depends not only on the adhesive strength but also on its ductility and stiffness. Very ductile adhesives tend to have low shear strength. However, when used in a joint, their ability to distribute the stress uniformly along the overlap (low stiffness) and deform plastically can give a joint strength much higher than with apparently strong but less ductile adhesives. A ductile adhesive is able to redistribute the load and make use of the less stressed parts of the overlap, whereas a brittle adhesive concentrates the load at the ends of the overlap giving a low average shear stress. Thus, in ideal cases, a strong, ductile, and flexible adhesive is desired [30]. Also ductile adhesives have more fatigue strength than the brittle adhesives.

4.2.2. Adherend properties

The most important adherend properties affecting the joint strength are the adherend modulus and its strength. The higher the adherend modulus, the lower will be its deformation at the ends of the overlap, where the load transfer takes place, and the lower will be the effect of the differential straining in the adhesive [8]. Strength is also important as adherend yielding can lead to premature failure in case of metallic adherends. This is because when the stress imposed at the end of overlap become more than the yield point of the steel, large plastic strains result, creating a plastic hinge. Also increase of the thickness of both adherends (proportional to elastic modulus) corresponds with an increase of the adherend axial stiffness and that will result into a more uniform distribution of the shear stress and thus an increase of the average shear strength.

4.2.3. Overlap lengths

The increase of the overlap of a bonded joint will result in an increase of the joint strength. The increase in overlap length seems not very effective as the average shear stress decreases while the peak stresses at the end of the overlap remain the same. The advantage of this low stress level in the middle of the overlap is the resistance to creep phenomena due to constant loading. Furthermore, the bonded joint becomes more robust, because local defects like voids in the adhesive have less effect on the load transfer [31].

A literature survey by Silva and Adams [32] compares the prediction of the joint strength with elastic models and the experimental results. The experimental results were obtained with simple lap joints (SLJs) made of brittle adhesive Redux 326 and high strength steel adherends [33]. Joint predictions are presented for different analytical models as shown in Figure 4-5. It can be seen that the models predict better for shorter overlaps than for longer overlaps with the experimental results. For larger overlaps, all the models tend to predict similar values and are 10-50% lower than the experimental values. A possible explanation for the relatively poor failure load predictions is the fact that brittle adhesives are difficult to characterize in bulk due to their high sensitivity to defects. However, a good point is that the predictions are always lower than the experiment values and are therefore regarded as safe for the design.

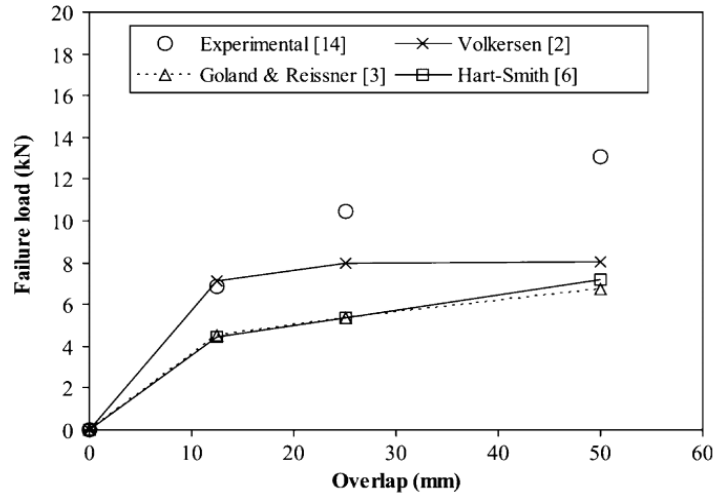


Figure 4-5: Overlap effect on Linear analysis: brittle adhesive (Redux326) and high-strength steel [34]

4.2.4. Adhesive thicknesses

The effect of the adhesive thickness on the bond strength of single-lap adhesive joints is still not perfectly understood. The classical elastic analyses such as those of Volkersen [8] or Goland and Reissner [35] predict that the strength increases with the adhesive thickness, whereas experimental results show the opposite. Practice shows that the lap-joint strength increases as the bond line gets thinner [36]. This can be seen in literature survey by Silva and Adams [32] in which the adhesive thickness effects for different models have been compared as shown in Figure 4-6. The experimental joint strength decrease as the adhesive thickness increases while the linear elastic analyses shows the opposite trend as shown in Figure 4-6.

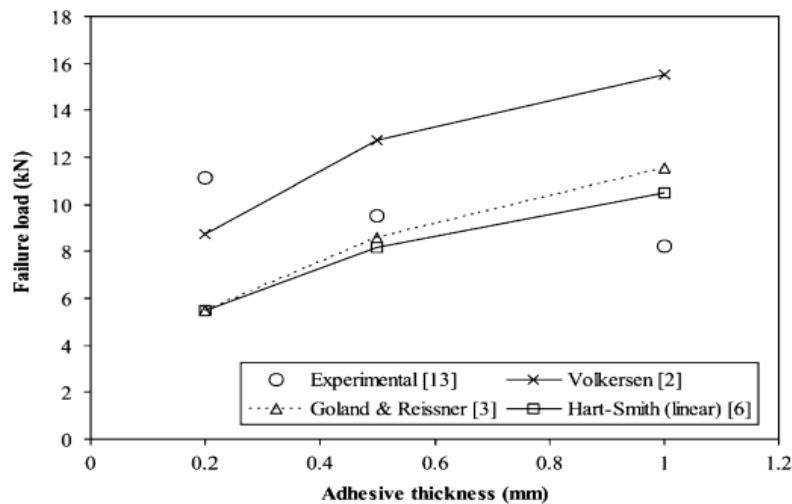


Figure 4-6: Adhesive thickness effect on linear analysis: adhesive (Hysol 9321) and high-strength steel [32]

According to Crocombe [37] thicker single-lap joints have a lower strength considering the plasticity of the adhesive. An elastic analysis shows that the stress distribution of a thin bondline is more concentrated at the ends of the overlap than a thicker bondline, which has a more uniform stress distribution. Therefore, a thin bondline will reach the yielding stress at a lower load than a thick bondline. However, when yielding does occur in a thicker joint, there is a less “elastic reserve” to sustain further loading, and thus, yielding spreads more quickly. Also other theories to explain the adhesive thickness on the strength of SLJs were introduced by Gleich *et al.* in 2001 [38] and Grant *et al* (2009). There are many theories that attempt to explain this fact and this subject is still controversial. However, Adams and Peppiatt (1974) explained that an increase in the bondline thickness increases the probability of having internal imperfection in the joint (voids and microcracks), which will lead to premature failure of the joints [39].

In another investigation, Hans Nordberg [40] has shown that with the increase in the adhesive thickness the fatigue strength also increases at the same number of cycles. For longer lives the increased bondline thickness does not seem to affect the strength.

4.2.5. Environmental effects

Water and humidity are two of the most damaging environmental factors for adhesive. The possible mechanisms by which water can degrade adhesive joints include [27]:

- plasticization
- swelling
- hydrolysis or crazing of the adhesive
- degradation or change of the interface resulting in loss of adhesion
- corrosion of the substrate

The fatigue life of lap joints is progressively reduced after pre-exposure to water. However, control in water absorption does not seem to affect the fatigue properties with more than 15% as shown in Figure 4-7 [40]. The control in water absorption can be done by:

- coating (encapsulating) the exposed edges of the joint with a water resistant sealant
- using a suitable primer/coupling agent will improve interfacial durability – a fluid primer that wets the surface will tend to fill discontinuities on the adherend surface

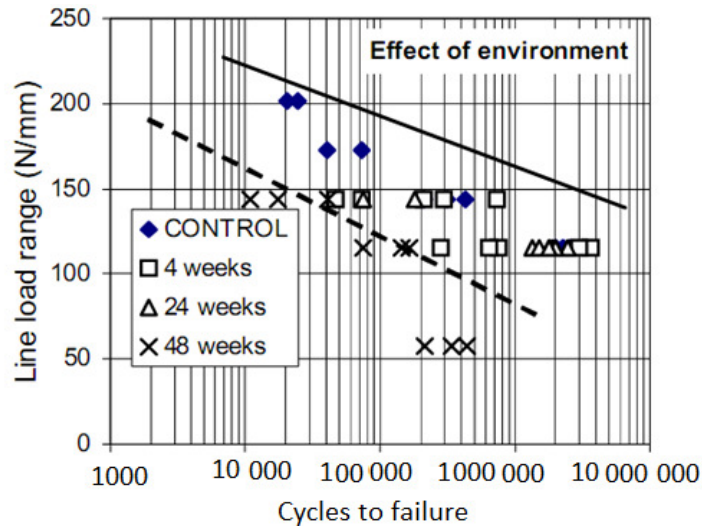


Figure 4-7: Fatigue of 1.5 mm AISI 304L stainless steel adhesive joints. Specimen immersed in water for 4 to 48 weeks [40].

4.3. Method to improve the joint strength

Adhesive joints are formed with a fillet of adhesive spew which is squeezed out under pressure while the joint is being manufactured. The assumption that the adhesive layer has a square end is thus unlikely to be realistic. Various authors have shown that the inclusion of a spew fillet at the ends of the overlap reduces the stress concentrations in the adhesive and the substrate. Modification of the joint end geometry with a spew fillet spreads the load transfer over a larger area and gives a more uniform shear stress distribution. The load transfer and shear stress distribution of a single-lap joint with and without fillet are schematically represented in Figure 4-8.

Adams and Peppiatt [39] found that the inclusion of a 45° triangular spew reduces the predicted maximum shear stress to 70 per cent of that obtained for the square ended adhesive layer for a single lap joint. Also the maximum transverse tensile stress when spew is present is reduced to 80 per cent of that given by Goland and Reissner. The National Physical laboratory [41] conducted a series of simulated experiments using finite element analysis (FEA) on CR1 Mild Steel/AV119 Epoxy for single lap joints. The results also show an increase in predicted failure load by 30% with the inclusion of a concave fillet as shown in Appendix E.

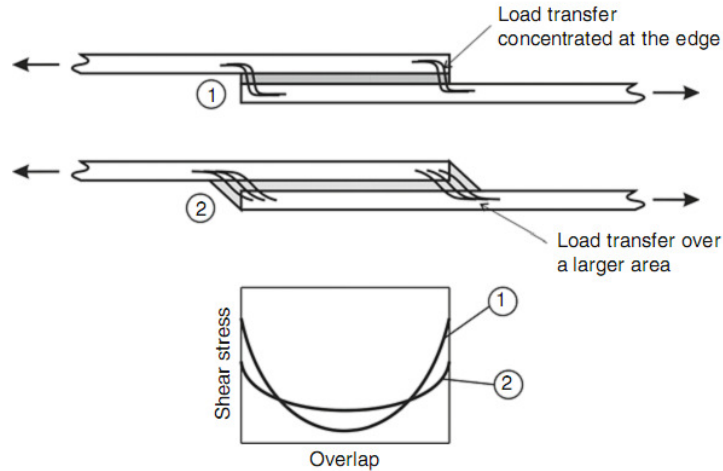


Figure 4-8: Load transfer and shear stress distribution in single-lap joints (1) with fillet and (2) without fillet [29]

4.4. Conclusion

A conclusion for this chapter along with a point of view for the bonded joint to be designed in this project has been discussed briefly here.

The bonded joint should be designed such that the load is transferred by shear stresses in the adhesive layer, whereas the tensile, peel or cleavage loads should be avoided or minimized as much as possible. The ideal adhesive selection would be a strong, ductile and flexible adhesive. The adherend selected should have higher elastic modulus and strength.

The results presented for the geometrical parameters: adhesive thickness and overlap length, illustrate the fact that elastic models are not appropriate to simulate the effect of these two parameters. This is due to the prediction of different results in comparison to experimental results. However, the overestimated joint strength because of increase in adhesive thickness can be compensated by the low joint strength prediction due to large overlap. Assuming this compensation, the elastic model has been implemented for design in this study.

It has also been considered that the porosity and the number of micro-cracks in the adhesive are less. In future it is required to do experiments for SLJs keeping the same material and adhesive properties as applied in this project. The experimental data is required to understand the actual behavior of the variation in the adhesive thickness and the overlap length. Also, the long term behavior and the effect of different environments on bonded joints need a lot of attention in the future. The inclusion of spew fillet leads to an improvement in the design. However, this has not been modeled in tower design for this project.

5. Design of adhesive bonded joints

This chapter presents the design of bonded joint with adhesive. Selection of the joint type for the joint in the tower is discussed briefly. Determination of loadings, material and adhesive properties and analytical models to be applied in the design procedure have also been introduced. Finally, the methods for the design checks are set up along with the S-N curve for adhesives and structural steel.

5.1. Adhesive bonding design procedure

A simple stepwise guideline to be followed for the bonded joint design is shown in Figure 5-1. The design starts with the selection of suitable joint type surveying all the positive and negative aspects of the joints. The loadings are introduced at the bonded joint as calculated before in the tower design section. A strong adhesive and an analytical model to be applied for the design are then selected. The approach for the optimization of geometrical parameters is also discussed. Finally design checks to be performed are presented. If the design checks do not fulfill then the approach is iterated many times with the change in the joint geometry. Results are displayed separately in the next two chapters for both objectives of the project.

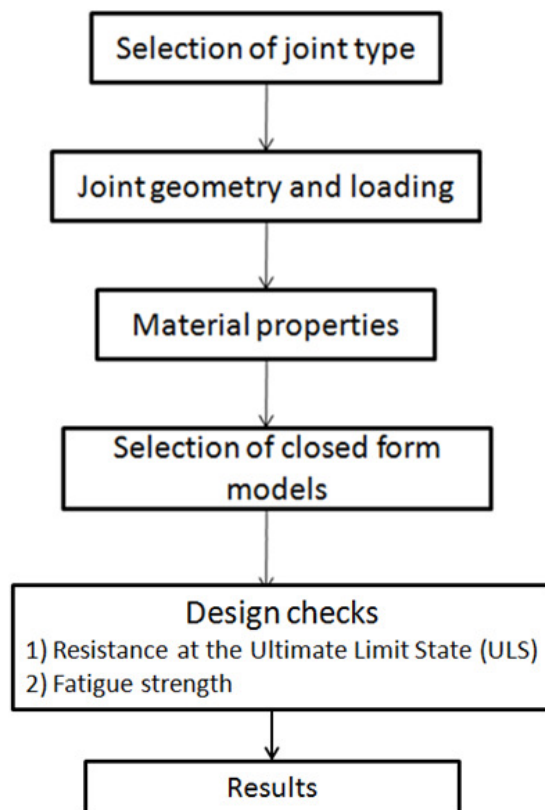


Figure 5-1: Steps for the design of a adhesive bonded joint

5.2. Selection of a joint type

5.2.1. Various types of joints

For a good joint design, the adhesive must be loaded in shear and the load-bearing area must be as large as possible. Peel loads are the greatest enemy of the designer of the bonded joints [26]. Wherever possible, the adhesive should be loaded in shear so that peel and cleavage stresses are avoided. Different joint designs can be implemented to overcome these problems. The most common forms of lap and strap joints are shown in Figure 5-2. Some are stronger than the others, but none is simpler to make in comparison to the single lap joint.

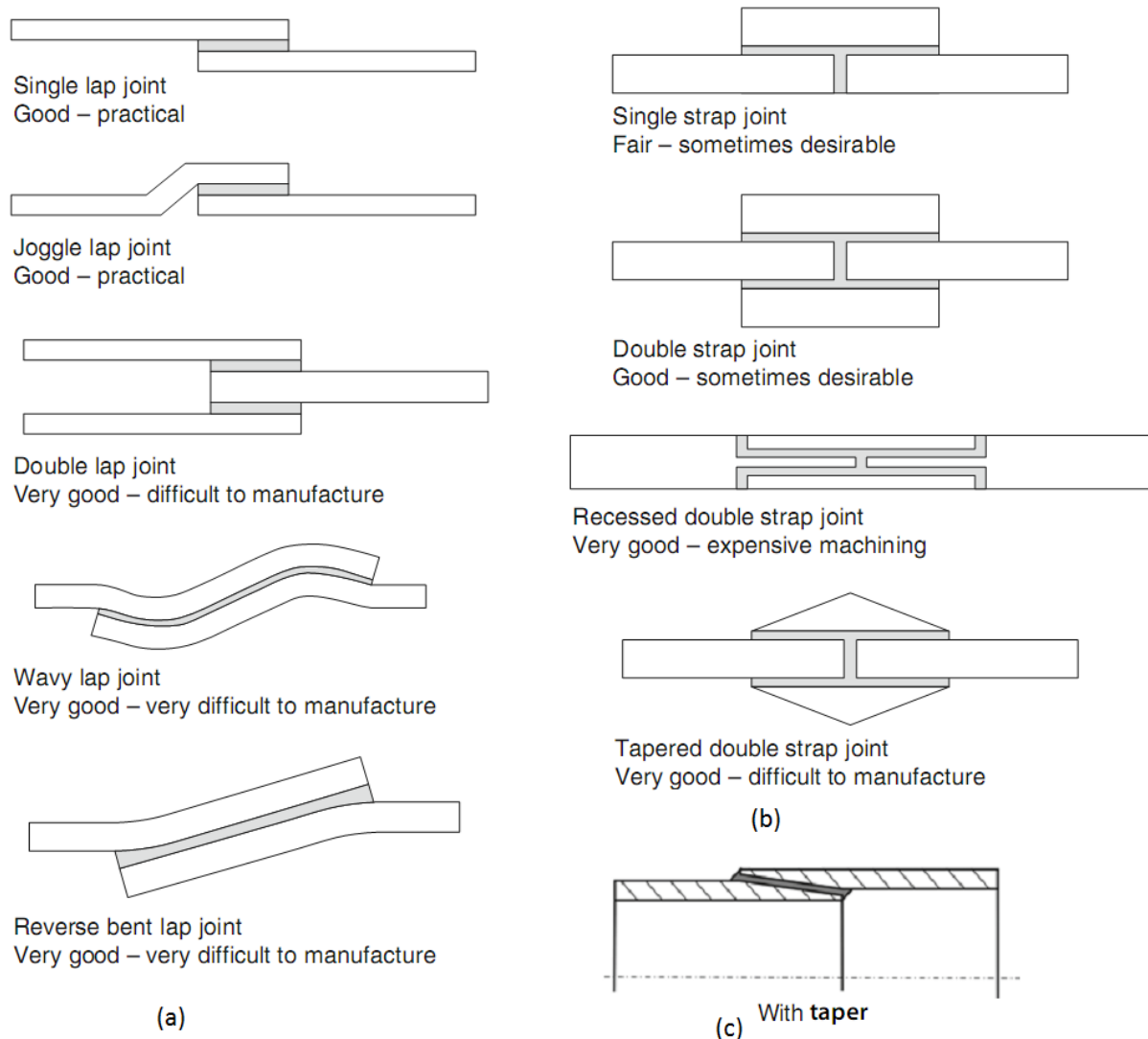


Figure 5-2: Joint configurations for (a) Lap joints [30] (b) strap joints (c) tubular joint with a taper [29]

5.2.2. Considerations for selecting a suitable type of joint

Single lap joint is the easiest joint to make with no complexity in its machining or manufacturing. Also with installation perspective, it is easy to assemble by just sliding the upper tower shell along the lower tower shell. This sliding squeezes the adhesives uniformly all over the bonded area and avoids extra assembly procedures. The circular geometry of the connection to be bonded with adhesive makes the final geometry look like a tubular joint as shown in Figure 5-3.

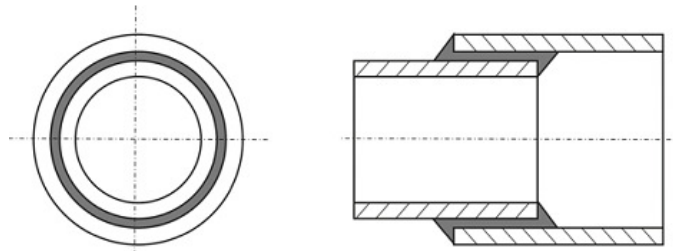


Figure 5-3: Tubular single lap joint [29]

The eccentric forces acting on the SLJ induce a bending moment in the joint. The bending moment causes additional tensile (peel) stresses to be induced in the adhesive layer, concentrated at the ends of the joint. The lack of symmetry causes joint rotation for lap joints. The rotation is much less for the tubular joints than for the plate joints as shown in Figure 5-4. This is because rotation causes hoop stresses in the tubular joint which constrain the rotation [42]. Thus the tubular-SLJ reduces the peel stress at the end of the adherend.

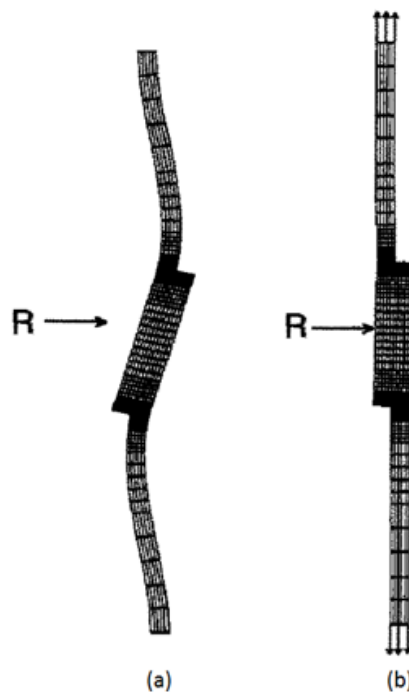


Figure 5-4: Rotation of joints in (a) Single lap plate joint (b) Single lap tubular joint [42]

Other types of joints are not considered for the following reasons:

- For tapered and scarf joint, the manufacturing of the tapering at a small angle by machining is difficult, especially with contoured edges. Frigyes Thamm has shown that the adherends have to be tapered to a fine edge if significant benefit is to be achieved, and this is usually impracticable [43]. During the bonding process the sharp edges are also critical in positioning, and pose problems after curing for Non Destructive Inspection.
- As in the case of single-lap joints, the strap joint with only one strap is subjected to peeling stresses because the load is not collinear. However the strap needs to be manufactured and machined separately. The joint with two straps reduces the bending moment and is therefore stronger, but it adds cost. The straps with a taper and the recessed joints are the most efficient but require a lot of machining. Strap joints will lead to extra assembly procedures with jigs and fixtures to hold and locate the parts accurately until the adhesive has cured.

Thus the aim is to design the tower joint without taper, but with low shear stresses to prevent creep. The selected joint is the single lap joint (SLJ) with a square edge around the circumferential end of the tower and foundation section.

5.3. Joint geometry and loading

The joint geometry data consists in the overlap length and the thickness of the adherends and adhesive layer. The load acting on the adherend is the maximum force per unit width which can be calculated from the extreme bending moment and the axial force (refer to section 3.5.1) and is given by:

$$Force/width = \left(\frac{M_y \cdot (D_o/2)}{I_{tower\ section}} + \frac{F_z}{\pi/4 \cdot (D_o^2 - D_i^2)} \right) \cdot t_w \quad 5-1$$

Where

$$I_{tower\ section} \quad \text{is the moment of inertia} = \frac{\pi}{64} (D_o^4 - D_i^4) [m^4]$$

$$t_w \quad \text{is the wall thickness of the tower [mm]}$$

5.4. Material properties

The adherend for the tower and foundation section wall is steel. 1-C epoxy is taken as structural adhesive which is good for metal bonding. The reference adhesive taken for this research is one-part hot curing toughened epoxy adhesive (ESP110) [26]. This is a metal (Aluminum) filled, paste adhesive designed to provide maximum resistance to impact, shear, cleavage and tensile loads. The durability, chemical resistance and high temperature performance are extremely good. ESP110 will bond to a wide variety of surfaces, including steel. ESP110 can withstand temperatures from -40° to +180°C. The adhesive chosen is an intermediate adhesive which is between brittle and ductile adhesive with good shear strength. The material properties of both adherends and adhesive used in the design are given in the Table 5-1.

Factor of safety (FOS) for adhesive

The partial safety factor by which the adhesive should be divided to give design values is taken as 3 [27]. This leads to allowable shear strength of 16.7MPa during design as shown in the Table 5-1. This includes the partial safety for the environmental conditions and the adhesive thickness.

Table 5-1: Material properties of adherend and adhesive

Adherend Properties (Steel)	
Modulus of elasticity, E (GPa)	210
Poisson ration	0.3
Adhesive Properties (ESP110)	
Ultimate shear strength, τ_{ult} (MPa)	50
Design shear strength (MPa) with FOS 3, τ_{allow}	16.7
Modulus of elasticity, E (GPa)	3.7
Shear Modulus, G (GPa)	1.35
Poisson ratio	0.37

5.5. Closed-form models

5.5.1. Types of models

Knowledge of the state of stresses inside the adhesive layer of an adhesively bonded joint is essential for joint strength prediction and joint design. However, adhesive bonded joints have a relatively complex stress distribution. The two methods for the stress analysis of lap joints are analytical and numerical methods. The former is a closed-form model employing classical linear theories in which some simplifications are used. The numerical methods use finite element methods to handle complex structures and nonlinear material properties where classical methods generally fail to work. The Finite Element Model (FEM) approach opens the possibility to analyze complex joint geometries, like spew fillet and adherend tapering, and to include geometrical and material non-linear behavior. Although the closed-form solutions have their limitations, they are easy to use, especially for parametric studies. The FE method is time-consuming and not easily applicable to routine design work. Consequently the former has been used for joint design in this project work. Comparison between different analytical models has been shown in the Table 5-2.

In this research work, the analytical model is selected to determine the stress distribution. The model is chosen for the selected material behavior and the geometry. The problem deals with bonding the tubular tower section, the peel stresses are negligible. So the Volkersen's simple lap joint theory can be used [44].

Table 5-2: Comparison between different analytical models [32]

Models	Adhesive elastic	Adhesive plastic	Adherend elastic	Adherend plastic	Isotropic adherends	Anisotropic adherends	Geometries covered	Results given
Volkersen	Yes	No	Yes	No	Yes	No	SLJ and DLJ	Shear stress
Goland and Reissner	Yes	No	Yes	No	Yes	No	SLJ	Shear and peel stresses
Hart-Smith	Yes	Yes	Yes	No	Yes	No	SLJ and DLJ	Shear and peel stresses
Bigwood and Crocombe	Yes	Yes	Yes	No	Yes	No	Sandwich	Shear, peel, and von Mises stresses
Adams <i>et al.</i>	Yes	Yes	Yes	Yes	Yes	No	SLJ and DLJ	Failure load
Frostig	Yes	No	Yes	Yes	Yes	Yes	SLJ	Shear and peel stresses

5.5.2. Volkersen model

The model used for this design as Volkersen model as described in [8]. Volkersen's analysis introduced the concept of differential shear, illustrated in Figure 5-5. The reduction of the strain in the adherends along the overlap (from A to B) and the continuity of the adhesive/adherend interface cause a non-uniform shear strain (and stress) distribution in the adhesive layer. It was assumed that adhesive deforms only in shear and that the adherend can deform in tension as shown in Figure 5-6. However, this analysis does not account for the bending effect caused by the eccentric load path of SLJs. Also adhesive stress variation across the adhesive thickness has not been considered. Volkersen's analysis also predicted that the thicker the adhesive, the higher is the strength. Unfortunately, this theory is not supported by the experimental evidence which shows that thicker bond line gives lower strengths [26].

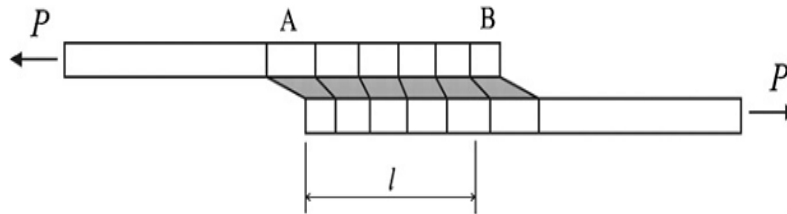


Figure 5-5: Deformations in loaded single-lap joints with elastic adherends [8].

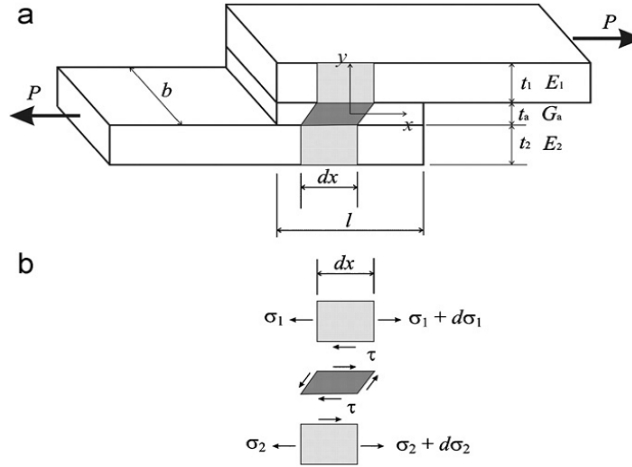


Figure 5-6: Single-lap joint analyzed by Volkersen [8]: (a) Geometry and (b) Elemental diagram

The adhesive shear stress distribution (τ) according to Volkersen is given by:

$$\tau = \frac{P}{bl} \frac{w \cosh(wX)}{2 \sinh(w/2)} + \left(\frac{\psi - 1}{\psi + 1} \right) \frac{w \sinh(wX)}{2 \cosh(w/2)} \quad 5-2$$

Where:

$$w^2 = (1 + \psi)\phi$$

$$\psi = t_t/t_b$$

$$\phi = \frac{G_a l^2}{E t_t t_a}$$

$$X = \frac{x}{l}, \quad -\frac{1}{2} \leq X \leq \frac{1}{2}$$

P	the applied load [N]
b	the joint width [mm]
l	overlap length [mm]
t_t	the top adherend thickness [mm]
t_b	the bottom adherend thickness [mm]
E	the adherend modulus [MPa]
G_a	the adhesive shear modulus [MPa]
t_a	the adhesive thickness [mm]
$\frac{P}{bl}$	average shear stress, τ_{avg} [MPa]

The origin of the longitudinal co-ordinate x is the middle of the overlap

5.5.3. Selection of failure criterion

The failure criterion chosen for linear elastic analysis in the design is maximum shear stress in the adhesive according to Volkersen's model. That is, the maximum adhesive shear stress is to be less than or equal to the maximum allowable adhesive shear stress as given by:

$$\tau \leq \tau_{allow} \text{ or } \left(\frac{f_{v,adh}}{\gamma_{M,adh}} \right) \quad 5-3$$

Where

τ is the shear stress in the adhesive layer (equation 5-2) [MPa]

$f_{v,adh}$ is the limiting shear strength value of adhesive [MPa]

$\gamma_{M,adh}$ 3.0 is the material factor for adhesive bonded joints

5.5.4. Linear elastic analysis

The simplest analysis considers the adherends to be rigid and the adhesive to deform only in shear. The adhesive shear stress is constant over the overlap length. This value for the shear stress can be interpreted as the average shear stress acting on the adhesive layer [45] and is given by:

$$\tau_{avg} = \frac{P}{b \cdot l} \quad 5-4$$

The stress in the sheet material is given by:

$$\sigma_{sheet} = \frac{P}{b \cdot t} \quad 5-5$$

Where:

t metal thickness (thickness of thinner sheet in joints made of different thickness) [mm]

σ_{sheet} stress in the sheet due to axial loads and bending moments [N/mm²]

For design purposes it is assumed that the resistance of the bonded joint can be described by the resistance of a unit width segment of tubular-single lap joint as shown in Figure 5-7. The relationship between stress level in sheet material and average shear stress in the adhesive can be found by equating the force per unit width in the sheet and in the adhesive and is given by combining equation 5-4 and 5-5 as:

$$\sigma_{sheet} = \frac{\tau_{avg} \cdot l}{t} \quad 5-6$$

Combining equations 5-2 and 5-6 give the shear stress distribution in the adhesive along the overlap which does not include the width term. This equation has been used in the design calculations and is given by:

$$\tau = \frac{(\sigma_{sheet} \cdot t) w \cosh(wX)}{l \cdot 2 \sinh(w/2)} + \left(\frac{\psi - 1}{\psi + 1} \right) \frac{w \sinh(wX)}{2 \cosh(w/2)} \quad 5-7$$

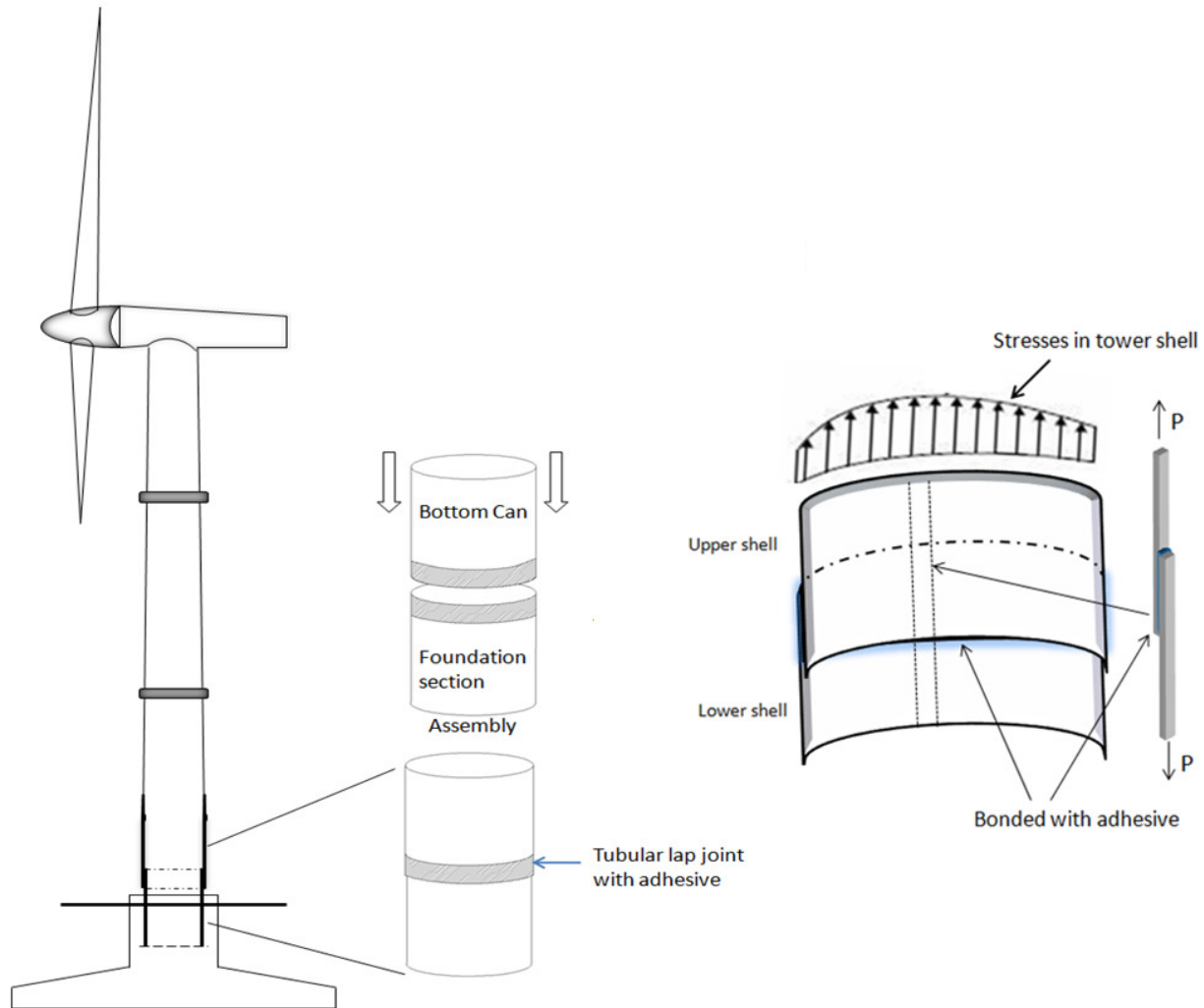


Figure 5-7: Principle of the proposed adhesive bonded connection

Design example with Volkersen model

To make the design process clearer in this project, an example has been discussed along with the design approach. The conclusion from this example will be used in the design of adhesive bonded connection for both the objectives of this project. The considered parameters for this joint geometry are: overlap length as 400mm, adhesive thickness 10mm and adherends thickness of 36.5 and 55mm, stress in the sheet = 234MPa. The shear stress distribution (red curve) along the overlap has been plotted in the Figure 5-8 using the Volkersen model (equation 5-7) implemented in Matlab (refer Appendix D).

The shape of the shear stress distribution in Figure 5-8 is non-linear which can be explained by the concept of differential shear as discussed in the chapter 5.5.2. The stresses are high at the end of overlap because of the maximum strain difference in the adherends at both ends of the adhesive layer. At the middle of the overlap both adherends have the same strain and thus lead to a lower shear stress. Figure 5-8 also illustrates the asymmetry in the peak stresses at the end of the joint. It can be seen that the peak shear stress at the side of the thick sheet becomes lower. This is because there is less deformation due to the higher stiffness of the sheet.

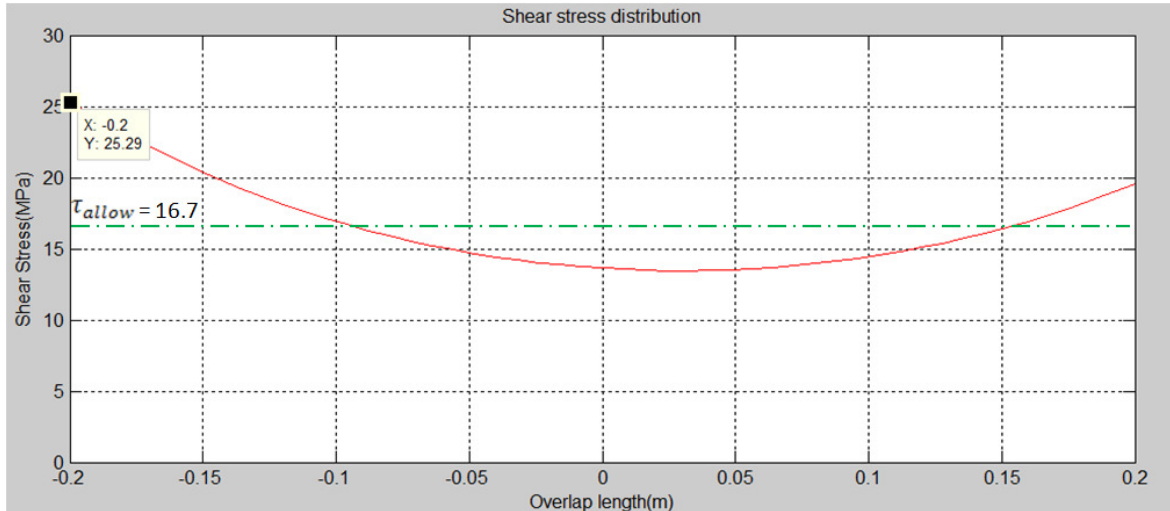


Figure 5-8: Shear stress variation along the overlap length, $l = 400\text{mm}$ (-200mm to +200mm), $t_o = 10\text{mm}$, $t_t = 36.5\text{mm}$ and $t_b = 55\text{mm}$

5.6. Design checks

The required design checks for the adhesive bonded connections are:

- Resistance at the Ultimate Limit State (ULS)
- Fatigue strength

5.6.1. Resistance at ULS

The simplified procedures for designing adhesively bonded joints are as follows:

- Calculate overlap length of the joint using the relationship between the stress level in the sheet material and the allowable shear stress in the adhesive as mentioned in equation 5-6.
- Check for the ultimate strength using the failure criterion equation 5-3.
- Optimize design geometry parameters.

Optimization of design parameters

The given geometry leads to peak stress higher than the allowable limit of the selected adhesive (τ_{allow}) as shown in Figure 5-8. Lowering of peak stress is possible with the optimization of the design parameters - overlap length and adherend thickness. Both the parameters are varied using Volkersen's model to achieve an optimized value for the safe bonding. It should be noted that width of the joint need not be optimized as the shear stress distribution is calculated per unit width. The thickness has been chosen as 10mm for the entire design of the tower.

The first geometry parameter to be optimized is the overlap length. Using Volkersen's model, a graph between the shear stress and different overlap lengths is plotted as shown in the Figure 5-9. It can be observed that the shape of stress curve level off with the effect of increase in overlap length. Thus, increasing the overlap length has virtually no benefit in reducing the peak stress. The next optimization step is to increase the adhesive thickness.

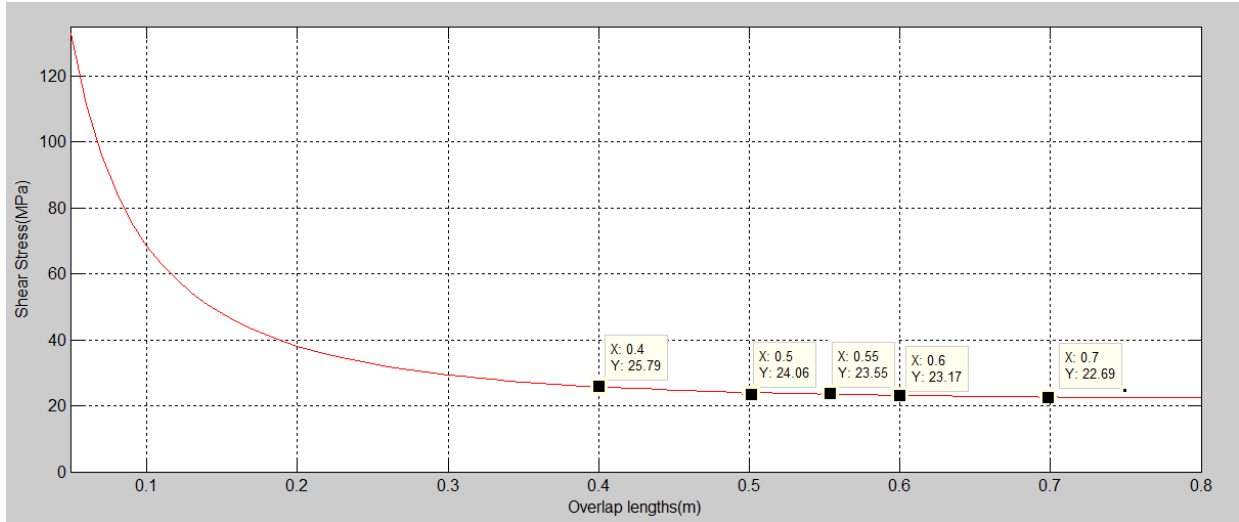


Figure 5-9: Shear stress variation against overlap length at thickness 10mm, $t_t = 36.5\text{mm}$ and $t_b = 55\text{mm}$

Unequal adherend thicknesses in a joint lead to asymmetry in the peak stresses at the end of the overlap. The effect of varying adherend thicknesses in a joint has been investigated here and the results are plotted as shown in the Figure 5-10. It can be illustrated from the figure that the unequal adherend thickness (blue and green curve) in a joint leads to asymmetric stress distribution at the ends of overlap. However if the adherend thicknesses are equal (violet, orange and black curve) then the stresses are symmetric at the end of joint and also peak stresses are lesser in comparison to the case of unequal adherend thicknesses. From Figure 5-10, it can be concluded that equal and thicker adherend will result in a reduction in the peak stress and confers a higher stability to the tower section.

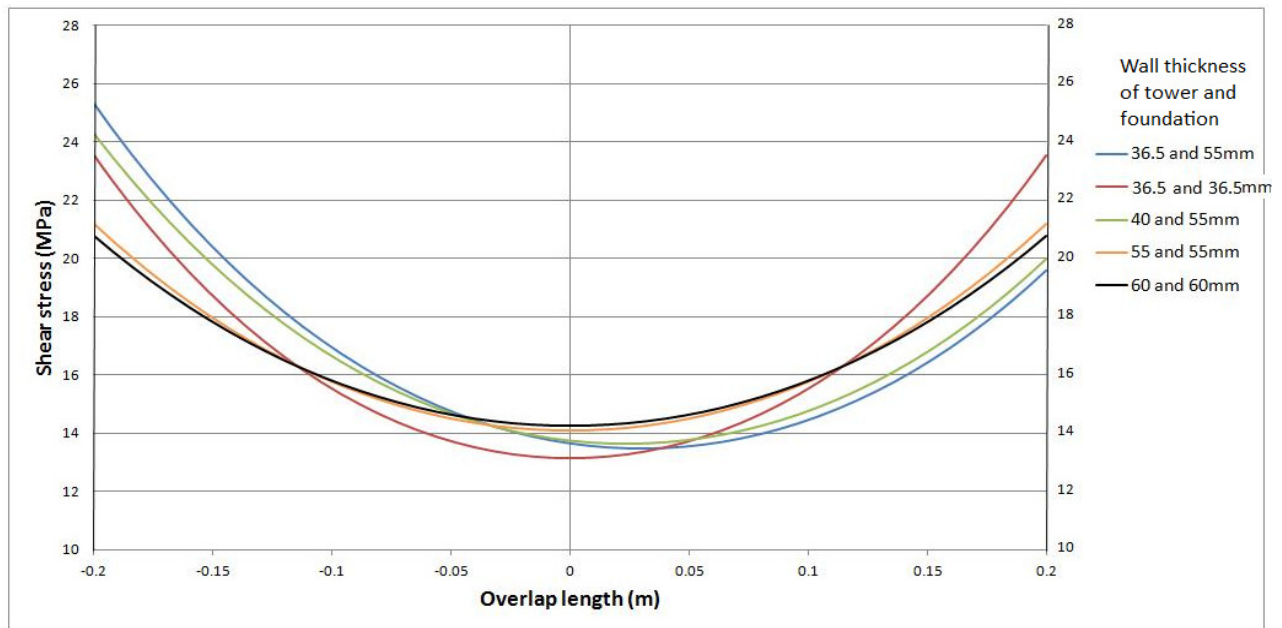


Figure 5-10: Effect of varying thicknesses of adherend in a joint on the peak stress at overlap length of 400mm

5.6.2. Fatigue check of the bonded joint

5.6.2.1. S-N curve of adhesive

The fatigue check for bonded connection has been performed with the same approach as discussed in the chapter 3.6.2. However, the S-N curve for the adhesive will be different when compared to the welding. The S-N curve of the adhesive used in this project is not available. It requires carrying out a test to get the S-N curve for ESP110. For this research, the S-N curve of toughened epoxy DP 490 has been used as a reference for fatigue check of the adhesive bonded connections. This curve has been taken from the fatigue test carried out by Robert Boyes as described in [46]. Fatigue tests were conducted at a constant test frequency of 20 Hz and R-ratio = 0.1. An S-N curve was plotted using the load range and number of cycles to failure as shown in the Figure 5-11.

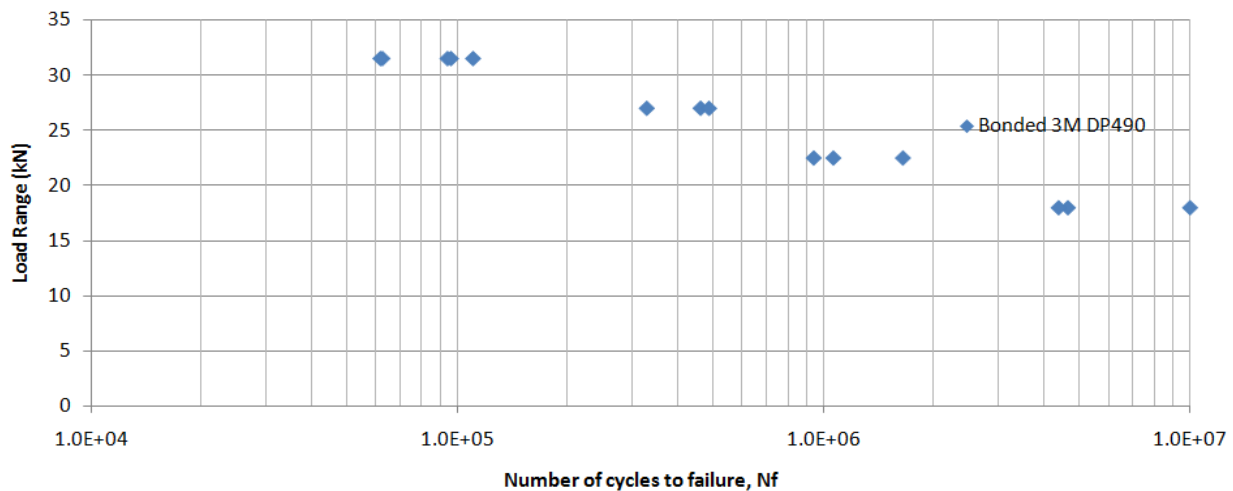


Figure 5-11: S-N curve for simple lap joint bonded with toughened epoxy system, DP 490. (Room temperature, 20 Hz, R = 0.1)

It can be noticed from Figure 5-12 that the S-N curve of the toughened epoxy adhesive is lower than the single epoxy adhesive used for this design. This leads to the fatigue assessment from this S-N curve giving a damage value higher than that obtained from the single epoxy adhesive. So the fatigue check with this curve will result in a safe design.

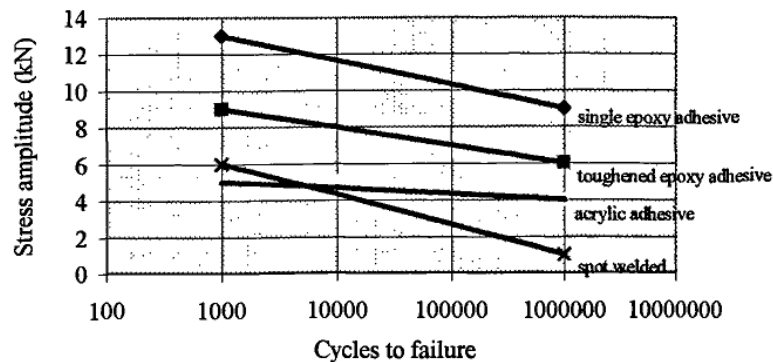


Figure 5-12: Dynamic fatigue of steel double-box hat structures [47].

However for the fatigue analysis in the Bladed, it is convenient to input stress ranges along with number of cycles. The load ranges of S-N curve plot in Figure 5-11 is converted to stress range by using the geometry of a test specimen as described in the [46]. In the Bladed, it is required to input the stress range in the descending order. However in the S-N curve plot in Figure 5-11, different numbers of cycles are marked for the same stress group. The means of the number of cycles for the same stress group were taken to plot the stress range versus number of cycles as shown in the Figure 5-13. The fatigue damage calculation will be performed in the Bladed after converting the stress ranges in to shear stress ranges (from equation 5-2) by using channel combination.

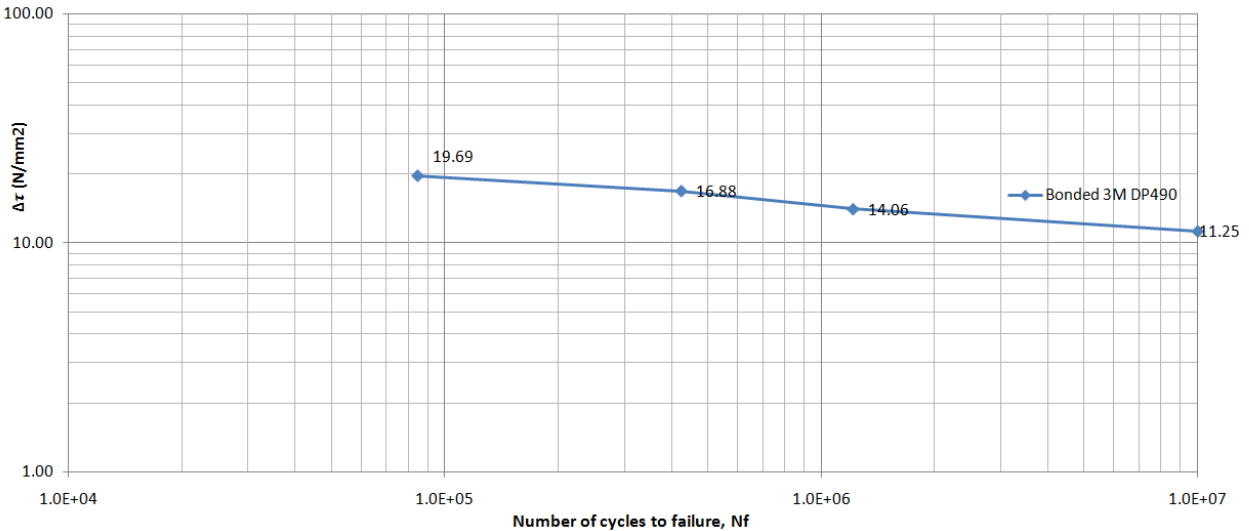


Figure 5-13: S-N curve for simple lap joint bonded with a toughened epoxy system (DP 490) to be used for the fatigue damage calculation of the designed joint. $f = 20\text{Hz}$ and $R = 0.1$

5.6.2.2. Safety factor for bonded joints

The partial safety factors are given in Table 5-3 according to IEC61400-1 edition 3 [7]. The partial safety factor for adhesive material is taken from 'adhesivestoolkit' [27]. The total safety factor is applied to the cyclic stress range for assessing the increment of damage associated with each fatigue cycle.

Table 5-3: Partial safety factors for fatigue analysis of adhesively bonded connections

Type	Partial safety factor
Loads, γ_f	1.0
Material (for welded and structural steel), γ_m	2
Consequences of failure (non fail safe structure components), γ_n	1.15
Total ($\gamma_f \cdot \gamma_m \cdot \gamma_n$)	2.3

5.6.2.3. S-N curve for structural steel

For the second objective of this research work, the welds between the cans are replaced with the adhesive bonded joints. It has been already discussed in the introduction to adhesive bonding that the bonded joints have more fatigue resistance. This improvement leads to possibility of reducing the wall thicknesses lower than that designed thicknesses with the fatigue assessment of the welds and thus, makes it significant to look for the fatigue in the steel.

The fatigue check of the steel will be performed with the same approach as done for welding, but with the different detail category and inverse slope. The detail category for the fatigue assessment of structural steel is taken as $\Delta\sigma_R = 160$ from the “Recommendations for Fatigue Design of Welded Joints and Components”, [48]. The inverse slope (m_s) in the range $N \leq 5 \cdot 10^6$ is 5 for structural steel. The S-N curve for structural steel is constructed according to the equations 3-18 and 3-19 as shown below in Figure 5-14.

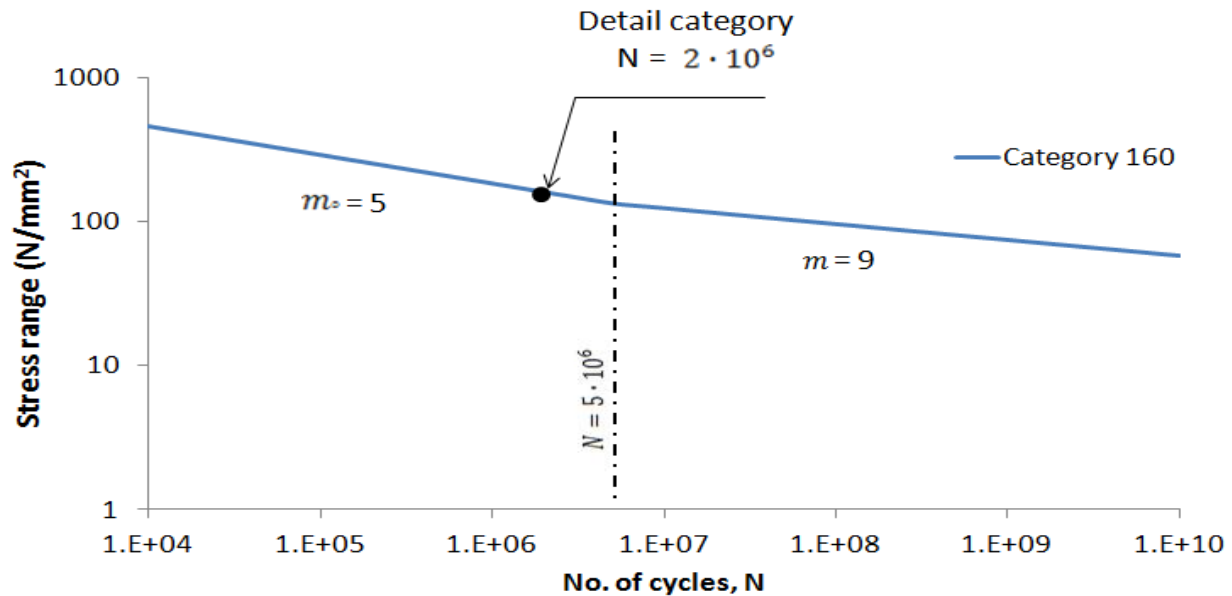


Figure 5-14: S-N curve for the structural steel

5.7. Modification in the can geometry

Bonding with adhesive could lead to increase or decrease in the wall thickness of the cans. This variation results in a big difference in the thicknesses between the next two adjacent cans to be welded and subsequently to high stress concentration in the welds. This problem can be solved by tapered wall in the vicinity of the welds so as to provide a stress flow as smooth as possible without major internal or external notches, discontinuities in rigidity and obstructions to strains.

The length of the transition should be at least 3 times the difference in depth as shown in Figure 5-15. The wall thicknesses difference with less than 3mm can be welded directly as the differences can be equalized within the weld. However, when the wall thickness differ more than 3mm at joints mainly stressed perpendicularly to the (butt) weld direction, the difference shall be smoothed by beveling or tapering according to Figure 5-15 prior to butt welding.

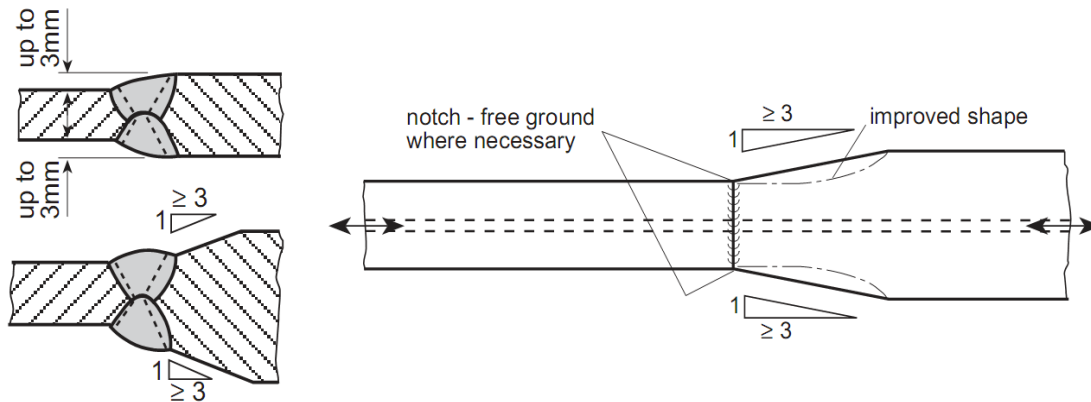
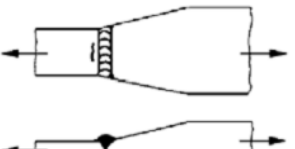


Figure 5-15: Transition in butt welds of unequal thicknesses

The detail category for weld between the cans in this project is taken as 80. For this detail category the tapering slope is considered as 1:5 from Table 5-4 given by the International Institute of Welding (IIW/IIS), IIW document XIII-1965-03 / XV-1127-03 [48]. The cost for machining a taper at the can's end should be also included in the final cost comparison if the taper is required in the final design with adhesive bonding.

Table 5-4: Detail Categories and tapering slope for welded parts of a component [48]

Type No.	Structural Detail	Description, Requirements and Remarks (St. = steel; Al. = aluminium)	Detail category $\Delta\sigma_R$ (FAT class)	
			Steel	Al
223		Transverse butt weld, NDT, with transition in thickness and width slope 1:5 slope 1:3 slope 1:2 Weld run-on and run-off pieces to be used and subsequently removed. Plate edges to be ground flush in direction of stress. Misalignment <10% Exceeding misalignment due to thickness step to be considered, see chapter 6.2.3.7.2		
			80	25
			71	22
			63	20

6. Bonding of tower base to the foundation instead of flange and cost comparison

This chapter presents the results of the first objective in the project. The chapter includes the required design parameters used for adhesive bonding. The results of the optimization steps, fatigue damage check and the natural frequency check are discussed briefly. Finally, the incurred costs for both the solutions are compared in detail.

6.1. Results of bonding tower base to the foundation

The section geometries of the tower base and the foundation are shown in Figure 3-5 and Figure 3-6. The tubular lap-joint is dimensioned after replacing the flanges from both the respective sections. The thickness of the adhesive is taken as 10mm [49]. This value is high to give enough manufacturing tolerance for the tower and foundation section.

As discussed in the section 3.5.1, the extreme loadings are calculated for the 50years Extreme Operating Gust as presented in Table 3-5. The types of loadings considered at the tower foundation are axial and bending moments. The loading at the adherend is calculated as the maximum force per unit width using the equation 5-1.

The overlap length is calculated using the relationship between the stress level in the sheet and the allowable shear stress in the adhesive using equation 5-6. This gives the overlap length approximately 400mm. From the optimization conclusion discussed in section 5.6.1, the adherend thickness and the overlap length are optimized to have less material usage. The adherend thicknesses are varied from 55mm to 70mm to determine the overlap length until the peak adhesive shear stress is less than the maximum allowable adhesive shear stress. The material volume for the increase in tower section thickness, foundation slab thickness and overlap length is also calculated as shown in Table 6-1.

Table 6-1: Effect on overlap length and material volume with increase in tower and foundation wall thicknesses

Tower base thickness (mm)	Foundation wall thickness (mm)	Peak shear stress (MPa)	Overlap length (mm)	Increase in material volume (mm ³)			
				Can	Foundation	Overlap	Total increase in volume
55	55	16.62	770	0.6425	0.0	0.5552	1.198
57	57	16.60	720	0.707	0.0586	0.5383	1.3039
60	60	16.64	660	0.8040	0.1464	0.52	1.4704
63	63	16.59	630	0.9012	0.2341	0.521	1.6563
67	67	16.64	590	1.0310	0.3508	0.52	1.902
70	70	16.65	570	1.1283	0.4382	0.525	2.0915

From the Table 6-1, it can be observed that with the increase in both of the wall thicknesses, the overlap length decreases. However, if we notice the material volume of the overlap length, there is no change. Thus, increase in both the wall thicknesses with the same magnitude, does not affect the overlap material but there is a significant increase in the overall material cost. For the perspective of material saving, the overlap length is increased with the wall thicknesses as small as possible.

The other advantage of increasing the overlap length is that stress in the central zone is reduced. From an adhesive performance point of view, an area of low stress means that the joint will not suffer from creep under loads. From Figure 6-1 (a) and (b), it can be observed that the overlap length of 770mm leads to reduced shear stress in the central zone in comparison to the overlap length of 660mm. Thus, the final overlap length is taken as 770mm and both the wall thicknesses as 55mm. Note that the thickness of the tower section is only increased for the bottom-most can.

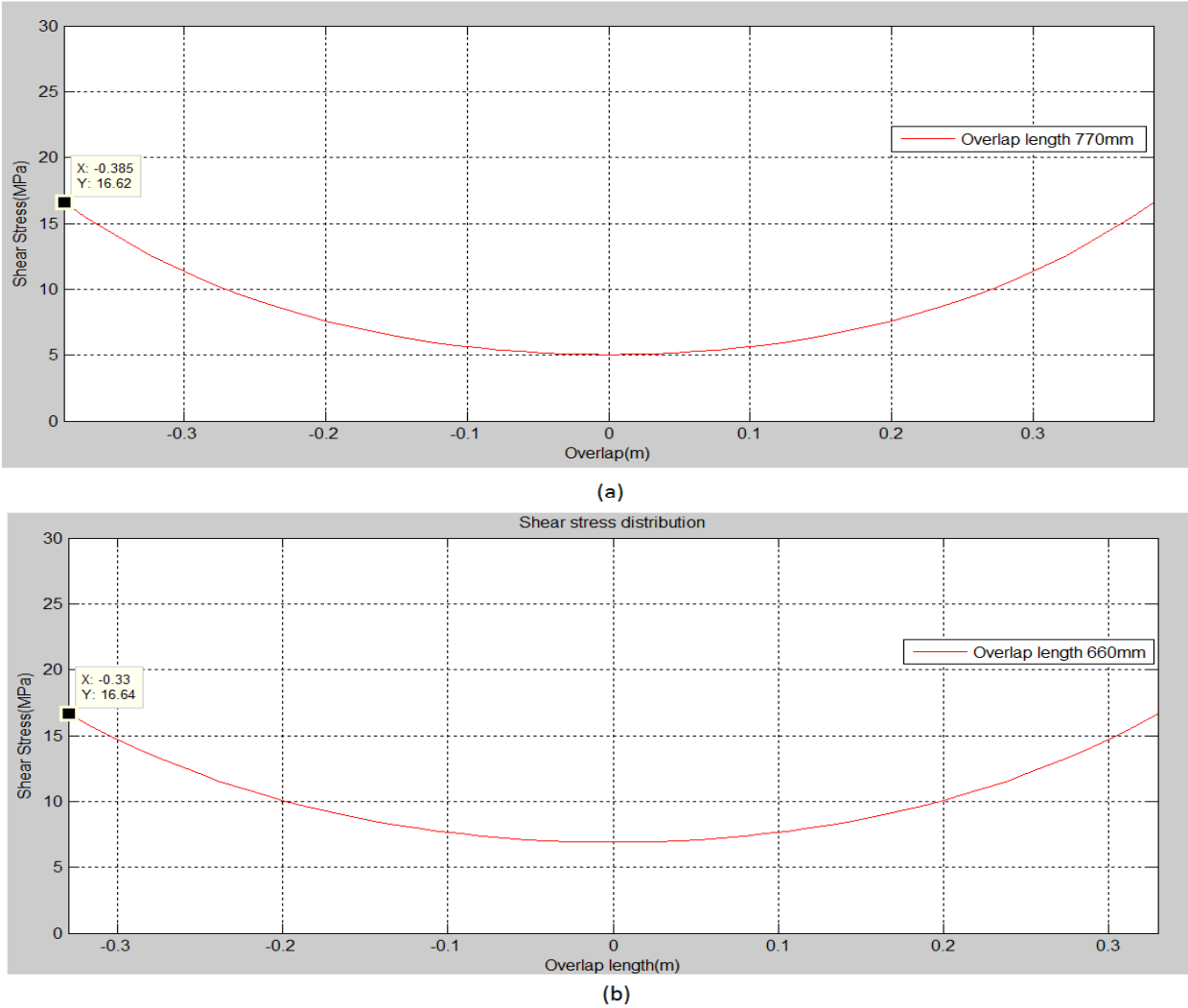


Figure 6-1: Shear stress variation along the overlap length for (a) both wall thickness 55mm, $l = 770\text{mm}$ and (b) both wall thickness 60mm and $l = 660\text{mm}$

The fatigue damage is calculated in the Bladed as discussed in the section 5.6.2. Applying the Goodman correction [22], the accumulated damage value is 0.4 which is less than 1. Thus, the bonded joint may survive for at least the planned service life of the turbine.

Figure 6-2 shows the campbell diagram of the turbine with the bonded tower base and foundation. It can be clearly seen that the first fore-aft and side-to-side tower frequencies are placed between the excitation frequencies (1P and 3P) throughout the operational range of the wind turbine.

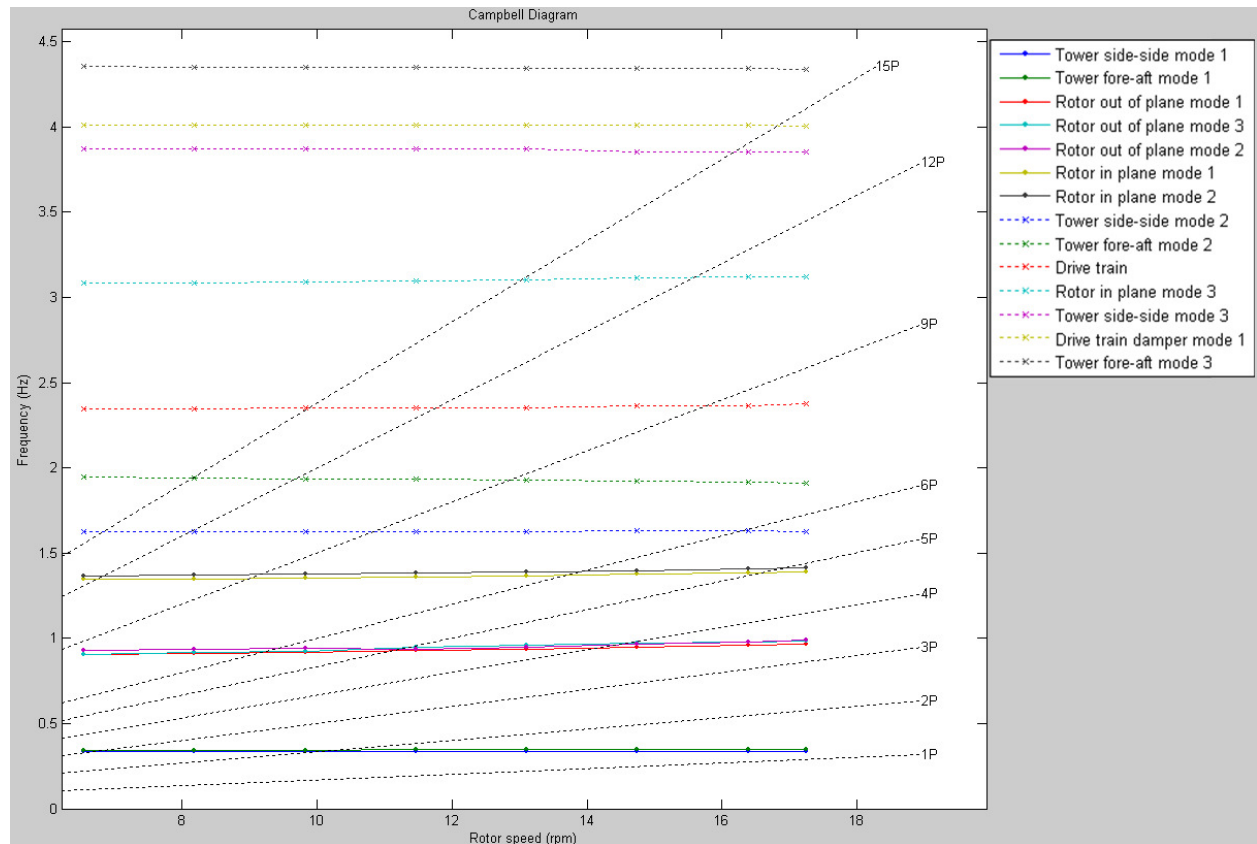


Figure 6-2: Campbell diagram for the turbine with bonded tower base to foundation.

6.2. Final geometry

The final optimized geometry parameters of bonding the tower base with the foundation instead of flanges are:

- Overlap length = 770mm
- Tower wall section thickness = 55mm
- Foundation wall thickness = 55mm
- Adhesive thickness = 10mm

6.3. Cost analysis

The material and the fabrication costs for the existing and the proposed solutions have been compared and other construction aspects are discussed qualitatively in this section.

6.3.1. Flange fabrication cost

The material costs for the bottom-most flange and bolts have been taken from the reference [15]. The cost details in the reference [15] are provided by Repower Energy Systems in December 2007. The flange cost in this study is approximated same as cost per unit volume of the flanges given by Repower and are put in Table 6-2.

Machining and drilling operations in the flanges are tedious and expensive. The fabrication costs for flanges are also included in this estimation. In an American study [50] this operation was estimated to cost about 3000\$ (2411€) per piece. The bolting assembly cost is also included in the Table 6-2. The values are taken from the reference [5]. The total rough estimation of the flange cost at the base is given in the Table 6-2.

6.3.2. Flange welding cost

Two conical cans or the flanges (at towers end) of the tower segments are joined with the circumferential welds. Submerged arc welding technique is recently used to weld different sections in the tower. The cost for the circumferential weld is calculated as [51]:

$$K_{cir} = k_F(\theta_w \sqrt{\kappa \rho V_{total}} + (1.3 \cdot 0.1559 \cdot 10^{-3} \cdot t^2 \cdot (\kappa - 1) \cdot L_{wi})) \quad 6-1$$

Where:

κ	number of element to be assembled which in our case is 2.
θ_w	difficulty factor expressing the complexity of the assembly = 2
ρ	density of the material = 7,850kg/m ³
L_{wi}	circumference of the can [m]
t	wall thickness[m]
R	radius of the conical tower [m]
V_{total}	total volume of two sections getting welded [m ³] = $2\pi R t L_{wi}$
K_{cir}	longitudinal weld cost [\$]
k_F	labour cost factor [\$/min] = 1\$/min [51]

The calculated costs of flange welding at the tower base and the foundation are put in the Table 6-2. The flange material accounts for most of the costs in the reference tower.

Table 6-2: Cost of foundation flange connection

	Unit price (€)	Amount	Total price (€)
Flange material (D=4190mm)	12756	2	25512
Bolt material (M42* 325 10.9))	23.4	140	3276
Machining and Drilling	2411	2	4822
Welding assembly cost	2157	2	4314
Bolt assembly cost			752
		Total	38676

6.3.3. Adhesive bonding cost

The costs of adhesive bonding include the costs of the extra steel and the adhesives applied. The cost of steel is taken approximate €1.4/kg from the WindPACT project (NREL/TP-500-40566) after escalating the cost using the PPI⁹ (Producer price index) to the appropriate year Euros [52]. The price of ESP110 adhesive is around 122£ (or 140€) per 320ml [53]. However, ordering in bulk, for basket of 5liter with items more than 10 baskets, the total price can be reduced by factor of 3.5. This factor has been estimated from the price charts of the adhesive [54]. It has been considered that the adhesive is heat cured by a heating blanket at 120°C, having power supply from a generator. The heating blanket costs around 500€ and the generator can be hired at the price of 500€ for one day [49].

The Table 6-3 shows the change in dimensions before and after bonding the foundation to the tower base. Using these geometry details, the cost of bonded connection replacing flanges are calculated as presented in Table 6-4.

Table 6-3: Dimension of bottommost can before and after bonding

Bottommost can		
Dimensions	Before Bonding	After bonding
Bottom can length, m	2.43	2.43+0.77= 3.2
Wall thickness, mm,	36.5	55
Outer diameter, m	4.19	4.23
Inner diameter, m	4.12	4.12
Overlap of tower wall		
Overlap length, mm	770	
Thickness, mm	55	

⁹ The Producer Price Index (PPI) program measures the average change over time in the selling prices received by domestic producers for their output.

Table 6-4: Cost of adhesive connection

Component	Amount	Unit Price (€)	Total price (€)
Overlapped wall	4359kg	6102	6103
Extra Material in can	4663kg	6530	6530
Machining cost for tapering	2	2411	4822
Adhesive material	110liter	140€ per 320ml with reduction factor 3.5	13750
Heating blanket	1	500	500
Generator hiring	1	500	500
Total			32204

6.4. Cost comparison

Table 6-2 and Table 6-4 include all the major costs that need attention to be added quantitatively. From these rough estimations, it appears that the total costs for this bonded connection can be cut down with a maximum of 17%. The savings are here around 6472€.

The minor costs incurred have been discussed qualitatively in this section. The formation of the bonded joint also requires surface treatment of the bonded area, application of adhesive material, control of production area conditions (moisture and dust). The incurred cost for these procedures can be assumed to compensate with the following two investments for flanges: maintenance and flatness check. A routine maintenance of tightening the bolts half yearly or annually is required. This will also add to the cost incurred on the flange connection. Also a check of the flange's flatness and tilt using easy-laser equipment needs to be performed to assure perfect bolting.

The installation costs with the cranes are not included, as it is assumed to be same for both of the solutions. However, extra jigs will be required to hold the tower in position during heat curing. This cost will be very low and has been ignored. The labour cost for the heat curing is also not included in comparison to the labour cost for assembly of bolts. This curing process is just spreading of the heating blanket around the bonded joint and giving the power supply, hence this cost has not been considered too. The non-destructive testing is required for both the solutions, so the cost of inspection is not compared for this process.

The adhesive thickness of 10mm reflects the prerequisite of higher manufacturing tolerances in the can and the foundation section in the region to be bonded with adhesive. If the tolerances are not met during the manufacturing then machining is required. However, during welding of flanges, if tolerances are also not met, additional machining is required here. Thus, these costs are based on the manufacturing technique and are not included.

The design of bonded connection has not been modeled with the influence of environmental conditions (moisture and water), creep and temperature effect. The inclusion of these factors could estimate the bigger dimensions than what designed now. However a reliable safety of factor is taken in the design to counterbalance effects of these factors.

Another drawback of the flange connections which may be taken into account is the long delivery time, typically between three and four months. If 45° triangular spew fillet is also modeled perfectly in the design, the cost can be possibly further reduced by 15%. This leads to the possibility of achieving the overall cost reduction by 25% (or approximately 10,000€) for the flange at the tower base.

7. Bonding of the cans instead of welds and cost comparison

This chapter presents the results for the second objective of this project. The adhesive bonded connections are less prone to fatigue. So it might be possible to reduce the wall thickness and save material in the entire tower. The reference tower will be redesigned with the bonded connections and the results will be discussed in detail. Finally, the potential cost benefits with the proposed assembly solution will be assessed.

7.1. Results of bonding the cans

The reference tower dimensions as presented in Table 3-11, are the input for the design of the entire tower with the bonded connections instead of the welds. The material and the adhesive properties are same as given in the Table 5-1. The bonded tubular lap joint is dimensioned after replacing each weld between the cans along the tower. The thickness of the adhesive is taken as 10mm. The extreme loadings at each can's height are taken as calculated for the reference tower, presented in Table 3-6.

In this section, the cans connections are bonded and checked for the allowable shear stress ($<16.7\text{MPa}$) and the fatigue. Accordingly, the tower dimensions are optimized as done for the bonded joint in the objective one. The results are displayed in the Table 7-1. For the bottom and the middle section of tower (or up to height 56m), it can be seen that with bonding, the wall thickness (t_2) increases and also use extra overlap material. Thus, the material saving in these sections are not possible. However from the height 56m onwards, there can be seen decrement in the wall thickness (t_2) from the wall thickness (t_1). The volume of overlap material and decrement in thickness are calculated and put in the Table 7-1. These bonded cans are dimensioned according to static and fatigue resistance.

The wall thicknesses (t_2) are lower than the thicknesses (t_1) which are based on the fatigue assessment of welds. As discussed in the chapter 5.6.2.3, it is significant to look for the fatigue in the steel. The fatigue damages of the steel for the reduced thicknesses (t_2) have been calculated as shown in the Table 7-1. It can be seen that fatigue damage value is less than 1, thus there might be no fatigue for at least the planned service life of the turbine.

Table 7-1: Detailed analysis of bonding cans with adhesive and remarks for the possibility of using adhesive

Tower section	Height m	Wall thickness at stability check, mm	Reference tower wall thickness, t_1 , mm	Thickness after bonding, t_2 , mm	Fatigue damage of steel	Overlap mm	Overlap volume m^3	Decrement in thickness volume, $V(t_1)-V(t_2)$, m^3	Remarks on perspective of saving material with adhesive
Bottom section	12	27.5	31	55	–	750	–	–	Not possible
Middle section	32	25	28	50	–	600	–	–	Not possible
Top section	56	19	22	20.3	0.006	580	–	–	Not possible
	60	17.4	20.5	19	0.005	430	0.0638	0.0523	Possible
	64	15.6	19	17	0.013	290	0.0379	0.0674	Possible
	68	13.5	18	15	0.021	200	0.0219	0.0976	Possible
	72	11	17	14	0.018	130	0.0112	0.0940	Possible
	76	7.8	17.5	12	0.004	70	0.0041	0.0725	Possible

7.2. Cost comparison

Table 7-2 shows the cost saving from the circumferential adhesive bonding in the tower from height 60m till the top. All the major relevant costs are included which are incurred for the welded and the bonded connections. Minor costs are ignored as this is a factory assembly process. It can be seen in the Table 7-2 that the cost savings are only possible for the top two cans with a maximum benefit of 1000€. It does not seem to be a better option to bond only two cans for such a small profit, and keeping all the other cans to be welded to each other. This will also interfere the serial welding of all the cans. So the circumferential bonding with adhesive does not contribute to the cost or material saving.

Table 7-2: Cost saving from the circumferential bonding

Height m	Overlap cost a, €	Adhesive applied cost, b, €	Saving in wall thickness cost (Decrease in thickness volume), c, €	Welding cost of can, d, €	Cost saving (c+d-a-b), €
60	701.162	4637	574.777	800	-3964
64	416.521	3033	740.726	770	-1939
68	240.681	2021	1072.624	730	-459
72	123.088	1268	1033.06	690	332
76	45.059	660	796.775	650	741

8. Conclusion and recommendations

The current work proposes a new assembly solution with adhesive for replacing the bottom-most flange and the welds in a tower sections. The conclusions reached are presented below after investigating the feasibility of implementing the bonded connections. After this some recommendations are presented.

8.1. Conclusion

For the welds in the entire tower, fatigue was the predominant phenomenon for determining the wall thicknesses. The Volkersen model has been implemented to design the adhesive bonded joints. The proposed bonded joint is a tubular-single lap joint. The design is prepared for the following two cases:

- 1) Connection between the tower base and the foundation section (replacing the flange), and
- 2) Connection between the cans for the entire tower (replacing all the welds).

With adhesive bonding, it was observed that static resistance of the bonded connections at Ultimate Limit State has a dominating effect on the wall thickness. Using Volkersen's model, it was observed that the shape of stress curve levels off with the increase in overlap length. Thus, increasing the overlap length had virtually no benefit in reducing the peak stress, which only left the possibility of increasing the adherend thickness.

A study of shear stress distribution showed that the unequal adherend thickness in a joint caused asymmetry in the peak stresses at the end of the overlap. For equal adherend thicknesses, the peak stresses were found symmetric and also of lesser magnitude in comparison to the case of unequal adherend thickness.

After comparing the cost for both the proposed cases with already existing design in the reference tower, the following conclusions can be drawn:

- For the first case, it appears that the bottom-most flange costs can be cut down by a maximum of 17% if the environmental conditions, creep, and temperature effect are not modeled in the design. The maximum potential savings in this case has been estimated as 6,500€. The adhesive bonded joint seems to be a feasible assembly solution for replacing the flange. However, it is observed that bonded connection adds extra material to the bottommost can. The inclusion of 45° triangular spew fillet can further reduce the dimensions leading to reduced cost of adhesive bonded connection.
- From the second case, the cost saving can be achieved only for the top two cans in the entire tower with a maximum saving of 1,000€. The remaining cans get thicker with bonded joints in comparison to the welded joints, leading to the use of more material. Thus, it is not feasible to bond only two cans for such a marginal cost saving, keeping all the remaining cans to be welded to each other.

As a final word, the adhesive bonded joint is an economically feasible assembly solution for the replacement of the flanges. The replacement of welds in the entire tower is also possible by bonded joints; however, in comparison to the existing solution it is not a feasible solution in terms of material and cost saving.

8.2. Recommendations for future work

The cost analysis performed on the current tower geometry and material highlighted a potential for savings of about 17%, i.e. around 6,500€. Hence, it is strongly recommended to further investigate the feasibility of implementing this solution.

Analytical models used for the design always behave differently from the experimental solutions. The design models used for bonded connections are simple and are based on limiting assumptions which do not explicitly account for all the parameters involved. Experimental results are neither available in the literatures for the geometry considered in this project. Therefore, it is required in the future to test experimentally for the perfect stress distribution result.

The modeling of spew fillet in the design can lead to a further saving in the material. This has not been modeled during the tower design in this project. Hence, the modeling of the spew fillet for further improvement in the design needs to be investigated.

The S-N curve to be applied for certain geometry in the design process requires the S-N curve of the same geometry. This is because the S-N curve for adhesive bonded connections depends on the geometry of the connections [55]. Hence, there is a need for experimentation to obtain reliable S-N curves for designing each connection in this project.

To propose comprehensive design recommendations other aspects must be addressed, from the designer point of view:

- Improving adhesive joint design using fracture mechanics
- Behaviour of a cylindrical connection, including the effects of peel forces.
- Effects of different environmental conditions (moisture and water), creep and temperature on the bonded connections

Finally, the surface preparation, interface properties, adhesive application and installation processes should be also analyzed.

9. Bibliography

- [1] *Wind Energy Market 2010/2011.*: German Wind Energy Association (BWE).
- [2] E. Hau, *Wind Turbines fundamentals, technologies, application, economics*, 2nd ed.: Springer, 2006.
- [3] W. Wallace. Applied Bolting Technology Products. [Online].
http://www.appliedbolting.com/pdf/ABTP_and_GL_Wind_Turbine_Flange_Bolt_Squirters.pdf
- [4] D.A. Dillard, *Advances in structural adhesive bonding.*: Woodhead publishing limited, 2010.
- [5] A. Verma, "Overview of current connection methods and selection of optimal potential area to be bonded with adhesives," Delft University of Technology, System Integration Project-II 2011.
- [6] GL-Garrad Hassan. [Online]. <http://www.gl-garradhassan.com/en/software/GHBladed.php>
- [7] "IEC 61400-1 Ed.3: Wind turbines - Part 1: Design requirements," International Electrotechnical Commission, IEC, 2005.
- [8] O. Volkersen, *Luftfahrtforschung* , vol. 15, pp. 41–47, 1938.
- [9] Danish Wind Industry Association. [Online].
<http://guidedtour.windpower.org/en/tour/manu/towerm.htm>
- [10] I. Lavassas, G. Nikolaidis, P. Zervas, E. Efthimiou, I.N. Doudoumis and C.C. Baniotopoulos, "Analysis and design of the prototype of a steel 1-MW wind turbine tower," *Engineering Structures*, vol. 25, pp. 1097-1106, 2003.
- [11] C.C. Baniotopoulos, "Design of Wind-Sensitive Structures," in *Wind Effects on Buildings and Design of Wind-Sensitive*, T. Stathopoulos and C.C. Baniotopoulos, Ed. Thessaloniki, Greece: Springer.
- [12] M. Seidel, "Entwicklung der Turmbauwerke für die Multi-MW-Klasse," in *Tagungsband Deutsche Windenergie-Konferenz (DEWEK)*, Wilhelmshaven, 2002.
- [13] GAMESA. [Online]. <http://www.gamesa.es/en/products-and-services/wind-turbines/design-and-manufacture/manufacturing-and-assembly-process.html>
- [14] Cooper & Turner. [Online].
http://www.cooperandturner.co.uk/documents/brochures/Wind_brochure3_08_web.pdf
- [15] W. Husson, "Friction Connections with Slotted Holes for Wind Towers," Luleå University of Technology, PhD Thesis ISSN: 1402-1757, 2008.
- [16] "Appendix 8.3: Vestas V90 transport guidelines," Vestas wind systems A/S, 2005.
- [17] N. Diepeveen and M. Segeren, Personal communication for 3MW Bladed file, 2011.

- [18] H.J.T. Kooijman, C. Lindenburg, D. Winkelaar, and E.L. van der Hooft, "DOWEC 6 MW PRE-DESIGN: Aero-elastic modelling of the DOWEC 6 MW pre-design in PHATAS," DOWEC and ECN, public report: Re-print of a confidential report ECN-CX--01-135 DOWEC-F1W2-HJK-01-046/9, September 2003.
- [19] "General specification V90-3MW VCRS 60Hz," Vestas Wind Systems A/S, class 1: Document no.: 0000-4797 V02, 2009.
- [20] Enercon Wind Turbines Technology and Service. [Online].
http://www.ledsjovind.se/entorp/Technologie&Service_Eng.pdf
- [21] "Guidelines for Certification of Offshore Wind Turbines," Germanischer Lloyd, WindEnergie, Edition 2005.
- [22] *Guidelines for Design of Wind Turbines*, 2nd ed. Denmark: DNV/Risø, 2002.
- [23] "Eurocode 3. Design of steel structures-Part 1-1: General rules and rules for buildings," DS/ENV1993-1-1,.
- [24] Dansk Ingeniørforening, 1998.
- [25] A.J. Kinloch, *Adhesion and adhesives: science and technology*.: Chapman & Hall, 1987.
- [26] J. Comyn and W.C. Wake R.D. Adams, *Structural adhesive joints in engineering* , 2nd ed.: Chapman & Hall, London, 1997.
- [27] The adhesives design toolkit. [Online]. www.adhesivestoolkit.com
- [28] A. Kwakernaak, "AE4740 Lecture notes: Adhesive bonding," Adhesion Institute, Delft University of Technology, 2011.
- [29] E.M. Petrie, *Handbook of adhesives and sealants*.: McGraw-Hill, New York, 2000.
- [30] L.F.M. da Silva, A. Ochsner and R.D. Adams, *Handbook of adhesion technology*, 1st ed.: Springer, 2011.
- [31] L.J. Hart-Smith, "Effects of flaws and porosity on strength of adhesive bonded joints," *Proceedings of 29th Annual SAMPE Symposium and Exhibition, April 3-5, 1984*.
- [32] L.F.M. da Silva, R.F.T.Lima and R.M.S. Teixeira, "Development of a Computer Program for the Design of Adhesive Joints," *The Journal of Adhesion*, vol. 85, no. 12, pp. 889–918, 2009.
- [33] L.F.M. da Silva, R.D. Adams and M. Gibbs., "Manufacture of adhesive joints and bulk specimens with high-temperature adhesives," *International Journal of Adhesion & Adhesives*, vol. 24, pp. 69-83.
- [34] L.F.M. da Silva, P. J.C. das Neves, R.D. Adams, A. Wang and J.K. Spelt, "Analytical models of adhesively bonded joints—Part II: Comparative study," *International Journal of Adhesion & Adhesives*, vol. 29, pp. 331–341, 2009.

- [35] M. Goland and E. Reissner, "The Stresses in cemented joints," *Journal of Applied Mechanics*, vol. 66, pp. A17–A27, 1944.
- [36] L.F.M. da Silva, T.N.S.S. Rodrigues, M.A.V. Figueiredo, M.F.S.F. de Moura and J.A.G. Chousal, "Effect of Adhesive Type and Thickness on the lap shear strength," *The Journal of Adhesion*, vol. 82, no. 11, pp. 1091–1115, 2006.
- [37] A.D. Crocombe, "Global yielding as a failure criterion for bonded joints," *International Journal of Adhesion and Adhesives*, vol. 9, pp. 145–153, 1989.
- [38] D.M. Gleich, M. J. L. van Tooren, and A. Beukers, "Analysis and evaluation of bondline thickness effects on failure load in adhesively bonded structures," *Journal of Adhesion Science and Technology*, vol. 15, no. 9, pp. 1091–1101, 2001.
- [39] R.D. Adams and N. A. Peppiatt, "Stress analysis of adhesive-bonded lap joints," *The Journal of Strain Analysis*, vol. 9, pp. 185–196, 1974.
- [40] H. Nordberg, "Fatigue Properties of Stainless Steel Lap Joints," *SAE International*, 2005.
- [41] W R Broughton, L E Crocker and J M Urquhart, "Strength of Adhesive Joints: A Parametric Study," NPL Materials Centre, National Physical Laboratory, ISSN 1473-2734, July 2001.
- [42] J.D. Whitcomb and K. Woo, "Analysis of debond growth in tubular joints subjected to tension and flexural loads," *Computers and structures*, vol. 46, no. 2, pp. 323-329, 1993.
- [43] F. Thamm, "Stress Distribution in Lap Joints With Partially Thinned Adherends," *The Journal of Adhesion Volume*, vol. 7, no. 4, pp. 301-309, 1976.
- [44] Z.C. Roza and M.J.L. van Tooren, *Finite Difference Methods for stress analysis of adhesive bonded joints - The design of a MATLAB adhesive toolbox*, Aerospace materials, Ed.: Delft University Press, 1998.
- [45] L.F.M. da Silva, P.J.C. das Neves, R.D. Adams and J.K. Spelt, "Analytical models of adhesively bonded joints—Part I: Literature survey," *International Journal of Adhesion & Adhesives*, vol. 29, pp. 319–330, 2008.
- [46] R. Boyes, "Adhesive bonding of stainless steel: strength and durability," Sheffield Hallam University, PhD Thesis 1998.
- [47] T.B. Jones and N.T. Williams, *SAE International Congress and Exposition*, 1986.
- [48] A. Hobbacher, International Institute of Welding (IIW/IIS), IIW document XIII-1965-03 / XV-1127-03, Update July 2004.
- [49] H. Poulis, Personal communication, 2011.
- [50] N.W. Lanier, "LWST Phase I Project Conceptual Design Study: Evaluation of Design and Construction Approaches for Economical Hybrid Steel/Concrete Wind Turbine Towers," National Renewable

Energy Laboratory, NREL/SR-500-36777, January 2005.

- [51] P.E. Uys, J. Farkas, K. Jarmai and F. van Tonder, "Optimisation of a steel tower for a wind turbine structure," *Engineering Structures*, vol. 29, pp. 1337–1342, 2007.
- [52] L. Fingersh, M. Hand and A. Laxson, "Wind Turbine Design Cost and scaling model," National Renewable Energy Laboratory, Technical report NREL/TP-500-40566, December 2006.
- [53] Glue Online. [Online]. http://www.glueonline.co.uk/shop/Cyanoacrylate_Adhesives.html
- [54] krayden Inc. [Online].
<http://krayden.distone.com/itBrowse.asp?act=search&pgf=grid&pg=8&pl=PBAD&sb=-rel&pgl=12>
- [55] Rene Alderliesten, Personal communication, 2011.
- [56] L.F.M. da Silva, T.N.S.S. Rodrigues, M.A.V. Figueiredo, M.F.S.F. de Moura and J.A.G. Chousal, "Effect of Adhesive Type and Thickness on the lap shear strength," *The journal of adhesion*, vol. 82, no. 11, pp. 1091–1115, 2006.
- [57] L.F.M. da Silva, R.D. Adams and M. Gibbs, "Manufacture of adhesive joints and bulk specimens with high-temperature adhesives," *International Journal of Adhesion & Adhesives*, vol. 24, pp. 69-83, 2004.
- [58] R.D. Adams and V. Mallick, *The Journal of Adhesion*, vol. 43, no. 1-2, 1993.
- [59] W.E. de Vries and V.D. Krolis, "Effects of deep water on monopile support structures for offshore wind turbines".
- [60] Dansk Ingeniørforening, 1983.
- [61] R. Alderliesten, Personal communication, 2011.
- [62] SeeBA Energiesysteme GmbH. [Online]. www.seeba-online.de
- [63] M. Seidel, "Experiences with two of the world's largest wind turbine towers," in *European Wind Energy Conference*, Madrid, 2003.
- [64] M. Kühn, "Dynamic and Design Optimisation of Offshore Wind Energy Conversion Systems," DUWIND, Delft University of technology, PhD thesis 2001.
- [65] Cooper and Turner and McLean Buchanan and Wilson. [Online].
http://www.cooperandturner.co.uk/documents/brochures/Wind_brochure3_08_web.pdf
- [66] A. Bromage and A. Tricklebank, "Concrete Towers for Onshore and Offshore Wind Farms," The Concrete Center, 2007.

Appendix A. Load case descriptions

Extreme load case descriptions

Design load case:	DLC 1.3	
Operating conditions:	Power production	
Wind conditions:	Extreme turbulence model (ETM)	
Type of analysis:	Extreme	
Partial safety factors:	Normal	
Description of simulations:		
Load case identifier	Mean wind speed (m/s) (mid bin)	Longitudinal turbulence intensity (%)
DLC_1.3_bin1	4	70.8
DLC_1.3_bin2	8	40
DLC_1.3_bin3	12	30
DLC_1.3_bin4	16	24.6
DLC_1.3_bin5	20	21.5
DLC_1.3_bin6	23.5	19.7
Comments: 10 minute simulations Rayleigh wind distribution Turbulence scaling parameter, $c=2$		

Design load case:	DLC 2.3		
Operating conditions:	Power production plus loss of electrical grid connection		
Wind conditions:	Extreme operating gust (EOG)		
Type of analysis:	Ultimate		
Partial safety factors:	Abormal		
Description of simulations:			
Load case identifier	Vhub (m/s)	EOG gust (m/s)	Grid loss phasing
DLC_2.3_a	10.3	5.795	tstart gust + 0 tstart gust + 2.45 tstart gust + 4 tstart gust + 5.25
DLC_2.3_b	12.3	6.448	
DLC_2.3_c	14.3	7.100	
DLC_2.3_d	20	8.960	
DLC_2.3_e	25	10.590	
Comments: Steady wind with transient gust (gust period = 10.5s) One minute simulations Gust occurs 10s into simulation Wind gradient exponent (exponential model), $\alpha = 0.2$ Grid loss phasing indexed x=1 (t=10s), x=2 (t=12.45s), x=3 (t=14s), x =4 (t=15.25s)			

Design load case:	DLC 4.2	
Operating conditions:	Normal shut-down plus deterministic gust	
Wind conditions:	Extreme operating gust (EOG)	
Type of analysis:	Ultimate	
Partial safety factors:	Normal	
Description of simulations:		
Load case identifier	Vhub (m/s)	EOG gust (m/s)
DLC_2.3_a	10.3	5.795
DLC_2.3_b	12.3	6.448
DLC_2.3_c	14.3	7.100
DLC_2.3_d	20	8.960
DLC_2.3_e	25	10.590
Comments:		
Steady wind with transient gust (gust period = 10.5s)		
One minute simulations		
Gust occurs 10s into simulation		
Wind gradient exponent (exponential model), $\alpha = 0.2$		
Shut down occurs at start of gust		
Starting azimuth angle varied from 0-90deg in 30deg intervals (indexed 1-4).		

Design load case:	DLC 5.1	
Operating conditions:	Emergency shut-down	
Wind conditions:	Normal turbulence model (NTM)	
Type of analysis:	Ultimate	
Partial safety factors:	Normal	
Description of simulations:		
Load case identifier	Mean wind speed (m/s) (mid bin)	Longitudinal turbulence intensity (%)
DLC_5.1_a	10.3	20.7
DLC_5.1_b	12.3	19.28
DLC_5.1_c	14.3	18.26
DLC_5.1_d	20	16.48
DLC_5.1_e	25	15.58
Comments:		
Three dimensional three component Kaimal turbulent wind field (1 min sample)		
Shut down occurs 10s into simulation		
Wind gradient exponent (exponential model), $\alpha = 0.2$		

Design load case:	DLC 6.1	
Operating conditions:	Idling	
Wind conditions:	Extreme wind model(turbulent) (Vhub = V50)	
Type of analysis:	Ultimate	
Partial safety factors:	Normal	
Description of simulations:		
Load case identifier	Mean wind speed (m/s)	Longitudinal turbulence intensity (%)
DLC_6.1	50	11
Comments:		
Three dimensional three component Kaimal turbulent wind field (10 min sample).		
Wind gradient exponent (exponential model), $\alpha = 0.11$		

Fatigue load case descriptions

Design load case:	DLC 1.2	
Operating conditions:	Power production	
Wind conditions:	Normal turbulence model (ETM)	
Type of analysis:	Fatigue	
Description of simulations:		
Load case identifier	Mean wind speed (m/s) (mid bin)	Longitudinal turbulence intensity (%)
DLC_1.2_bin1	4	34.4
DLC_1.2_bin2	8	23.2
DLC_1.2_bin3	12	19.5
DLC_1.2_bin4	16	17.6
DLC_1.2_bin5	20	16.5
DLC_1.2_bin6	23.5	15.8
Comments:		
10 minute simulations		
Rayleigh wind distribution		

Appendix B. Definition of adhesive related terms

Adhesive: Non-metallic substance capable of joining materials by surface bonding (adhesion), the bonding possessing adequate internal strength (cohesion).

Adhesive failure: Failure of an adhesive bond, such that separation appears to be at the adhesive/adherend interface as shown in figure below.

Bond-line: The layer of adhesive, which attaches two adherends.

Bond strength: The unit of load applied to tension, compression, flexure, peel, impact, cleavage, or shear, required to break an adhesive assembly with failure occurring in or near the plane of the bond.

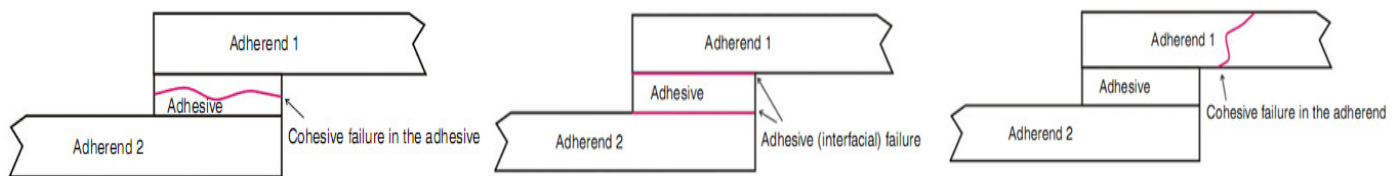


Figure: Examples of cohesive and adhesive failures [30]

Cohesion: It only involves intermolecular attractive forces within a single substance

Cohesive failure: Failure within the body of the adhesive or adherend (i.e. not at the interface) as shown in Figure.

Fatigue: Dynamic—alternate loading in shear or tension-compression. Static—maximum load sustained for long periods of time in tension or shear; tests are also used to determine creep.

Fatigue life: Number of cycles necessary to bring an adhesive bond to the point of failure when the bond is subjected to repeated cyclic stressing under specified conditions.

Fatigue strength: The force that a joint will withstand when it is applied repeatedly for an infinite number of cycles.

Lap joint: Joint made by placing one adherend partly over another and bonding together the overlapped portions.

Substrate: An adherend, a material upon which an adhesive is applied.

Interphase: The region between the adhesive and the adherend.

Interface: The interface, different from the interphase, is a plane of contact between the surface and the two materials. It is within the interphase. It is useful to define and measure the surface energy.

Appendix C. Adhesive and material properties

Table: Adhesive properties (E is the Young's modulus, ν is the Poisson's ratio, σ_y is the tensile yield strength, σ_r is the tensile strength, ϵ_r is the tensile failure strain, τ_y is the shear yield strength, τ_r is shear strength, γ_r is shear failure strain and CTE is the coefficient of thermal expansion) [26], [56], [57] and [58]

Property	Adhesives			
	Redux 326	AV 119	Hysol 9321	MY 750/HY 956
E (GPa)	4.44	3.05	3.87	3.18
ν	0.35	0.35	0.35	0.35
σ_y (MPa)	50.9	28.6	22	
σ_r (MPa)	50.9	67.1	46	86.2
ϵ_r (%)	1.28	8	3.8	6.4
τ_y (MPa)	36.5	49	25	
τ_r (MPa)	36.5	49	33	
γ_r (%)	3.63	30	6.4	
CTE ($^{\circ}\text{C}^{-1}$)				56.7×10^{-6}

Table: Properties of metallic adherends (E is the Young's modulus, ν is the Poisson's ratio, σ_y is the tensile yield strength and CTE is the coefficient of thermal expansion) [26], [56], [57] and [58]

Properties	Adherends		
	Mild steel	High-strength steel	Aluminium
E (GPa)	210	210	75
ν	0.3	0.3	0.3
σ_y (MPa)	270	1080	280
CTE ($^{\circ}\text{C}^{-1}$)			22×10^{-6}

Appendix D. Matlab code for Volkersen Model

Variation of peak shear stress against different overlap length

```
% variation of shear stress when bonding length is changed from 50mm to
% 2m keeping the adhesive thickness 10mm
clear all
clc

tw = 55*10^-3; % Tower section wall thickness (m)
tf = 55*10^-3; % Tower foundation wall thickness (m)
v = 0.35; % Poisson ratio
E = 210*10^9; % Young's modulus for both tower and foundation
section(Pa)
ta = 10*10^-3; % Adhesive thickness (m)
Ea = 3.7*10^9; % Modulus of elasticity (Pa)
Ga = 1.35*10^9; % Shear Modulus (Pa)

% Bending and Axial stress calculation on joint section

di = 4.19-2*0.035; % Inner diameter (m)
do = di + 2*tw; % Outer diameter (m)
M = 85.404*10^6; % Bending moment (Nm)
Sb = M*do*0.5*64/3.14/(do^4-(di)^4); % Bending stress
Sa = 3*10^6 * 4/3.14/(do^2-di^2); % Axial stress
Stotal = Sb+Sa; % Total stress
l = 0.05;

for i=1:196
    x = -l/2;
    phi = Ga*l^2/E/tw/ta;
    Si = tw/tf;
    w = sqrt((1+Si)*phi);
    X = x/l;
    % Adhesive shear stress
    Taumax(i) = (Stotal*tw/l/1000000)*((0.5*w*cosh(w*X)/sinh(w/2))+(((Si-1)/(Si+1))*w*0.5*sinh(w*X)/cosh(w/2)));
    l = l + 0.01;
end

plot(0.05:0.01:2, Taumax, 'r')
axis([0.05 2 0.0 135]), grid
xlabel('Overlap lengths(m)'), ylabel('Shear Stress(MPa)')
```

Shear stress distribution along the overlap length

```
% Shear stress distribution along the overlap length taking origin of
% longitudinal coordinate x at the middle of overlap length
clear all
clc

tw = 55*10^-3; % Tower section wall thickness (m)
tf = 55*10^-3; % Tower foundation wall thickness (m)
v = 0.35; % Poisson ratio
E = 210*10^9; % Young's modulus for both tower and foundation section, Pa
ta = 10*10^-3; % Adhesive thickness (m)
Ea = 3.7*10^9; % Modulus of elasticity (Pa)
Ga = 1.35*10^9; % Shear Modulus (Pa)
l = 0.77;

% Bending and Axial stress calculation on joint section

di = 4.19-2*0.035; % Inner diameter (m)
do = di + 2*tw; % Outer diameter (m)
M = 85.404*10^6; % Bending moment (Nm)
Sb = M*do*0.5*64/3.14/(do^4-(di)^4); % Bending stress
Sa = 3*10^6 * 4/3.14/(do^2-di^2); % Axial stress
Stotal = Sb+Sa; % Total stress

% Parameters calculation
phi = Ga*l^2/E/tw/ta
Si = tw/tf;
w = sqrt((1+Si)*phi)
x = -l/2;

for i=1:51
X = x/l;

% Adhesive shear stress
Tau(i) = (Stotal*tw/l/1000000)*((0.5*w*cosh(w*X)/sinh(w/2))+(((Si-1)/(Si+1))*w*0.5*sinh(w*X)/cosh(w/2)));
x = x+0.0154;
end

plot(-0.385:0.0154:0.385, Tau, 'r')
title('Shear stress distribution')
axis([-1/2 1/2 0.0 30]),grid
xlabel('Overlap length(m)'),ylabel('Shear Stress(MPa)')
```

Appendix E. Table showing the failure loads for fillet

Table showing the predicted failure load for concave fillet versus no fillet [41]

Table A3: FEA Strength Predictions for CR1 Mild Steel/AV119 Epoxy Single-Lap Joints - von Mises Material Model
(concave fillet versus no fillet)

Case	Adhesive Thickness (mm)	Adherend Thickness (mm)	Bond Length (mm)	Predicted Failure Load (N)				
				Maximum Shear Stress	Maximum Tensile Stress	Hill's Failure Criterion	Maximum Shear Strain	Maximum Tensile Strain
1 (no fillet)	0.25	2.5	12.5	4,225	4,240	2,241	6,043	7,507
2 (no fillet)	0.25	2.5	25.0	5,077	5,088	2,688	6,672	9,773
3 (no fillet)	0.25	2.5	50.0	6,577	6,525	3,743	10,076	13,217
4 (fillet)	0.25	2.5	12.5	6,285	6,295	4,076	8,711	7,395
5 (fillet)	0.25	2.5	25.0	7,655	7,715	4,900	10,168	9,526
6 (fillet)	0.25	2.5	50.0	10,482	10,656	6,683	13,512	12,833

Table A4: FEA Strength Predictions for CR1 Mild Steel/AV119 Epoxy Single-Lap Joints - Linear Drucker-Prager Material Model
(concave fillet versus no fillet)

Case	Adhesive Thickness (mm)	Adherend Thickness (mm)	Bond Length (mm)	Predicted Failure Load (N)				
				Maximum Shear Stress	Maximum Tensile Stress	Hill's Failure Criterion	Maximum Shear Strain	Maximum Tensile Strain
1 (no fillet)	0.25	2.5	12.5	5,330	5,264	2,659	-	-
2 (no fillet)	0.25	2.5	25.0	6,401	6,328	3,217	7,406	9,394
3 (no fillet)	0.25	2.5	50.0	8,777	8,666	4,498	10,164	13,027
4 (fillet)	0.25	2.5	12.5	6,110	6,105	4,426	7,985	7,280
5 (fillet)	0.25	2.5	25.0	7,540	7,517	5,321	10,594	9,282
6 (fillet)	0.25	2.5	50.0	12,287	12,175	7,219	13,930	12,727

